E.T.S. de Ingeniería Industrial,
Informática y de Telecomunicación

GNSS-R systems for soil parameters determination

Grado en Ingeniería
en Tecnologías de Telecomunicación

Trabajo Fin de Grado

Rodrigo Moreno Cordón

Luis Javier Serrano Arriezu

Patrizia Savi

Pamplona, Julio 2018

upna Universidad Pública de Navarra
Nafarroako Unibertsitate Publikoa

Resumen

La Reflectometría en Sistemas Globales de Navegación por Satélite (GNSS-R) es una tecnología basada en la utilización de las señales procedentes del Sistema Global de Navegación por Satélite (GNSS) la cual, estudiando las reflexiones de dichas señales sobre superficies tanto sólidas como líquidas, nos permite obtener información acerca de la composición del terreno.

Estos sistemas pueden presentarse como radares mono-estáticos o bi-estáticos. Es decir, no hay necesidad de que el transmisor y el receptor estén juntos, lo que ofrece la posibilidad de realizar mediciones de señales GNSS con receptores pasivos terrestres o basados en aeronaves aviones o drones.

Durante las últimas décadas, esta ciencia ha encontrado su nicho en aplicaciones para la determinación de diversas características de la superficie terrestre, yendo desde la estimación de la densidad de la nieve y el hielo hasta la caracterización de la humedad del sustrato.

El objeto de esta tesis es el de estudiar algunos de los usos potencialmente más relevantes de las tecnologías GNSS-R desde puntos de vista tanto teóricos como experimentales, ofreciendo resultados conclusivos y allanando el camino para futuras investigaciones en esta materia.

Extensas investigaciones acerca de la determinación de la constante dieléctrica del terreno y del espesor de la nieve han sido llevadas a cabo. Además del análisis de la eficiencia y beneficios que presentan las configuraciones GNSS-R linealmente polarizadas, en sustitución de las polarizaciones circulares más comúnmente utilizadas.

El método utilizado para caracterizar los parámetros del terreno es el análisis de la interacción entre los campos electromagnéticos de las señales GNSS directamente recibidas y los campos electromagnéticos de las señales reflejadas sobre la superficie terrestre.

Las señales transmitidas por GPS, las cuales pueden interpretarse como combinaciones lineales de componentes de polarización horizontal y vertical, son polarizadas circularmente a derechas (RHCP) mientras que las señales reflejadas están

predominantemente polarizadas circularmente a izquierdas (LHCP) para ángulos de incidencia típicos.

El porqué de la predominancia de sistemas GNSS-R polarizados circularmente es entendible teniendo en cuenta estos datos. No obstante, cuando se realizan los cálculos pertinentes para el análisis de señales circularmente polarizadas existe la necesidad de descomponer dichas componentes circulares en lineares.

Teniendo esto en cuenta, se desarrollaron modelos matemáticos que proveen herramientas para poder trabajar directamente con señales de polarización circular en este campo. Por lo tanto, uno de los propósitos principales de esta tesis es la de demostrar la eficiencia de esta tecnología, presentando sus inconvenientes y beneficios, y presentando mediciones que sostienen su utilidad.

Con esta meta, se presentan campañas de medición de la profundidad de la nieve con sistemas polarizados linealmente, y se discuten sus resultados, demostrando que son una excelente opción para medir dicha profundidad y el contenido de agua equivalente de la nieve.

Por otro lado, la obtención de la constante dieléctrica del suelo es investigada estudiando campañas de medidas previas, y realizando una nueva utilizando un sistema GNSS-R proporcionado por el Politecnico di Torino.

Esta configuración se compone de dos antenas tipo parche de polarización circular, dos front-end comerciales SiGe y un software de adquisición y post-procesado de datos (Jia, Notarpietro y Savi, 2014).

Finalmente, los resultados obtenidos en esta tesis muestran los beneficios de los sistemas GNSS-R tanto para la determinación de la constante dieléctrica del sustrato como para la de la profundidad de la nieve, junto con la exposición del potencial de las configuraciones GNSS-R linealmente polarizadas. Aparte de presentar resultados concluyentes, se espera que esta investigación sirva de referencia para futuros estudios en este campo.

Abstract

Global Navigation Satellite System Reflectometry (GNSS-R) is a GNSS based technology that uses its receiving reflected signals, either from liquid or from solid surfaces, and compares them in order to obtain information about the soil's composition.

GNSS-R systems can present a bi-static or multi-static schema. That is, there is no need for the transmitter and receiver to be together, what offers the possibility to measure GNSS signals with either ground-based or aircraft-based passive receivers.

Along the last years, this technology has found its application in many subjects, going from the soil moisture determination to the snow and ice depth sensing.

This thesis aims to study some of the most relevant uses of GNSS-R from both theoretical and experimental points of view, offering conclusive results and paving the way to further investigations on these topics.

Extensive research has been carried out on the dielectric constant of the soil and the snow depth determination, together with the analysis of the utility of the linearly polarized GNSS-R configurations instead of the common circularly polarized ones.

The mechanism used to characterize the soil's parameters is by analysing the interaction between the directly received electromagnetic field and the one field scattered from the surface.

GPS transmitted signals are right-hand circularly polarized (RHCP) while the surface's scattered signal is predominantly left-hand circularly polarized (LHCP) for typical incidence angles.

Why most of the existing research has been based on circularly polarized models is directly understandable observing these facts. However, when conducting computations about the circular polarization there is indeed a need of decomposing the circular components in linear ones.

Regarding this fact, mathematical models were developed in order to provide tools to work directly with linearly polarized signals. Thus, one of the purposes of this thesis is the

demonstration of the efficiency carried by this technology by presenting its pros and cons and giving measurements that sustain its usefulness.

Following this path snow depth measurement campaigns, which uses linearly polarized systems, are presented and their results are discussed. Proving that these GNSS-R systems are a great option for measuring snow depth and equivalent water content.

On the other hand, soil's dielectric constant retrievals are investigated examining previously measurements' campaigns and conducting another one using a GNSS-R system provided by the Politecnico di Torino.

This setup was composed by two circular polarized antennas, two commercial SiGe's front-ends and data acquisition and data post-processing software (Jia, 2014).

Finally, the results obtained in this thesis show the benefits of GNSS-R systems for both dielectric constant and snow depth determination, and the potential of the linearly polarized configurations. Furthermore, this research is hoped to serve as a reference to future studies working in these subjects.

Acknowledgement

Reaching the end of this university period, I could not be more grateful than having had the honour of working on this project at the Politecnico di Torino in such an enriching research environment.

Particularly, I must show my deepest gratitude to the professor Patrizia Savi who has been a real mentor during these months, and without whose tutelage and help I would not have been able to reach these objectives.

I have also to express my absolute gratitude to my sending institution on this Erasmus+ program, the Universidad Pública de Navarra, and to my professor Luis Javier Serrano Arriezu who made this whole experience become possible. The inner UPNA's engineering school ETSIIT, its affiliated, and even the unaffiliated who have contributed to my education also have my entire gratitude, rightfully.

As it could not be otherwise, I have to truly thank my family whose support has always helped me to overcome any obstacle and surpass myself, even from the distance. And my friends, whose support has been palpable during the whole exchange program, have the absolute right to be object of my gratitude as well. Above all, I must thank A.U. because, essentially, she is my lighthouse.

Last but not least, I am willing to extend the thanks to all the fabulous people who I have met in Torino, with whom I have had such amazing and rewarding experiences and from whom I have learned so much.

Counting on your help, I will continue working hard and doing my best with the aim of making the world a better place.

Contents

List of Figures

List of Tables

1. Introduction

1.1. Global Navigation Satellite System

GNSS (Global Navigation Satellite System) is a global position and tracking system which uses a constellation of satellites to provide autonomous and geo-spatial location around the globe through microwave transmission (L-Band). Assisted by the data processing of the receiver device as well, this bilateral schema guarantees accuracy in synchronization and positioning.

Although the first objective in developing this system was for military use, the tremendous utility of GNSS technology meant that many countries considered investing in it during these last years in order to provide positioning, navigation and tracking services for its population.

By December 2016, some countries had already deployed satellite systems, focusing first on covering their own regions but later on working to expand their coverage around the world, which is nowadays their current task.

Some of them are: Russia with GLONASS (24 satellites in orbit), the European's Union Galileo with 14 operational satellites, 2 testing only, 2 unavailable, 2 retired, and 4 commissioning (Constellation Information | European GNSS Service Centre, 2017) the USA's Global Positioning System (GPS) with 31 satellites in orbit; or China, who is in the process of expanding its system into the global BeiDou-2 GNSS by 2020 (Tao, 2018).

1.2. GNSS-R

Global Navigation Satellite System Reflectometry is based on receiving GNSS reflected signals either from the sea or from the Earth, and comparing them in order to obtain information about these surfaces compositions.

Ground-based or aircraft-based, the GNSS-R passive receivers differ from other microwave sensing systems because of their bi-static radar system, what means that there is a significant distance separating the transmitter and the receiver as shown in Figure 1 (Jin, 2014)

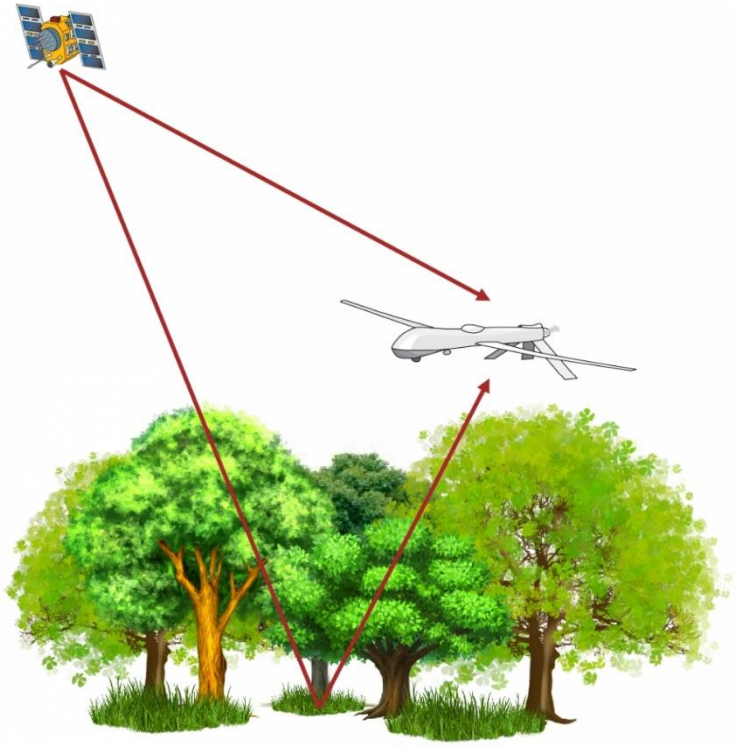

Figure 1: GNSS-R bi-static air-based radar system (http://www.coregalproject.com/pages/technology, s.f.)

Furthermore, this schedule can be also expanded to a multi-static radar system in which the receiver gets at the same time multiple signals coming from many transmitters (Jin, 2014) (Shuanggen Jin, 2011)(see Figure 2).

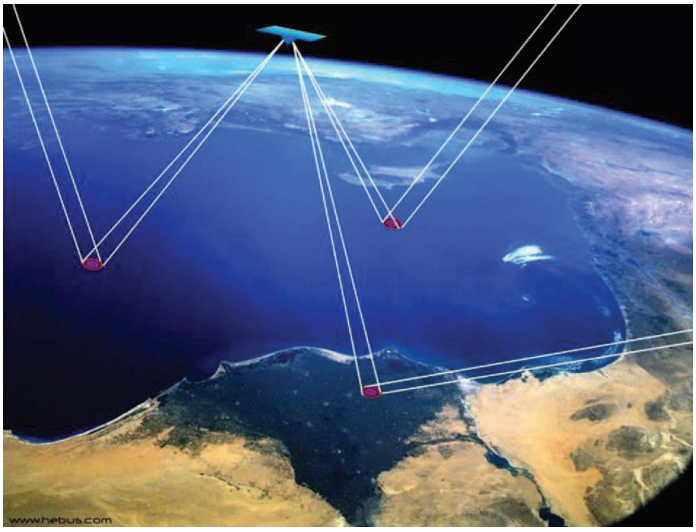

Figure 2: GNSS-R multi-static radar system (Valery U. Zavorotny, December 2014)

Separating the different signals from each GNSS satellite by its modulation, the receiver is capable of recognizing as a well-known signal the one direct from the satellite, so consequently it would be able to compare this reference signal with one the scattered signal from the reflecting surface.

Therefore, GNSS-Reflectometry is currently being a fundamental work tool in many fields as soil parameters or moisture determination, snow depth (Berardelli, 2009), weather prediction models, wind speed, wave motion (Gleason, 2005) (Clarizia, 2009), detection of buried objects, ocean altimetry (Martin-Neira M. , 1993) and soil nutrients.

1.3. GNSS-R Applications

Since 1996, when the first proposal of studying the ground dielectric permittivity showed up (Adnan Kavak, 1996), the use of the multipath surface interference of GNSS signals has risen as an efficient method for monitoring this data with, firstly ground-based (Valery U. Zavorotny, December 2014) and later even air-based, GNSS passive receivers.

Using the L-Band GNSS signals, the density of the surface's vegetation can be inferred from the attenuation and scattering around the specular direction, which provides an estimation about the biomass ratio of increment in this zone (P. Ferrazzoli, 1995, 2012 Online).

Soil moisture and vegetation density sensing have already shown their robustness from ground-based stations measuring multi-path reflectometry and interferometric patterns (Kristine M. Larson, 2008) (Larson & Small, 2014). Proving it by retrieving an error between 3-4% when applying these interferometric techniques for determining the bare soil moisture due to the surface roughness (Valery U. Zavorotny, December 2014) (N. Rodriguez-Alvarez, 2011).

Apart from that, as previously mentioned, GNSS-R also has several uses in the fields of earth surface sensing, going from wave motion and ocean patterns to buried objects detection.

Altimetry measurements is one of them, commonly used to determine both ocean and ice surface height. Being the first foreseen application for GNSS-R systems, it depends on whether the reflected power from the surface is enough in order to enable precise observations.

Executed by at least four radio-links (one can also be used but in particular cases when a good a priori information is available), GNSS-R measured surface height can be averagely estimated around an area in absolute or relative terms.

Wind speed and waves measurement has also been a topic of study for GNSS-R systems, even when it does not give the wind speed itself, but it is able to determine the surface roughness, which is closely correlated with the wind stress on the sea surface.

In fact, many ocean applications are in need of knowing the wind stress measurements, while other application as meteorological ones are based on the effective wind indeed.

Therefore, in order to come to a common solution for both of them, the relationship between these parameters, linked to the drag coefficient, is currently being the study issue for many researches.

Furthermore, during these last decades, snow depth determination has been as well one of the relevant topics for which GNSS-R was applied.

Actually, its relevance when measuring the amount of water stored in the snowpack and forecasting the rate of melt are essential for management of water supply and flood control systems (Shi & J.Dozier, 2000).

Thus, using GNSS-R multipath models together with circularly or even linearly polarized setups, we are able to determine its thickness and its equivalent water content.

1.4. Brief history of GNSS-R for land parameters determination

Land parameters determination has been a researching issue since 1952, when the Gardner and Kirkham's group firstly proposed this sensing at Iowa State College. Leading to a primary Time Domain Reflectometry (TDR) technique, which was later introduced, by a group of Canadian researchers for this purpose (Campanella, 2014).

Meanwhile, the history of GNSS-R can be barely understood without a brief look at the born and development of GNSS itself.

Born in 1960 as a project from the United States, the Transit satellite system was the first satellite-based geo-positioning system (Worth & Warren, Transit to Tomorrow. Fifty Years of Space Research at The Johns Hopkins University Applied Physics Laboratory, 2009).

Developed for military use jointly by DARPA and the Johns Hopkins Applied Physics Laboratory, and sponsored by the Navy, it provided accurate location information to its Polaris ballistic missile submarines meanwhile being also useful as a navigation system.

This first satellite was based on the Doppler-Delay effect: travelling through a well-known path, the Transit broadcasted signals of a well-known frequency as well. Therefore, the receiver only had to monitor the frequency shift due to the satellite movement, evaluate it between a short interval, and then it was able to determine a particular position by distinguishing if it was located whether to one side of the satellite or to the other (Kershner & McClure, 1998).

After many years being used only for military purposes, it was freely available for civilian use until its withdrawal in 1996, when it ceased navigation service and was made obsolete by the Global Positioning System (GPS).

NAVSTAR-GPS (NAVigation System and Ranging - Global Position System) also known as GPS, is one of the already functional GNSS systems and the only one having worldwide range currently. Born in 1973 as a project from the United States Department of Defence (National Research Council, 1995), the Global Positioning System (GPS) was also developed for military use. However, it was not until 1983 when the US's President Ronald Reagan made it freely available for civilian use after Korean Air Lines Flight 007 was shot down for entering the URR's prohibited airspace (Organization, 2008).

Subsequently in early 1990s, the southern California Permanent GPS Geodetic Array (PGGA) established the first operational GPS for civilian use.

Later on, in 1993, its satellite constellation achieved initial operational capability (IOC) and finally NAVSTAR-GPS was declared with Full Operational Capability (FOC) by Air Force Space Command (AFSPC) in April 1995 (Observatory, 2011).

As well as GPS, GLONASS (*Global'naya Navigatsionnaya Sputnikovaya Sistema* or GLObal NAvigation Satellite System) is also a space-based satellite navigation system that follows the guidelines of the GNSS technologies.

Developed by the Soviet Union (and now by Russian Federation), it provides services of radio-navigation both for the civilian use and for the military use of Russian Aerospace Defence Forces.

Apart from these already operational GNSS systems, there are many countries who are currently working on their main constellations, in order to fully develop their operability systems during these next years.

As an example of them, we can remember Galileo satellite navigation system. Created by the European Space Agency (ESA, European Union), the aim of this 24 satellite constellation is to provide to the MEOSAR system a global search and rescue function.

Galileo get its Early Operational Capability (EOC) denomination in 2016 (Agency, 2016), which meant that it was able to provide services with a weak signal, but thanks to the European effort and investment on the this technology, it is expected to reach Full Operational Capability (FOC) in 2019 (Commission, 2015), and finally it will reach its 30-satellite constellation by 2020.

As well as Europe, China is also developing its own satellite constellation under the name of BeiDou-2 (formerly known as COMPASS). This is an expansion from their previous Asia-Pacific regional service (BBC, 2012), looking forward to into global coverage, and evolving from the first generation BeiDou Navigation Satellite System (also known as BeiDou-1).

Becoming operational in December 2011, it was able to provide this Asian-Pacific services with a partial constellation of 10 satellites.

Four years later, in 2015, China launched the project BeiDou-3, the BeiDou's third generation, which is supposed to finally provide global coverage with millimetre-lever accuracy by 2020, using nothing less than 35 operational satellites (Wang L. , 2016).

These last years, GNSS has being developing signals models increasing their amplitude and bandwidth, what leads to more accurate positioning systems, thanks to a shorter signal-acquisition time and to an easier indoor-navigation schema.

For example, Galileo is spanning its E5a+E5b signal bandwidth beyond 60MHz, and other issues as altimetry resolution are also being developed. As Weiquiang Li has shown, regarding her improvements by factors between 1.5 and 1.7 only by inter-modulating the signals (Li, et al., The Impact of Inter-Modulation Components on Interferometric GNSS-Reflectometry, 2016).

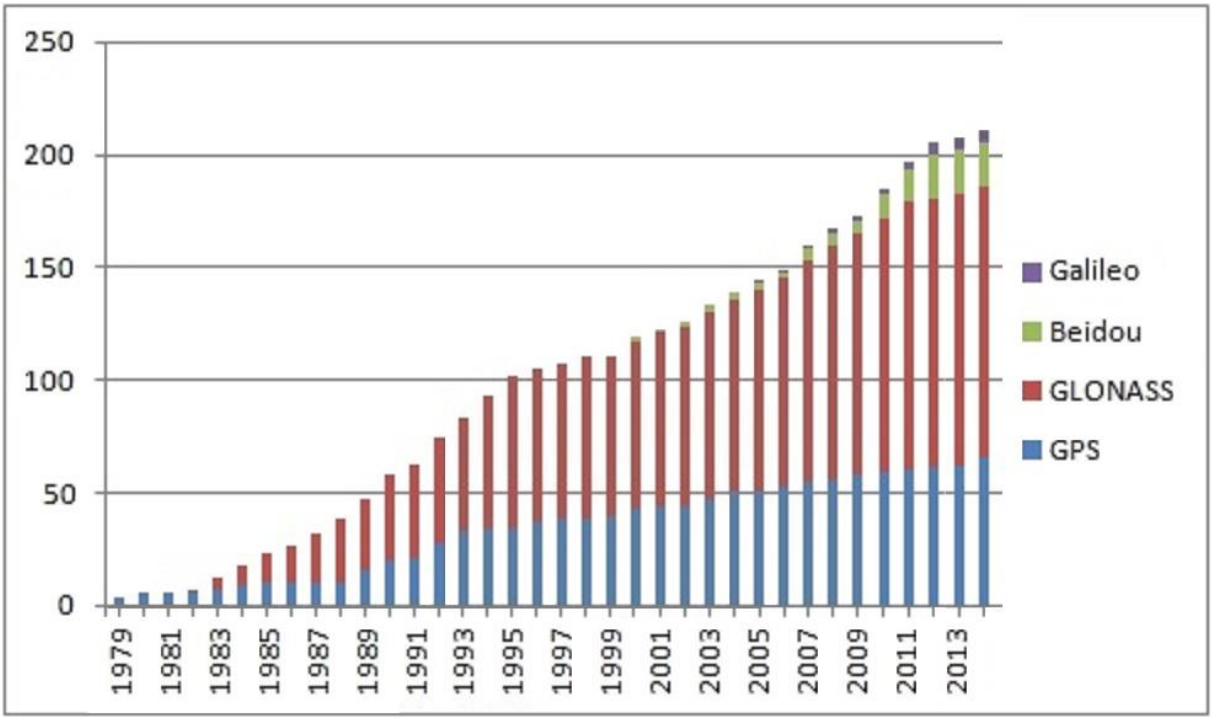

Figure 3: Launched GNSS satellites 1978 to 2014. (Credit: Wikipedia).

Concurrently, while GNSS systems were evolving in such a way, a fundamental application of them was also developing on the background. That was, in fact, GNSS-Reflectometry (GNSS-R).

The earliest studies shown an effective manner to sense soil moisture in the top surface layers (0-4 and 0-2 cm) with P-band (0.775 GHz) and L-band (1.4 GHz) signals, respectively (Wang & Schmugge, 1980) (Njoku & O'Neill, 1982).

A few years later, it was only 1998 when Giovanni Piccardi conceived the first GNSS-R model for bi-static reflections (Picardi, Seu, G. Sorge, & Martin Neira, 1998) (Martin-Neira, Kern, & D'Addio, 2017). And no much time passed until Valery U Zavorotny and Alexander G Voronovich proposed the second one, using a terminology closer to radar theory that is widely used nowadays (Voronovich, 2000).

It proposed fitting the model to the rising edge of the observed waveform, what provides a better accuracy when estimating of the delay of the echo.

This technology is being a study issue even now. As an example of it the recent proposal of Weiquiang Li of adapting it to air-based systems can be seen, a concept to partially measure the expected echo shape in flight (Martin-Neira, Kern, & D'Addio, 2017).

Therefore, as the GNSS-R technology evolved during the last decades, its applications also did so, being the land parameter determination its main issue from the very first moment.

The oldest researching project regarding this subject could be the one leaded by A. Kavak, W. J. Vogel, and G. Xu in 1996, who used a six-channel, C/A code processing, CiPS receiver with an almost omni-directional patch antenna to measure three types of ground to characterize 1.575 GHz specular ground reflections and properties, defining the use of GNSS-R for the following decades.

They matched the computer simulated values with the experimentally obtained results, estimating the patterns that would determine the electrical characteristics (conductivity and dielectric constant) of surfaces as grass, asphalt or water (Kavak, Xu, & Vogel, GPS multipath fade measurements, 1996).

This same researching group continued using and developing this emergent system for many years. Also succeeding when they derived ground electrical characteristics by the matching of those simulated and measured signals, and the fading produced when comparing directly received L-band signals with the ones reflecting specularly from the ground (Kavak, Vogel, & G. Xu, Using GPS to measure ground, 1998).

Being in a tireless evolving process, GNSS-R is being used with many aims (soil moisture, snow depth, vegetation density…) but always following strategies as the ones previously mentioned: comparing simulations with empirical measurements of circular polarized antennas.

In fact, the linear polarization has always been almost taken apart from the equation, concerning only a few studies about its potential.

One of them, and even one of the first researches about GNSS-R, showed up in 1998.

It was the researching group formed by V. U. Zavorotny and A. G. Voronovich the one who suggested a reception of the scattered by using a simple signal at two orthogonal linear

polarizations with analysing their ratio, in order to mitigate the adverse effect of the surface roughness in GNSS-R moisture retrievals (Valery U. Zavorotny, December 2014).

But later on, a simpler approach was examined experimentally for which only the circular cross-polar component of the reflected field was acquired (D. Masters, Initial results of landreflected GPS bistatic radar measurements in SMEX02, 2004), often normalized by the land reflected co-polar signal, and actually ended including both circular components in (A. Egido, 2012) (Valery U. Zavorotny, December 2014).

Different models appeared along the years, many of them studying this polarization dilemma.

The effects of the different polarization state on reflected signals from rough surfaces was the researching point of Zavorotny in 2000. He proposed a theoretical description based on a homogeneous soil model, showing that the ratio of two orthogonal polarizations received power proved to be independent of the surface roughness factor and sensitive to the soil moisture (Zavorotny & Voronovich, 2000).

This theoretical model was empirically corroborated in 2012 (Egido, et al., 2012).

In 2011, a researching group reviewed the potential applications of bistatic radar observations including a list of possible approaches and algorithms for the wide range of its applications, concluding that the received power is sensitive to the forest biomass without showing the typical saturation of radar backscattering measurements (Cardellach, Fabra, Nogués-Correig, Oliveras, & Rius, 2011).

During those years, a more practical study was being under research at the same time. Estimating the above-ground, but following the Multipath and Interference Pattern Technique (IPT), it provided a deeper analysis on the soil moisture over dense and packed vegetation layers, with high vegetation water content (Rodriguez-Alvarez, et al., 2011).

Recent researches have also gone deeper into the airborne-based GNSS-R measurements, as a study did in 2014 when three scientific flights were performed in order to acquire GNSS reflectometry (GNSS-R) polarimetric observations over a wide range of terrain conditions

obtaining the georeferenced right–left and right–right reflectivity components and discussing them (Egido, et al., 2014).

And shortly afterwards, only a few years ago, a first polarimetric GNSS-R measurement from a stratospheric flight was carried out over Boreal forests showing different GNSS codes by polarimetric ratio maps (Carreno-Luengo, et al., 2015).

1.5. Aim of the Thesis

Reaching at this point, we already have an overall view of the situation of the GNSS-R technology over the last years and its current issues.

Therefore, it is difficult not to notice some of its aspects that nowadays generalized but might cause standstill if we do not try to broaden horizons in any of them.

The extended use of circular polarized antennas could be seen as one method commonly used (and actually perfectly functional) that is really focusing all the researchers' attention during the last decades, as seen before. But, why do not we have a look to the linear polarized antenna's systems?

Being during this last years a secondary subject of study, GNSS-R system based on linear polarized antennas has being a bit disregarded.

Therefore, the study of measured data using linear polarized antennas for GNSS-Reflectometry for land parameter determination will be one of the main subjects of this thesis.

Together with this aim comes the objective of studying and furthering the use of GNSS-R linearly polarized systems for the determination of snow depth, as it is an important component of the climate system and a critical storage component in the hydrologic cycle so, having the technology to measure it, its characterization should be carried out.

Meanwhile, when doing this researching work, some measurements about the determination of the soil dielectric constant have been conducted with the GNSS-R system provided by Politecnico di Torino.

Regarding the fact that in this case linearly polarized antennas have been used, it is remarkable to highlight that the aim of these campaign is to provide useful measured data for further studies about this subject.

2. Basic principles of GNSS

2.1. Global Navigation Satellite Systems

GNSS is a navigation system composed by a constellation of satellites in Medium Earth Orbit (MEO, 20000km and above) used for positioning and location users in any part of the globe, whether on land, sea or air.

These satellites transmit ranges of signals in order to determine the position, velocity and time (PVT) of the static or mobile user by measuring differential computations of the distances using a minimum of three satellites of known position, which number can be extended to four satellites in order to provide altitude information.

Each of these satellites has its own modulation and, being used as transmitters, they make receivers know those in advance in order to differ the signals from one satellite to another. They possess navigation payloads, atomic clocks and other subsystems which guarantee great precision when estimating the user's position.

Another way to provide that is arranging them in different planes within the MEO orbits, in order to ensure the best Geometric Dilution of Precision (GDOP), therefore these orbits are chosen as a compromise between accuracy, global coverage and launch cost.

Furthermore, when designing the constellation, special attention is paid to the selection of the number and the orbits of the satellites, assuring always enough visible quantity of them from anywhere in the world, reaching for signal availability and accuracy.

2.2. GNSS Positioning Process

The more accurate distance measurement is, the more accurate the final location estimation will be. In practice, the receiver captures the L-band signals emitted by the satellites that contain the position of the satellite and the exact time it was transmitted. The position of the individual

satellite is transmitted in a data message called *ephemeris* data, together with the *almanac* data, which gives information about the time and status of the entire satellite constellation .

On the other hand, in order to provide the propagation time of the signal and thereby determine the satellite-to-user range, ranging codes as CDMA (code division multiple access) are used. This is a spread-spectrum technique that encoded the data with unique pseudo-random noise (PRN) sequences, achieving higher rates (Jin, 2014).

Estimating the PVT is a labour of four satellites, as previously said, computing three position coordinates and one clock error as four unknowns.

The user segment compares the broadcast time, which is encoded in the transmission, with the time of reception, measured by an internal clock, so that the propagation time (or transit time) of the signal from the satellite is measured.

Bearing this in mind, it only performs two measurements of the GNSS signals: a comparison between the received code with a locally generated copy (this is called Pseudorange), and a differentiation between the received carrier signal phase and the one from a receiver-generated signal at the same frequency (this is called the carrier phase observable) (Jin, 2014).

Thus, the location of the user after the position of the satellite can be obtained from both, the ephemerides from the navigation message, as well as from the carrier phase observables, respectively. Reaching, this second one, a millimetric precision, but lacking the accuracy of the Pseudorange because of an ambiguity in the number of times the carrier wavelength (Jin, 2014).

In order to guarantee a precise estimation about the user's location each satellite uses an atomic clock, which provides nanosecond accuracy, enabling him to be synchronized with the whole constellation.

Each measurement of the distance places the receiver in a spherical shell of radius equal to the measured distance, thus, taking several measurements and looking for their intersection point, the position can be actually inferred.

However, this estimation is not easy to compute in some cases due to the delays. For example, when the mobile receiver is rapidly moving, the position of the signal moves while signals from several satellites are received. In addition, radio signals have a slight delay when they pass through the ionosphere.

Finding the shortest tangent line to four spherical shells centered on each of the four satellites, receivers reduce errors using combinations of multiple signals and correlations (Hegarty & Chatre., 2008). Then the partial data, affected by noise and constantly changing, is combined in an estimated single position, time, and speed.

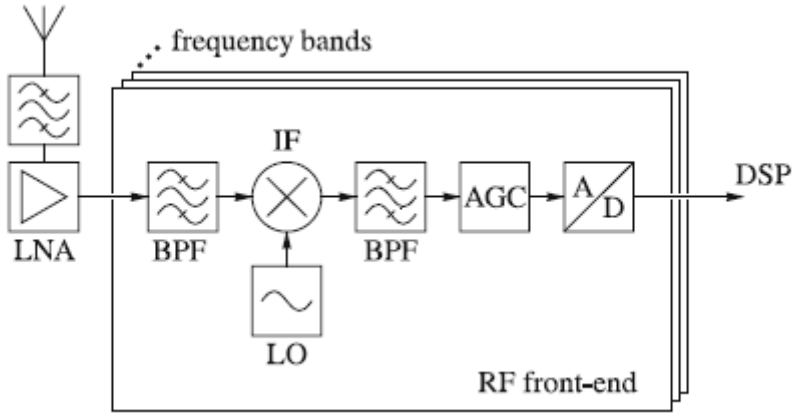

Figure 4: GNSS receiver (Hofmann-Wellenhof, et al., 2008)

2.1. GNSS Signals

Satellite navigation systems can be classified, based on their signals, into passive and active as well as into one-way (uplink = earth-to-space; downlink = space-to-earth) and two-way ranging systems.

Anyway, the main GNSS systems are passive one-way downlink ranging systems. The satellites emit modulated signals that include the time of transmission to derive ranges as well as the modeling parameters to compute satellite positions (*ephemeris* and *almanac* data).

We can observe how the emitting satellite works in the (Figure 5: Composition of the navigation satellite).

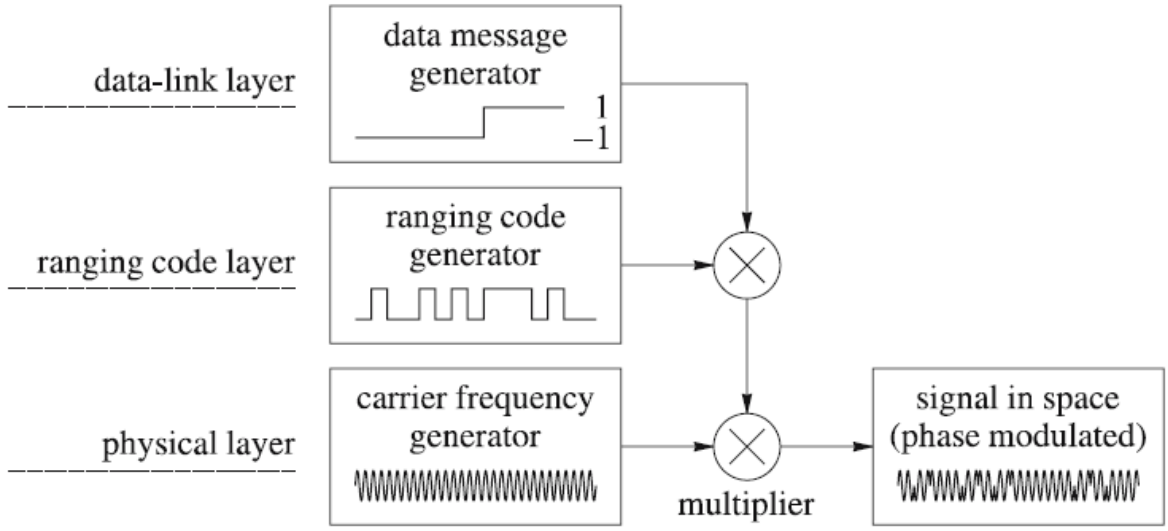

Figure 5: Composition of the navigation satellite (Hofmann-Wellenhof, et al., 2008)

The code layer is based on a continuous but periodic modulated signal exploited within correlation techniques.

A problematic issue in which satellite systems have to focus more than anything is in synchronization. Therefore, periodicity is strictly synchronized to the time system of the satellites and to the data message, containing in the data-link layer the time of transmission, satellite *ephemeris, almanac*, etc. (Hofmann-Wellenhof, et al., 2008).

Satellite navigation uses circularly polarized signals by definition, in order to get round the Faraday Rotation effect, the polarization fading caused by earth and the cross-polarization losses caused by the satellite's movement.

Therefore, satellites generate a signal by modulating a ranging code, according to the spectral shaping scheme, and the data message onto the carrier frequency, and the multiplexing these different signals into one right-handed circularly polarized, which emitted from the satellite

antennas. But we cannot ignore that under certain circumstances, specular reflecting surfaces change the right-handed circular polarization (RHCP) to left-handed circular polarization (LHCP) and vice versa, what will have especial interest for us when using GNSS-R systems, as we will see on chapter 4.

Summarizing GNSS systems, we can observe that they mainly use carrier signals between the frequencies represented in the table below, together with their specific modulations and multiplexing methods (Table 1: GNSS signals).

System	Carrier	Modulation	Multiple Address
GPS	L1/L2/L5 L1C/L2C	BPSK/BOC/MBOC/QPSK	CDMA
Galileo	E1/E5/E6 E5a/E5b	BOCc/CBOC Alt BOC BPSK	CDMA
GLONASS	L1/L2/L3	BPSK/QPSK	FDMA/CDMA
BeiDou	B1/B2/B3	MBOC/BOC Alt BOC QPSK	CDMA

Table 1: GNSS signals (Jin, 2014)

All GNSS systems work between the Ultra High frequencies, defined by the ITU. Thus, their carriers goes from 300 MHz to 3 GHz frequency ranges, 1m to 1dm wavelength range, and are part of one of the UHF related bands: B / C / D / E bands (NATO) and L / S bands (IEEE).

These specific bands correspond to the following frequency ranges, shown in Table 2.

NATO LETTER BAND DESIGNATION				BROADCASTING
NEW NOMENCLATURE		OLD NOMENCLATURE		**BAND DESIGNATION**
BAND	FREQUENCY (MHz)	BAND	FREQUENCY (MHz)	
A	0 – 250	**I**	100 – 150	Band I 47 – 68 MHz (TV)
				Band II 87.5 – 108 MHz (FM)
		G	150 – 225	Band III 174 – 230 MHz (TV)
B	250 – 500	**P**	225 – 390	
C	500 – 1 000	**L**	390 – 1 550	Band IV 470 – 582 MHz (TV)
				Band V 582 – 862 MHz (TV)
D	1 000 – 2 000	**S**	1 550 – 3 900	
E	2 000 – 3 000			
F	3 000 – 4 000			
G	4 000 – 6 000	**C**	3 900 – 6 200	
H	6 000 – 8 000	**X**	6 200 – 10 900	
I	8 000 – 10 000			
J	10 000 – 20 000	**Ku**	10 900 – 20 000	
K	20 000 – 40 000	**Ka**	20 000 – 36 000	
L	40 000 – 60 000	**Q**	36 000 – 46 000	
		V	46 000 – 56 000	
M	60 000 – 100 000	**W**	56 000 – 100 000	

Table 2: EU, NATO, US ECM frequency designations (Radio spectrum, 2018)

Furthermore, as we can see in (Table 1: GNSS signals), generally, GNSS applies a CDMA (Code Division Multiple Access).

This is, as seen before, a spread-spectrum technique that uses a unique randomizing sequence PRN (pseudo random noise).

The PRN is a signal similar to noise which satisfies one or more of the standard tests for statistical randomness. Although it seems to lack any definite pattern, pseudorandom noise consists of a deterministic sequence of pulses that will repeat itself after its period (Federal Standard 1037C).

Therefore, we can conclude that GNSS signals are composed by three main elements to take into account: Carrier, ranging code (PRN codes) and navigation data (ephemeris, clock bias parameters, almanac, etc.).

3. Basic Principles of GNSS-Reflectometry

3.1. Introduction and categories

Global Navigation Satellite System - Reflectometry is a method of remote sensing, based on GNSS systems, generally used to obtain information about the earth surface in different environments either liquid, solid, barren or covered by vegetation.

This can be done analysing the GNSS reflected signals in the receiver.

Therefore, depending on the transmitter-receiver infrastructure, we can differ some different schemas of GNSS-R technologies:

Bi-static Radar systems are the ones in which there exists a significant distance between transmitter and receiver.

On the other hand, we can find multi-static Radar systems, which differ from the bi-static ones due to receiver, who is getting at the same time multiple signals coming from many transmitters (Jin, 2014) (Shuanggen Jin, 2011)(Figure 2).

Apart from this, GNSS-R systems can also be ground-based (Figure 6) or air-based (Figure 1).

This implies taking into account different issues when working with them, as happens in the satellite tracking process, but it also carries different vantages: the possibility of separating the radio-links by modulation or even using the delay and Doppler information from air-based received signals (Jin, 2014).

Figure 6: Static measurement setup (Jia, 2014)

For some applications it is desirable that both direct and reflected radio-links interference with each other, being then gathered by a single antenna.

But what is more common is finding systems in which these two contributions are received by two different antennas: one pointing to the transmitter to gather direct ray, while the other to the surface, to collect the surface-Earth scattered signals.

3.2. Geometry

The amount of received reflected radio-links could be as large as the number of direct ones.

Therefore, considering the huge number of the simultaneously received signals, the spatial coverage observed by a nadir-looking antenna is nothing else than a gapped and irregularly sampled image of the Earth surface.

Indeed, the amount of GNSS received signals can go from about 15 if measuring from the Earth surface to even more when working with an air-based system (the higher the receiver's altitude, the higher the number of signals).

Consequently, the formed image is compound by the mosaic of glistering zones produced by the reflected signals, giving a synoptic view of hundreds of kilometres across-track but not about the distance between them.

In order to analyse the potential time-space coverage of a hypothetical GNSS-R it is useful to focus on the specular reflection points rather than on the glistering zones. What provides an idea of the spatial coverage by ground-tracking the GNSS constellations when move along their orbits.

These specular points are the surface's exact location where the specular reflections take place (Figure 7). Theoretically, they are defined as the points characterized by an equality between the incident angle and the reflection angle in the plane that includes both transmitter and receiver, making the waves coming from a single direction be reflected in another single direction as well.

Specular points make reference to the surface points scattering the GNSS signals such specular way, but in most scenarios two different scatterings take place at the same time, this specular scattering together with the diffuse scattering.

In contrast with the specular one, diffuse scattering is characterised for reflecting the incidental signal in a broad range of directions.

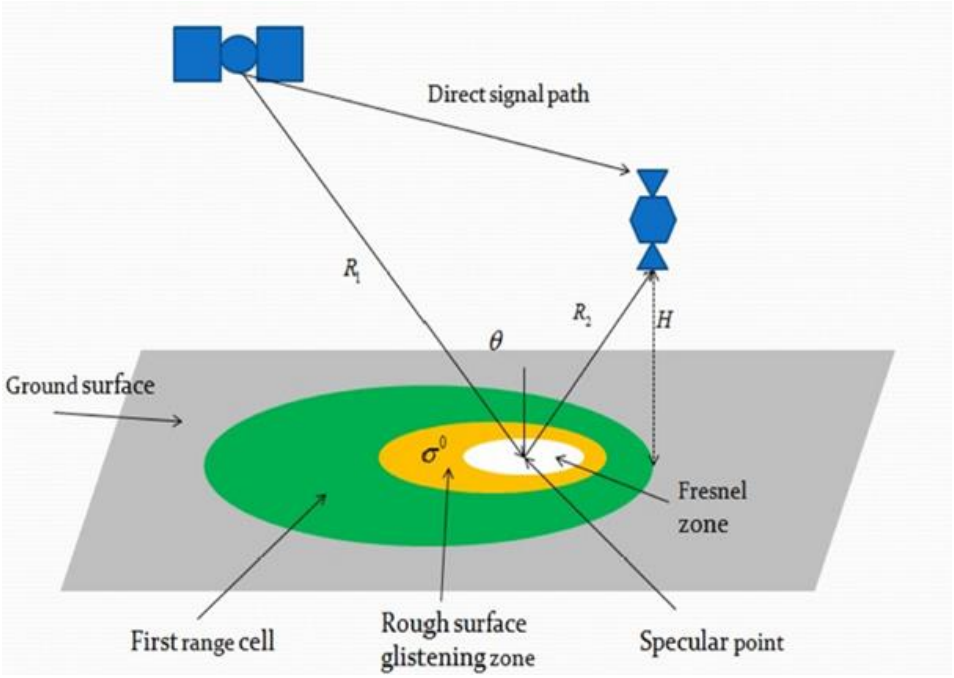

Figure 7: Geometry and scattering zones (Jin, 2014)

Specular scattering appears to be dominant when the scattered signals are reflected from smooth surfaces, which means in terms of λ that the topographic accidents in those are insignificantly large compared to the electromagnetic wavelength.

In these cases, the signal's power is reflected by an active region called Fresnel zone (Figure 7) coherently, and its size is determined that the differential phase change across the surface comparing with the specular point is limited to π radians (Beckmann & Spizzichino, 1963).

On the other hand, when the surface's roughness cannot be deprecated, the diffuse scattering becomes dominant, causing more signal power to be scattered incoherently by an expanded active region surrounding the Fresnel, also called "glistening zone" (Figure 7).

This zone is defined by Geometrical Optics as the one composed by the surface's *facets* whose reflection points towards the receiver above a probability threshold. By definition, a *facet* is a surface patch of size of curvature of the order of the electromagnetic wavelength (λ).

Therefore, the rougher the surface, the larger the resulting glistering zone (Figure 8).

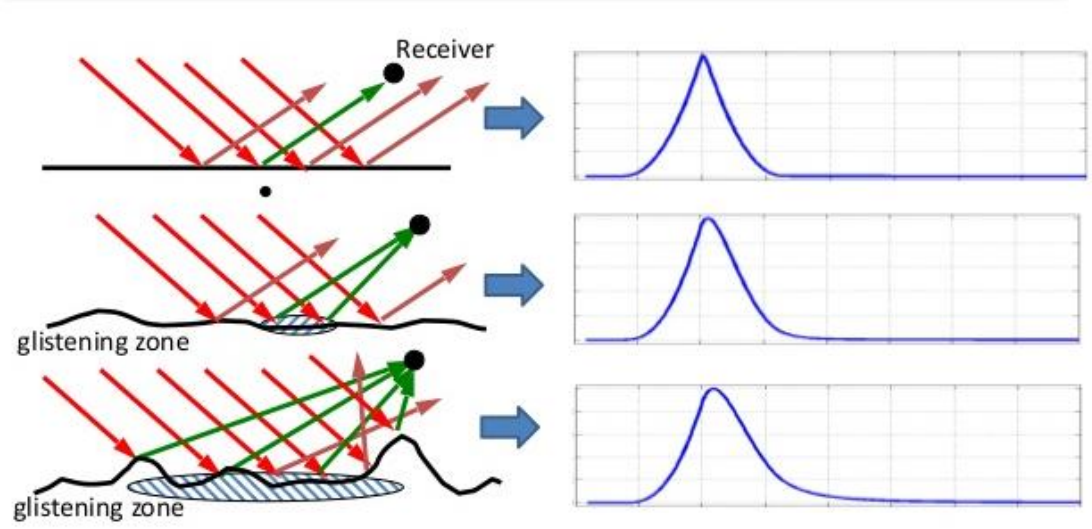

Figure 8: Glistening Zone and Multipath (Garrison, 2016)

Supposing a flat-Earth model (Figure 9) and assuming that the scattering plane is mathematically our Y-Z plane, we can infer that the specular point corresponds to the center of coordinates for the ellipse:

$$1 = \frac{y^2}{a^2} + \frac{x^2}{b^2} \tag{1}$$

So, the specular point will be:

$$a = \frac{\sqrt{2H\Delta\rho}}{(\sin e)^{\frac{3}{2}}} \tag{2}$$

$$b = \frac{\sqrt{2H\Delta\rho}}{(\sin e)^{\frac{1}{2}}} \tag{3}$$

where $\Delta\rho = \Delta\tau \times c$, being $\Delta\tau(x,y) = \tau(x,y) - \tau_{spec}$ the relative delay to the specular radio link, $\tau(x,y)$ the travelling time along the radio-link and τ_{spec} after reflecting at the specular point.

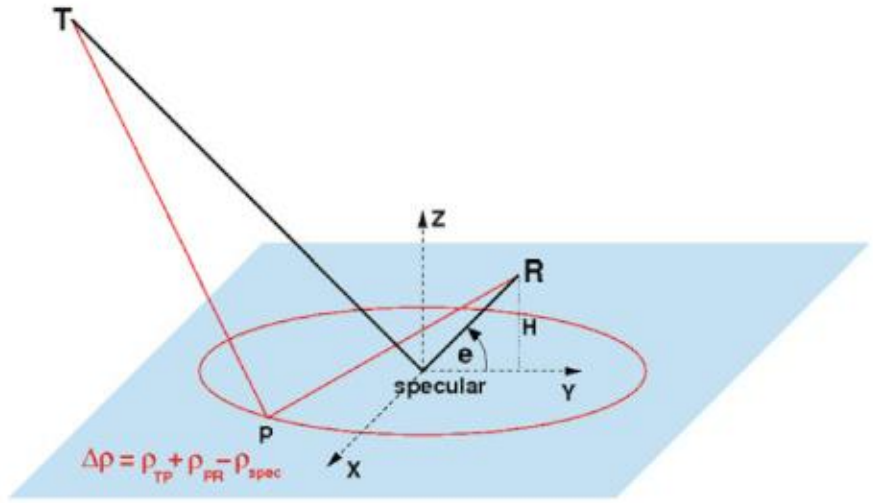

Figure 9: Iso-Delay ellipse in flat-surface approximation (Jin, 2014)

Being *e* the elevation angle complementary to the incidence one, and H the receiver's altitude.

Anyway, we have to consider that until now we are taking into account only the scattering coming from the surface's specular Fresnel zone. Indeed, there could appear any other contributions from areas away from the specular one as well.

Therefore, we should regard the incoherent scattering due to the diffuse reflections, what adds power to the trial of the waveform, distorting it and spreading its delay as we can see in the Figure 10 **(b)**.

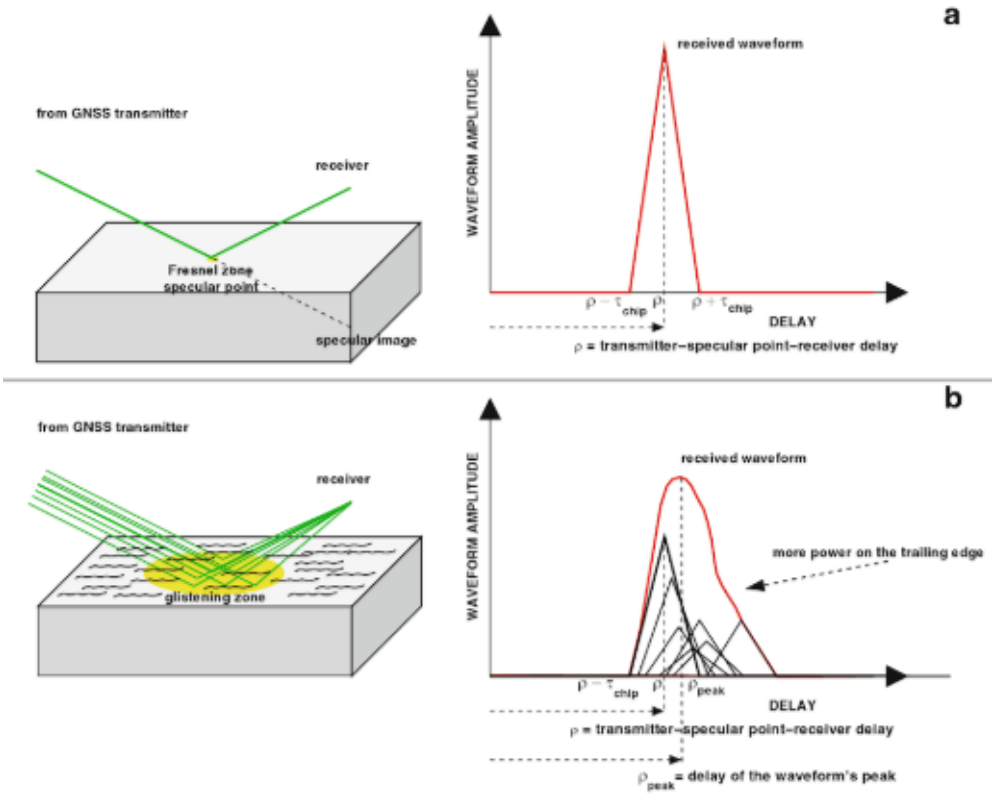

Figure 10: Waveform from specular (a) vs. diffuse (b) scattering (Jin, 2014)

Also, the signal contribution given by diffuse scattering has different Doppler frequency than the specular itself, whose effect over the Earth surface is characterized at each point of the reflecting zones with respect to the specular points on Doppler-Delay mappings as follows in the Figure 11.

In there, we can observe ellipses that actually are a plotting representation of the iso-range ellipses (lines of equal delay across the surface) and iso-Doppler hyperbolas (lines of equal Doppler frequency across the surface) across the Earth.

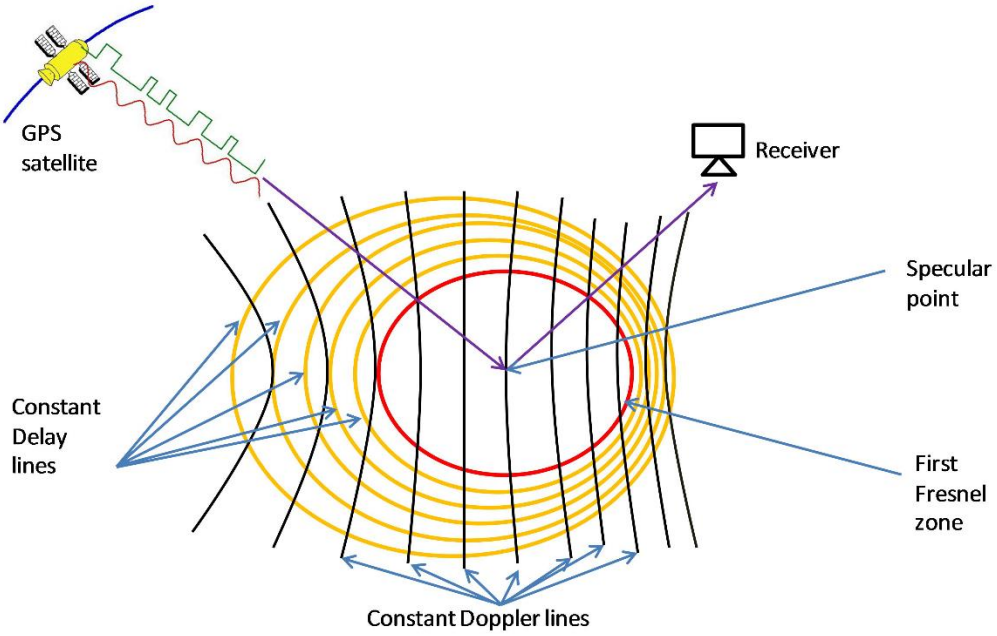

Figure 11: Delay and Doppler spreading across the surface (Pei, 2014)

This characterization will lead us to the well-known Delay-Doppler Map (DDM), which mapped those hyperbolas at any point on the surface with a width determined by the GNSS PRN code chip for the delay and by the coherent integration time for the Doppler.

And from them we can extract information about the SNR, who will greater when the surface of reflection was the smoother and the soil moisture the higher.

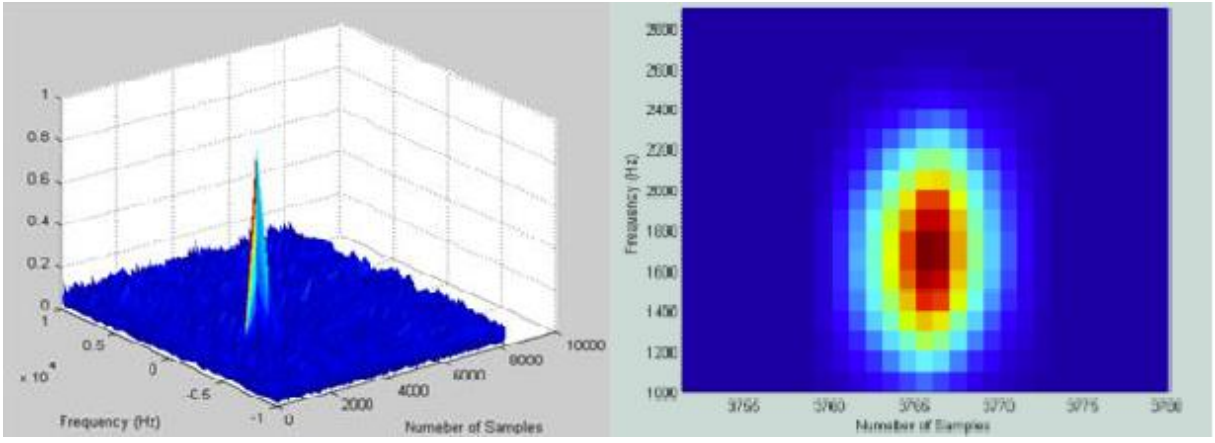

Figure 12: 3D Delay-Doppler Map (Jia, 2014)

3.3. Bistatic-Radar

As stated before, the bistatic-radar schemas present always more than one paths for the reflected signals, actually the same number of reflected radio-links as the amount of direct ones, which involves all the received GNSS signals at that moment.

But eventually the equations charactering this behaviour have turn out to be derived in the same way as the monostatic-radar's ones, getting to a general expression for the incoherent scattering as the following:

$$P^r = \frac{P^t G^r G^t \lambda^2 \sigma^0 A}{(4\pi)^3 R_1^2 R_2^2} \tag{4}$$

What also can be written in integral form:

$$P_{qp}^i = \frac{P^t G^t}{4\pi R_1^2} \frac{G^r \lambda^2}{4\pi} \iint_A \frac{\sigma^0}{4\pi R_2^2} dxdy \tag{5}$$

And whose symbols are explained in Table 3.

VARIABLE	MEANING
P^r	Received signal power
P^t	Transmitted signal power
G^t	Transmitter antenna gain
G^r	Received antenna gain
λ	signal wavelength
R_1	distance between specular point and transmitter
R_2	distances between specular point and receiver
σ^0	scattering coefficient per unit area
A	surface
I	incoherent power
Q	polarization received
P	polarization transmitted

Table 3: Bistatic Radar variables

Apart from this, as studied before, there exist two different types of scattering, the specular and the diffuse. Thus, the isolation of each of these cases when characterizing a model has being an issue which has leaded to the development of formulas that calculates separately the power reflectivity from specular and diffuse scatterings, depending on the reflecting surface.

In addition, a mathematical way to indicate if a surface is sufficiently "smooth" or not showed up in order to consider an only specular scattering situation; what was named after Rayleigh as it was his proposed criteria.

Anyway, as discussed in the previous section, in GNSS-R schemas reflected signals have always contribution from both coherent (specular reflection) and incoherent signal's power

(diffuse scattering). Thus, unfortunately, the Rayleigh criteria and the isolated-coherent scenarios appeared to be a qualitative approach to a more detailed need situation.

3.4. Scattering Components

The received power can then be expressed as a composite function with both coherent and incoherent contribution as follows:

$$P_{pq} = P_{pq}^{coh} + P_{pq}^{incoh} \quad (6)$$

Whose symbols are explained in Table 4.

Variable	Meaning
p	Incident wave polarization
q	Reflected wave polarization
$\boldsymbol{P_{pq}^{coh}}$	Coherent component
$\boldsymbol{P_{pq}^{incoh}}$	Incoherent component

Table 4: Signal Power Components

Therefore, it is important to analyse the theoretical and mathematical representations used to model these two power sources.

i. Coherent Component

In (De Roo & Ulaby, 1994) , the magnitude of the coherent component was defined for an incident signal with circular left-handed polarization, and a reflected one with circular right-handed polarization as:

$$P_{lr}^{coh} = \Gamma_{lr} \frac{P_t \lambda^2 G_t G_r}{(4\pi)^2 (R_1 + R_2)^2} \quad (7)$$

And

$$\Gamma_{lr} = |R_{lr}(\theta)|^2 \chi(z) \quad (8)$$

All the variables are listed in Table 5.

Variable	Meaning
Γ_{lr}	Reflectivity
P_t	Transmitted RHCP power
λ	Wavelength
G_t	Transmitter antenna gain
G_r	Receiver antenna gain
R_1	Distance between the satellite and the specular point
R_2	Distance between the specular point and the down-looking antenna
$R_{lr}(\theta)$	Fresnel reflection coefficient
$\chi(z)$	Probability density function of the surface heights z

Table 5:Coherent Scattering Variables

And, as far as the roughness of the terrain, can be modelled with a Gaussian distribution (Beckmann & Spizzichino, 1963).

$$\Gamma_{lr} = |R_{lr}(\theta)|^2 e^{-h\cos^2\theta} \quad (9)$$

Where *h* depends on the surface height standard deviation σ and the wave number *k*.

$$h = 4K^2\sigma^2 \tag{10}$$

As seen before, it is a fact that the rougher the scattering surface, the lowest the reflectivity, which is mainly depending on the absolute squared value of the Fresnel reflection coefficients.

So, for analysing these Fresnel reflection coefficients, as far as they are linearly polarized expressed, it is helpful to develop a manner to transform the circularly polarized components (GNSS transmit RHCP signals) into linearly polarized ones.

For this purpose, we use a transition matrix relating the reflection coefficients:

$$\begin{bmatrix} R_{ll} & R_{lr} \\ R_{rl} & R_{rr} \end{bmatrix} = \frac{1}{2}\begin{bmatrix} R_h + R_v & R_h - R_v \\ R_h - R_v & R_h + R_v \end{bmatrix} \tag{11}$$

Knowing γ is called the Grazing Angle, and it is the angle between the incident signal on the surface and the normal (line perpendicular to the surface at the point of incidence):

$$\gamma = 90 - \theta \tag{12}$$

And being ϵ_r the relative permittivity of the surface, which can be expressed on terms of the dielectric constant ϵ, the permittivity of vacuum ϵ_0, the wavelength λ and the electric conductivity σ

$$\epsilon_r = \frac{\epsilon}{\epsilon_0} - j60\lambda\sigma \tag{13}$$

We can get to an expression of each Fresnel reflection coefficients.

$$R_{lr}(\theta) = R_{rl}(\theta) = \frac{R_{vv}(\theta) - R_{hh}(\theta)}{2} \tag{14}$$

$$R_{rr}(\theta) = R_{ll}(\theta) = \frac{R_{vv}(\theta) + R_{hh}(\theta)}{2} \tag{15}$$

$$R_{vv}(\gamma) = \frac{\epsilon_r \sin(\gamma) - \sqrt{\epsilon_r - \cos^2(\gamma)}}{\epsilon_r \sin(\gamma) + \sqrt{\epsilon_r - \cos^2(\gamma)}} \quad (16)$$

$$R_{hh}(\gamma) = \frac{\sin(\gamma) - \sqrt{\epsilon_r - \cos^2(\gamma)}}{\sin(\gamma) + \sqrt{\epsilon_r - \cos^2(\gamma)}} \quad (17)$$

ii. Incoherent Component

In our case, we should define the incoherent component of the receiving power in terms of the bi-static radar equation, as follows:

$$P_{lr}^{coh} = \frac{P_r^t \lambda^2 G^t G^r}{(4\pi)^2 R_1^2} \iint_A \frac{\sigma^0}{4\pi R_2^2} dxdy \quad (18)$$

$$\sigma_{q,p}^0 = \frac{4\pi R^2 |E_p^2|^2}{A|E_q^i|} \quad (19)$$

where σ^0 is defined per unit area and represents the ability of the scattering surface of reflecting the incident signal.

Variable	Meaning
$\boldsymbol{P_r^t}$	Transmitted power right-hand polarized
$\boldsymbol{\sigma^0}$	Bistatic scattering coefficient or normalized radar cross section
$\boldsymbol{\lambda}$	Wavelength
$\boldsymbol{G^t}$	Transmitter antenna gain
$\boldsymbol{G^r}$	Receiver antenna gain
$\boldsymbol{E_p, E_q}$	Incident field, scattered field
$\boldsymbol{R_1, R_2}$	Distances to the specular point (Table 5)
$\boldsymbol{A}$	Illuminated surface of area
$\boldsymbol{R}$	Distance of the point of observation to the centre of A

Table 6: Incoherent Scattering Variables

In order to solve this, many assumptions and approximations have to be taken. Nevertheless, by doing so, several methods and mathematical models have been developed during the last years, giving an answer to the incoherent component characterization (3.5).

3.5. Surface Scattering

The study of the scattering phenomena starts from the point of the surface's characterization, observing their features for the sake of coming up with specialized methods to analyse them.

As studied in the previous chapters, many models have developed ways to do so but, particularly, some of them have actually proposed a widely approved way to identify a rough surface following a statistical description of it.

The shape of a random rough surface has shown to be describable by the surface height distribution function and the surface height correlation function as Nicolas Pinel and Christophe Bourlier proposed in 2013 (Pinel & Bourlier, 2013), or as previously studied in 1982 (Ulaby, Moore, & Fung, 1982).

As follows, the type of surface height was determined by a probability density function even Gaussian, Lorentzian or exponential, etc.

Thus, a rough surface was meant to be characterized by a Gaussian height PDF defining its surface's height probability density function with that distribution.

There is also another way to describe random rough surfaces, and it is the normalized height correlation function, which analyses the degree of the correlation between the heights of two locations with respect to their horizontal distance.

Once we are able to determine the nature of the reflection surface, we would be able to orientate the study of the scattering on it in one way or in another.

Indeed, these studies of modelling scattering of electromagnetic field due to surface rough have been taken for decades (Beckmann & Spizzichino, 1963), (Ulaby, Moore, & Fung, 1982).

Along these years, the in incoherent component has been modelled in several ways depending on different ranges of roughness: The Kirchhoff Approximation (KA), the Geometric Optics (GO) or Physical Optics (PO) solutions, the Small- Slope Approximation (SSA), the Small Perturbation Method (SPM), the Two-Scale Model, and the Integral Equation Model

i. The Kirchhoff Approximation (KA)

This approach suggests a solution in which the total fields (incident and scattered) at any point on the surface are approximated by the fields that would be present on an infinitely extended tangent plane at that point.

Therefore, the reflection is considered to be locally specular, depending only on the Fresnel coefficients within this local tangent plane and not on the surface elsewhere, what makes it a local approximation.

Thus, for this approach to be valid, every point on the scattering surface should represent a large radius of curvature compared to λ.

$$\boldsymbol{E}^{S}(\boldsymbol{r}) = K \int_{S}\{\widehat{\boldsymbol{q}[\boldsymbol{k_s}}} \times \left(\hat{\boldsymbol{n}} \times \boldsymbol{E}(\boldsymbol{r}')\right) + \eta\left(\hat{\boldsymbol{n}} \times \boldsymbol{H}(\boldsymbol{r}')\right))]\}e^{i(\boldsymbol{k_s}-\boldsymbol{k_i})\boldsymbol{r}'} d^2\boldsymbol{r}' \qquad (20)$$

As no analytic solution has been obtained for its expression, simplifying assumptions has shown up to solve it.

Further information and mathematical exhausted explanation can be found in (Ulaby, Moore, & Fung, 1982) (Jin, 2014) (Tsang, Kong, & Ding, Scattering of Electromagnetic Waves: Theories and Applications, 2000) (Tsang & Kong, Scattering of Electromagnetic Waves: Advanced Topics, 2002).

KA in Stationary-Phase Approximation (Geometric Optics, KGO)

It is applicable under the assumption that the phase factor of the KA equation is stationary, what implies that its derivate along the integration area is null.

This approach can be assumed, therefore, in cases when the surface's areas where this phase is constant, as well as in those where its local orientation is such that its local normal points towards the receiver (Ticconi, Pulvirenti, & Pierdicca, 2011) (Ulaby, Moore, & Fung, 1982).

Only applicable when the angle given by the incident (from transmitter) signals, corresponds to the one from the reflected signals (towards receiver) (Jin, 2014).

KA in Physical Optics Approximation (KPO)

Unlike the KGO approximation, this approach not only considers the contribution of the scattered fields over the well oriented surfaces, but also it considers the totality of contributions of the scattering fields over the whole rough surface.

ii. The small perturbation method (SMP)

It is based on formulating the scattering expanding the field in perturbation series of slopes of the surface as partial differential equation boundaries.

Then it is possible to find a solution in terms of plane waves that matches these surface boundaries' conditions.

Thus, this model is really appropriated for small slopes statistics scenarios, for Bragg scattering issues and for the assessing of polarimetric performances.

iii. The Integral Equation Method (IEM)

This method evaluates the integral equations of the electromagnetic field solving them iteratively from the charges and electric currents on the sea surface, using the induced one in the first iteration (KA) and the second one in the small slope statistics using the SMP.

Bridging the gap between KA and SPM and covering all roughness scales, the relative complexity of this method might seems firstly an objection, but indeed due to its accuracy it has been used extensively in the microwave region in recent years (Ticconi, Pulvirenti, & Pierdicca, 2011) (Jin, 2014).

iv. The Small Slope Approximation (SSA)

As the IEM, this method also gives a solution to unify the KA and the SPM, being applicable regardless from the signal's wavelength.

Provided that the slopes of the roughness are small compared to the angles of the incidence and scattering (Jin, 2014).

Anyway, it is restricted to single-scattering phenomena, being the non-local small-slope approximation a modification of the SSA when the multiple scattering from significantly distanced points cannot be overseen (Berginc & Bourrely, 2007).

v. The Two-Scale Composite Models

This method assumes a bilateral contribution to the scattered field, on the one hand the small-scale surfaces' roughness is modelled by the SPM and meanwhile, on the other hand, the large scale one is modelled by the KGO approach.

This approach is useful in some studies at describing real surface scattering, but it is disputable in the boundary selection between the slight rough surfaces and very rough surfaces (Jin, 2014).

3.6. Noise Contribution

Considered commonly an error, the Thermal Noise is an important factor to consider when conducting satellite measurements, as they are intercepted together with the expected GNSS signal.

Indeed, it is strongly dependent on the physical temperature from both the receiver's system and the environmental effects, making it important to differ its power from the signal's one when carrying GNSS measurements.

So, we can identify T_A as the Antenna Equivalent Temperature and T_e as the Equivalent Noise Temperature, composing together the Operative Temperature T_{op}

$$T_{op} = T_A + T_e \tag{21}$$

Which lead us to an expression of the Noise Power P_n depending on the total brightness temperature observed by the antenna

$$P_n = kT_{op}B \tag{22}$$

Where k is the Boltzman constant (k=1.380×10-23 J/K) and B is the noise bandwidth of the measurement system computed

$$B = \frac{1}{T_i} \tag{23}$$

And being T_i the integration time of 1 ms.

As well as the environment has a noisy contribution to the receiving process with the brightness temperature, it is also important to characterize the noise power introduced by the receiver as an intrinsic source.

Telecommunication receivers, are typically constructed as cascades of devices, what means that they are composed by a succession of stages to complete the receiving process, each one conducted by a different device.

Therefore, we can observe an own Gain G_i and contributing Noise Factor F_i for each of them, and even for the connecting cables. Leading us to take into account the inner noise contribution of the receiving system.

$$F_{tot} = F_1 + \frac{F_2}{G_1} + \frac{F_3 - 1}{G_1 G_2} + \cdots \tag{24}$$

Being each F_i the Noise Factor F of each device, also expressible in terms of T_e and the Standard Temperature T_0 (290º K).

$$F = \frac{T_e}{T_0} \tag{25}$$

i. Noise in the up-looking antenna

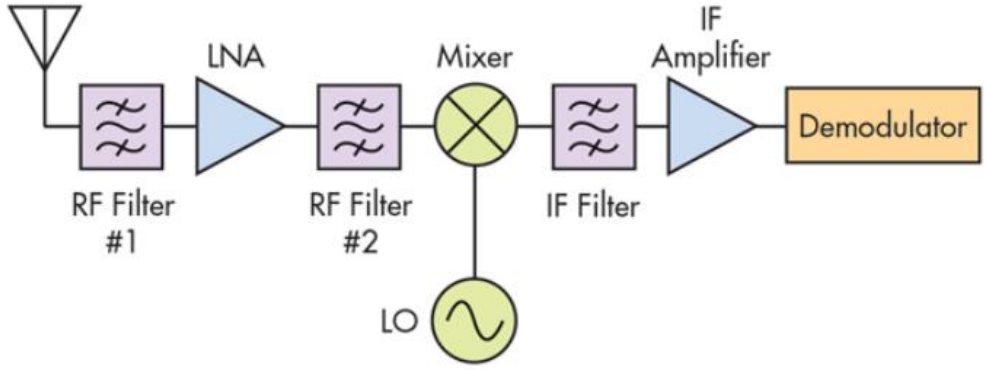

Figure 13: Receiver (http://www.mwrf.com)

Commonly, receivers are composed of many systems in cascade, as fitters, low noise amplifiers (LNA), demodulators, transmission lines, etc (Figure 13). But, in order to simplify it and make it possible to give an orientating noise contribution, we can present an example of a very basic receiver system only composed by two cables and a LNA (Figure 14).

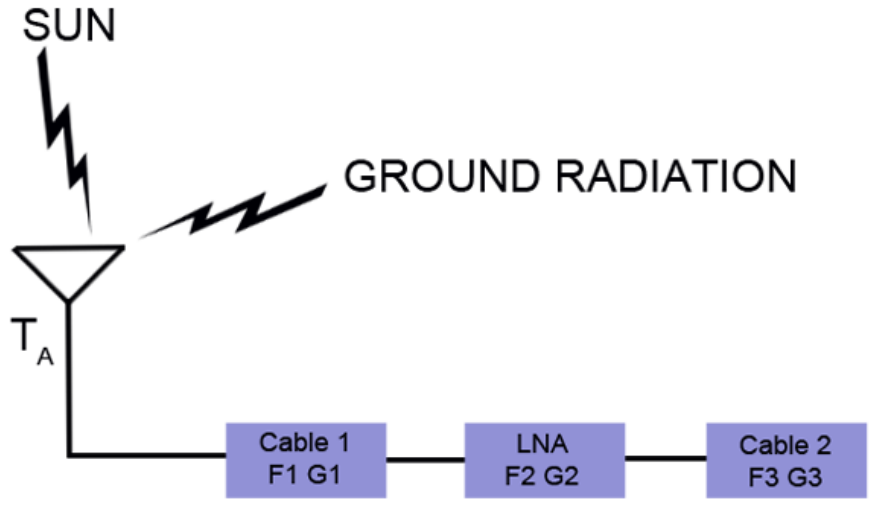

Figure 14:Basic receiver chain model (Campanella, 2014)

The antenna receives radiations coming from ground and Sun sources and it is characterized by a T_A = 100 K. Typical values of these parameters for commercial receivers can be found in the table below (Table 7):

	Cable 1	*LNA*	*Cable 2*
Gain – Loss [dB]	G_1 = -1	G_2 = 20	G_3 = -10
Noise Factor [dB]	F_1 = 1	F_2 = 3	F_3 = 10
Physical Temperature [K]	290	290	290

Table 7: Basic receiver typical parameters

So, computing the Noise Power from this, we obtain the results of Table 8

Noise Factor [dB]	***Top [K]***	***Bandwidth [Hz]***	***Pn [dB]***
2.5	*290*	*1000*	*-175*

Table 8: Receiver Noise Power

Thus, we can consider it a reference in order to know what to expect from the data processing process.

ii. Noise in the down-looking antenna

Being oriented towards the ground, the down-looking antenna is not affected in a considerable manner by the antenna brightness temperature, but the most important noisy contribution comes from the receiver's inner noise.

Anyway, fortunately it can be accounted and even corrected by the calibration process, which consists in referencing the current measurements to a previous well-known one's value.

For example, in (Campanella, 2014) they compared their measurements to well-known values from the water surface, from which they had known values of dielectric constant (ϵ = 80) and set the noise power accordingly. What leaded them to obtain a noise power for the RHCP antenna equal to -135.2 dB.

4. Measurements with GNSS-R

When analysing the SNR for the down-looking antenna in the chapter 4.2.ii we had to consider the non-coherent contribution of the received signals, meanwhile now we are able to overlook it as far as, when measuring the GNSS reflected signals, the reflecting surface was considered flat. Indeed, this simplifies enormously the signals processing.

Thus, we get to a basic definition of the SNR as:

$$SNR_{measured} = \frac{P_r}{P_n} \tag{26}$$

From which we can inference the Surface Reflectivity as we already know P_n in previous chapters and the SNR measured by the antenna

$$\Gamma_{lr} = \frac{SNR\ P_r\ G_{pr}\ (4\pi)^2\ (R_1+R_2)^2}{P_t\ \lambda^2\ G_t\ G_r} \tag{27}$$

Whose variables are defined in Table 5.

The Processing Gain G_{pr}, also known as correlation Gain, is adopted to increase the signal power with respect to the noise power as the signal GPS C/A code is de-spread during processing.

Thus, assuming the reflected signal is coherent over the coherent correlation interval of 1 ms (T_I), its value would depend on the chipping rate of the GPS L1 C/A code (1.023x10^6 Hz), and the T_I

$$G_{pr} = 10\log_{10}\left(1.023 \cdot \frac{10^6}{1000}\right) = 30.1\ dB \tag{28}$$

Therefore, if neglecting surface roughness (h=0), the Surface Reflectivity can be related to a coherent Fresnel Reflection Coefficient (Chapter 3.4.i) as:

$$\Gamma_{lr} = |R_{lr}(\theta)|^2 e^{-hcos^2\theta} = (R_{lr}(\theta))^2 \tag{29}$$

The GPS signal (RHLP transmitted) after being reflected from the earth is LHCP polarized, what makes it present a vertical and a horizontal component.

But, furthermore, it is possible to reduce its expression as done before due to the little difference between the vertical and horizontal component for high incident angles, neglecting the horizontal component. Obtaining:

$$R_{lr}(\theta) = \frac{R_{vv}}{2} \tag{30}$$

And introducing this one into the equation system from Chapter 3.4.i

$$R_{vv}(\gamma) = \frac{\epsilon_r \sin(\gamma) - \sqrt{\epsilon_r - \cos^2(\gamma)}}{\epsilon_r \sin(\gamma) + \sqrt{\epsilon_r - \cos^2(\gamma)}} \tag{31}$$

We obtain an expression for the Dielectric Constant of the Soil as the following

$$\epsilon_{soil}^2 \sin^2\gamma \left(\frac{1-R_{vv}}{1+R_{vv}}\right)^2 - \epsilon_{soil} + \cos^2\gamma = 0 \tag{32}$$

From which we can obtain a resulting value for ϵ.

4.1. Delay Doppler Maps and Delay Waveforms

When conducting GNSS-R measurements, it is common to use a representing tool to characterize the received signals, and the most appropriated ones are the Delay Doppler Map (DDM) (Figure 12)(Figure 15) and the Delay Waveform (DW) (Figure 16).

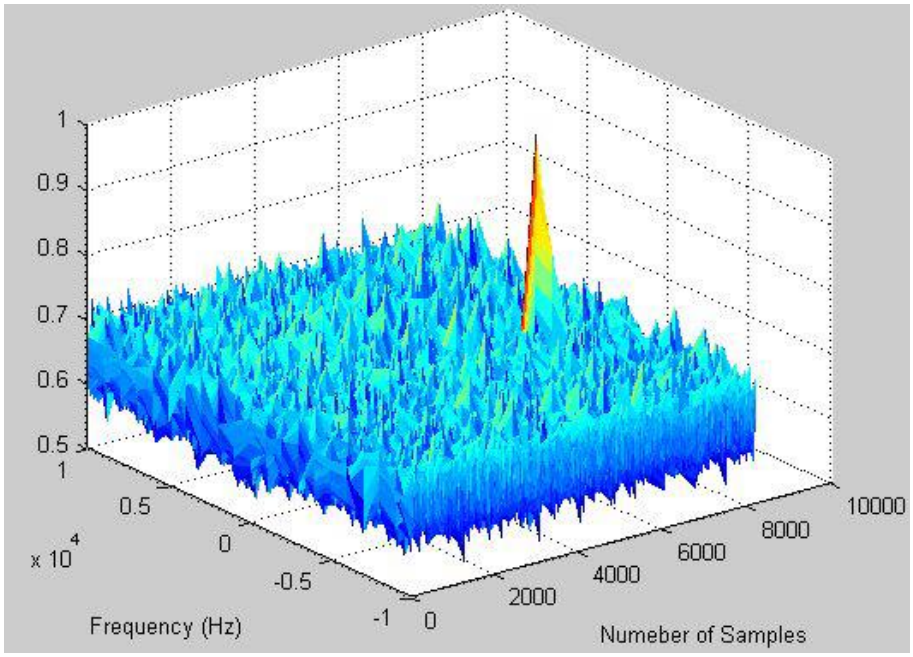

Figure 15: Delay Doppler Map (Pei, 2014)

In the Figure 15 we can observe a peak, it corresponds to the correlation power and as we can see it normalized to 1; as far as it corresponds the signal power.

Around the peak there appears a blue background that is the noise power distributed in other delays and frequencies.

On the other hand, the Delay Waveform (DW) is a valuable measure tool because it is very useful for helping us when characterizing the signal power along the number of samples, what makes it possible to observe if there have been different delays over the glistening zone.

This is recognizable because of the delay spread over the Number of Samples edge, instead of presenting the signal with a sharp triangle shape (Figure 16).

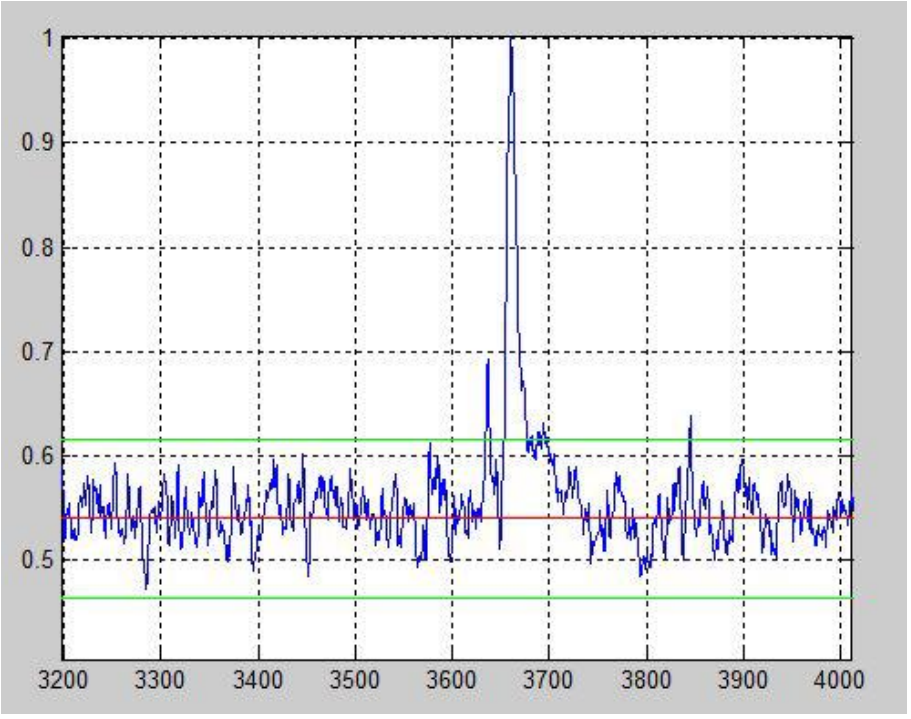

Figure 16: Delay Waveform (Pei, 2014)

Red Line	Averaged Noise Floor
Green Lines	Noise's Standard Deviation
Blue Line	DW

Table 9: DW

The Average Noise Floor is computed using the samples around the peak but with a margin of 8 before and 24 samples after it.

Meanwhile, the Standard Deviation covers an interval up and down of the mean, where the Noise Floor still present remarkable values.

These calculations are mean to evaluate the SNR taking into account this Noise Floor level (Chapter 4.3).

4.2. SNR and received signal power

When presenting the total noise power peak normalized to 1 and with the respect to the Average Noise Floor, it is possible to simplify the processed absolute SNR (Absolute Signal to Noise Ratio Φ_{peak}) in terms of this average $\overline{P_N}$:

$$\Phi_{peak} = \frac{1-\overline{P_N}}{\overline{P_N}} \tag{33}$$

So, the SNR of the received signal Φ for a given delay τ and a given Doppler frequency f can be expressed as:

$$\Phi(\hat{\tau}, \hat{f}) = \frac{G_D P_S \Lambda^2(\hat{\tau}-\tau) S^2(\hat{f}-f)}{P_N} \tag{34}$$

In Table 10 the meaning of these symbols is exposed.

VARIABLE	MEANING
$\boldsymbol{P_S}$	Signal power before spreading
$\boldsymbol{P_N}$	Noise power before spreading
$\boldsymbol{G_D}$	Processing gain*
$\boldsymbol{\Lambda, S}$	Attenuation ambiguity functions**
$\boldsymbol{\tau}$	Given delay
$\boldsymbol{f}$	Given doppler frequency

Table 10: Doppler SNR Variables

*The processing gain is ~30.1dB as far as it is due to the de-spread of the GPS C/A code.

**The Λ and S attenuation ambiguity functions describes the due to correlation misalignments along the frequency (delays).

Being the noise power before the spreading the same as the one shown in the chapter 3.6, but from which we can obtain an approximate value as follows:

$$P_N = P_n = kT_{op}B = k\big((F-1)290\big)B = k\big((F-1)290\big)\frac{1}{T_I} \cong -176.3 \text{ dBW} \quad (35)$$

Knowing that in Table 11 the meaning of these symbols is exposed.

$\boldsymbol{k}$	$\boldsymbol{1.380 \times 10^{-23}}$
$\boldsymbol{F}$	Between 1.0 – 2.5 dB
$\boldsymbol{T_I}$	1 ms

Table 11: SNR Variables' Values

Furthermore, when studying the case of Φ_{peak} we can infer a value approximately equal to 1 for the ambiguity functions, what leads us to a simpler expression for the signal power before spreading in which all the variables are known after the measurements, what makes it possible to obtain a value for P_S

$$P_S = \frac{\Phi_{peak}\, P_N}{G_D} \quad (36)$$

4.3. Satellite prediction and georeferencing

When working with a GNSS-R system, it is crucial to know the position of the transmitting GNSS satellite in the sky together with its relative position to our receiver.

That is why it is important to come up with a referencing frame which has to be able to correctly represent both the positions of the transmitter and the receiver, being that essential for determining the location of the specular point.

The Earth-centered Earth-fixed (ECEF) frame does so modelling the earth surface in a way that represents the user's position with respect to the center of the Earth (center of mass).

It is a geographic coordinate system and Cartesian coordinate system who uses X, Y, and Z coordinates as tools to graphic positions (Figure 17).

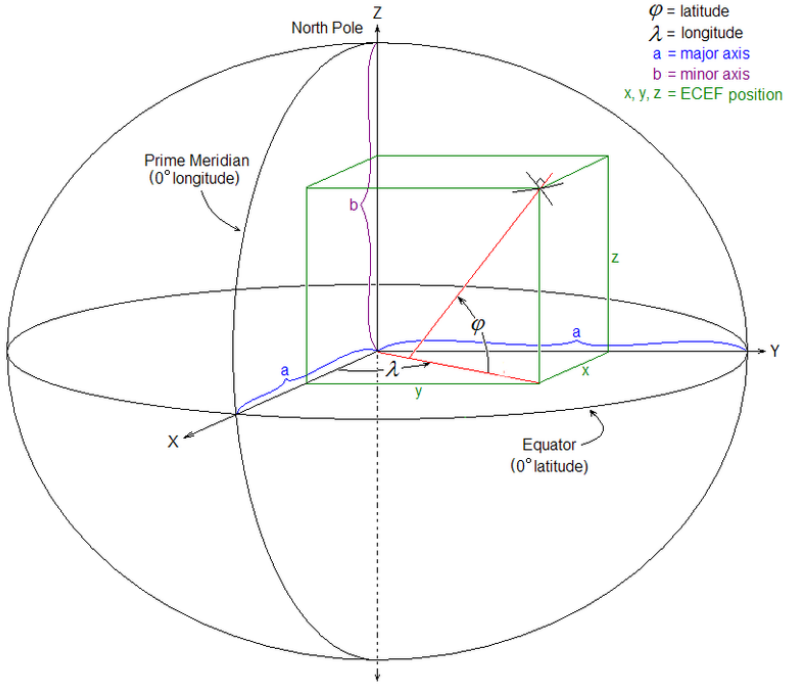

Figure 17: ECEF (https://en.wikipedia.org/wiki/ECEF, n.d.)

But, commonly, what we prefer to know is our position relatively to the Earth surface, instead of to its center. So that is why the World Geodetic System 1984 (WGS84) became popular as well.

This is a coordinates system in which the origin is meant to be located at the Earth's center of mass, being a reference surface for raw altitude data, and a gravitational equipotential surface (the geoid) that defines the nominal sea level.

Thus, all points on the geoid have the same gravitational potential and the force of gravity acts everywhere perpendicular to the geoid.

$$H \approx h - N \tag{37}$$

where all the parameters are listed in Table 12.

H	Orthometric height (elevation)
K	Terrain height with respect to the ellipsoid
N	Geoid height with respect to the ellipsoid

Table 12: Geoid variables

The orthometric height is the height of a body above the geoid or the height above the mean sea level.

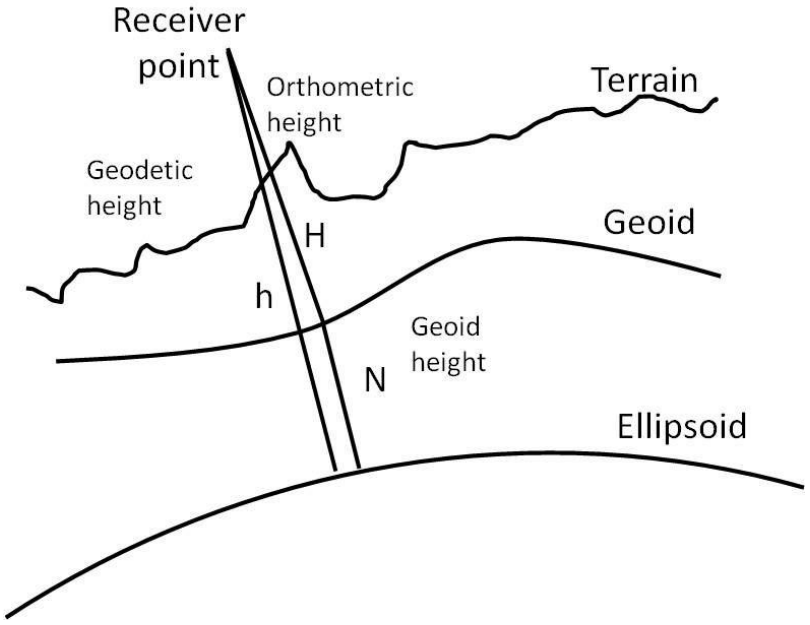

Figure 18: Geoid (Pei, 2014)

It is important to know in advance whether the height provided by the GNSS receiver or a certain map is geodetic height or orthometric height, as far as meanwhile orthometric height is commonly more useful, many maps tend to express the height of the terrain and features with respect to the geoid, as Google Maps does (Stillman, 2009).

The measurement campaigns presented in this thesis where done using the ECEF coordinate frame, assuming the surface was locally flat and with an equipotential height between the receiver and the specular point.

For these measurements, receiving locations were planned with Google Earth. Thus, elevation was actually the orthometric height along with longitude and latitude, so it had to be converted to geodetic height first, as its latitude, longitude and altitude with respect to WGS84 were further converted to ECEF frame for georeferencing specular points.

Further information about the measurement campaigns are explained later on each their particular sections.

5. Linear Polarization in GNSS-R System

During the last decades, most of the studies about GNSS-Reflectometry have focused almost only on a transmitter-receiver schema where both were using circular polarized antennas.

Thus, its use was spread across the different applications of GNSS-R being a researching topic when analysing the signal's propagation and reflecting performance.

Geometry and scattering models of these circularly polarized signals were thoroughly studied, as we have seen in Chapter 3, leading to solutions who takes this schema as an immovable start point when measuring soil parameters, snow depth, vegetation, etc.

Nevertheless, it should not be unseen the potential benefits that linear antennas would imply, not only simplifying the co/cross-polar dilemma of the circular polarization, but also making a much more straightforward scattering method.

Anyway, it is important to know the role of the circularly polarized systems in GNSS-R applications in order to understand the background of these technology, and the pros and cons of both configurations.

Receivers with circular polarized antennas actually present some benefits compared with the ones which use linear polarized antennas.

Firstly because of the polarization fading caused by earth to linear polarized antennas and the Faraday Rotation effect, which undergo a change in the polarization of electromagnetic waves traveling through ionized gases or through the earth magnetic field.

And even because maintaining a polarization coherence between transmitter and receiver helps the propagation process in terms of lower power losses.

In fact, building circularly polarized antennas into a satellite helps to minimize the effects of antenna cross-polarization losses on the ground as the satellite moves through space, what is the reason why in a GNSS-R schema the transmitters will always present a circularly polarized radiation.

Nevertheless, if we gave a look at linear polarized systems, we could realize that some of these disadvantages are not so difficult to overcome, and even some of them are not even issues if managed correctly as we will see later in this chapter.

As previously seen, the evolution of the GNSS systems through the years came hand in hand with the development of studies and researches about the usefulness of linear polarization.

Starting from using a simple signal at two orthogonal linear polarizations in order to mitigate the adverse effect of the surface roughness (Valery U. Zavorotny, December 2014), and going through theoretical descriptions of the ratio of two orthogonal polarizations received power and its relation with moisture (Zavorotny & Voronovich, 2000) (Egido, et al., 2012); the popularity of these systems increased during the last years, what encouraged tis study for many GNSS-R applications.

Indeed, this technology has found its use in many different scopes.

For example measuring biomass using bistatic-radars (Cardellach, Fabra, Nogués-Correig, Oliveras, & Rius, 2011), deeply analysing the soil moisture using IPT (Multipath and Interference Pattern Technique) (Rodriguez-Alvarez, et al., 2011), or observing terrain conditions using airborne-based and stratospheric GNSS-R linearly polarized systems (Egido, et al., 2014) (Carreno-Luengo, et al., 2015).

Above them all, the main use we will focus on this thesis is the snow depth determination, which is one of the subjects of our study (a more extended exhaustive analysis can be seen in Chapter 7) as far as it is a topic with such a potential and whose measurement can be easily conducted nearby around our area.

As we will see, linearly polarized receptors have shown to be really effective inferring snow depth and equivalent water content in many environments by analysing multipath patterns (Chapter 7).

The main problematic task that could come up when designing this kind of systems might be the unwieldy fading and polarization undesirable changes that occur during the signal's propagation.

Having this in mind, and assuming that GNSS satellites have circular polarized antennas, we can actually disregard them due to the fact that, when receiving with linear polarized systems, we are not taking part in the propagation process, that is, the resulting adverse effects on it will affect the circular polarized signal transmitted by the satellite regardless of our receiving system.

Furthermore, we can even get round the polarization loss due to the different antenna combination by designing our receiver in such a way that it could overcome the 3 dB losses resulting of this issue.

Besides, this technology is offering an advantage that should not be disregarded: mathematical estimations of the soil's dielectric constant given the measured data from linearly polarized antennas have been developed. So, further than measuring snow depth by the scattering multipath patterns, deeper studies on dielectric constant sensing would lead as well to a fully operational soil parameters determination technique.

Reached this point, the available installation of antennas with a linear polarization is no more to be discussed, but it is important to notice some aspects about it.

First of all, we already know the fact that working on this way implies an inevitable power loss (3dB) so, by assuming it as a designing issue, the election of the receiving antenna should take it into account; ensuring the most efficient device in terms of gain.

Besides, concerning the antenna's election, it is also remarkable the matter of following the transmitting satellite's position along its travel on the sky; maintaining the received signal within our receiver's radiation pattern most of the time.

Therefore, with a view of maintaining this situation the longer we can together with keeping in mind its entailing complexity, the simplest antenna's election turns out to be a linearly polarized patch antenna.

Unfortunately, the lack of resources and time have hampered us when trying to conduct soil moisture and snow depth measurements using this system, but an extended study about researches conducted on this way will be presented in Chapter 7.

Anyway, putting all this information together, we could easily assume that the risks of working with linearly polarized receivers is sufficiently low to guarantee good results if we managed it properly.

Summarizing, the benefits when measuring so many different surface's parameters using this technique shows us an alternative GNSS-R system whose potential is still to be exploited. Therefore, even when no further measurements have been done, this study is hoped to be a reference leading future researches to more rigorous conclusions.

6. Dielectric Constant Determination

6.1. Soil Dielectric Constant

In 1985, the Hallikainen's research group proposed a semi-empirical model to characterize the relationship between the signals reflectivity with the soil dielectric constant in terms of the volumetric water content of its surface knowing its relative percentages of silt, sand and clay (Ulaby, Hallikainen, & Dobson, 1985).

Indeed, it resulted giving the possibility of linking reflecting signals peak power to soil moisture as far as it was observed that, increasing the concentration of water in soil yield higher dielectric constant values, increments on the reflectivity occurred.

The wetness of the soil can be described in two different ways, considering the volume basis:

$$m_v = \frac{V_w}{V_t} = \frac{V_w}{V_{dry}} = \frac{W_w \rho_b}{W_{dry}} cm^3 cm^{-3} \tag{38}$$

Or considering the percentage by dry weight:

$$m_g = \frac{W_w}{W_{dry}} \times 100\% = 100 \frac{m_v}{\rho_b} (\%) \tag{39}$$

where W_w is the weight of the water in the sample; W_{dry} is the weight of the solid part of the sample; V_w is the volume of the water; V_{dry} is the volume of the solid part of the sample; V_t is the total volume of the sample, assuming it's equal to the volume of the solid part as the water takes place of the air and doesn't increase the total volume; ρ_b is the density of the sample mixture. The parameters are shown in Table 13.

VARIABLE	MEANING
$\boldsymbol{W_w}$	Sample's water weight
$\boldsymbol{W_{dry}}$	Sample's solid weight
$\boldsymbol{V_w}$	Volume of water
$\boldsymbol{V_{dry}}$	Volume of solid
$\boldsymbol{V_t}$	Total volume of the sample*
$\boldsymbol{\rho_b}$	Density of the sample mixture

Table 13: Wetness Soil Variables

*Assuming it's equal to the volume of the solid part as the water takes place of the air and doesn't increase the total volume.

But, since the dielectric constant of moist soils is proportional to the number of water dipoles per unit volume, the preferred measure for soil moisture is the volumetric.

The dielectric constant ϵ is considered as a function in terms of volumetric water content *mv*, the sand *S* and the clay textural *C*.

$$\epsilon = (a_0 + a_1 S + a_2 C) + (b_0 + b_1 S + b_2 C) m_v + (c_0 + c_1 S + c_2 C) m_v^2 \qquad (40)$$

For the study of remote sensing in the L-band we consider the coefficients in the row of frequency 1.4 GHz, giving the following polynomials for the dielectric constant:

$$\epsilon' = (2.862 - 0.012S + 0.001C) + (3.803 + 0.462S - 0.341C) m_v + (119.006 - 0.5S + 0.633C) m_v^2 \qquad (41)$$

$$\epsilon'' = (0.356 - 0.003S - 0.008C) + (5.507 + 0.044S - 0.002C) m_v + (17.753 - 0.313S + 0.206C) m_v^2 \qquad (42)$$

Being ϵ' and ϵ'' the real and imaginary parts respectively.

This is a semi-empirical model and requires the knowledge of the percentage of sand and clay to be applied. In the table below, summary values used in (Dobson, Ulaby, & Hallikainen, 1985) to validate the model are shown:

Field	Soil Type	Sand	Silt	Clay
1	Sandy	51.51	35.06	13.43
2	Loam	41.96	49.51	8.53
3	Silt Loam	30.63	55089	13.48
4	Silt	17.16	63.84	19
5	Silty Clay	5.02	47.60	47.38

Table 14: Textural component

For low values of m_v (for dry soils), the values of real part and imaginary part of ϵ are low. Increasing the water content in the soil, ϵ' increases significantly meanwhile, in contrast, ϵ'' does not change too much, remaining at low values when compared to the real part. It can be seen in the Figure 19.

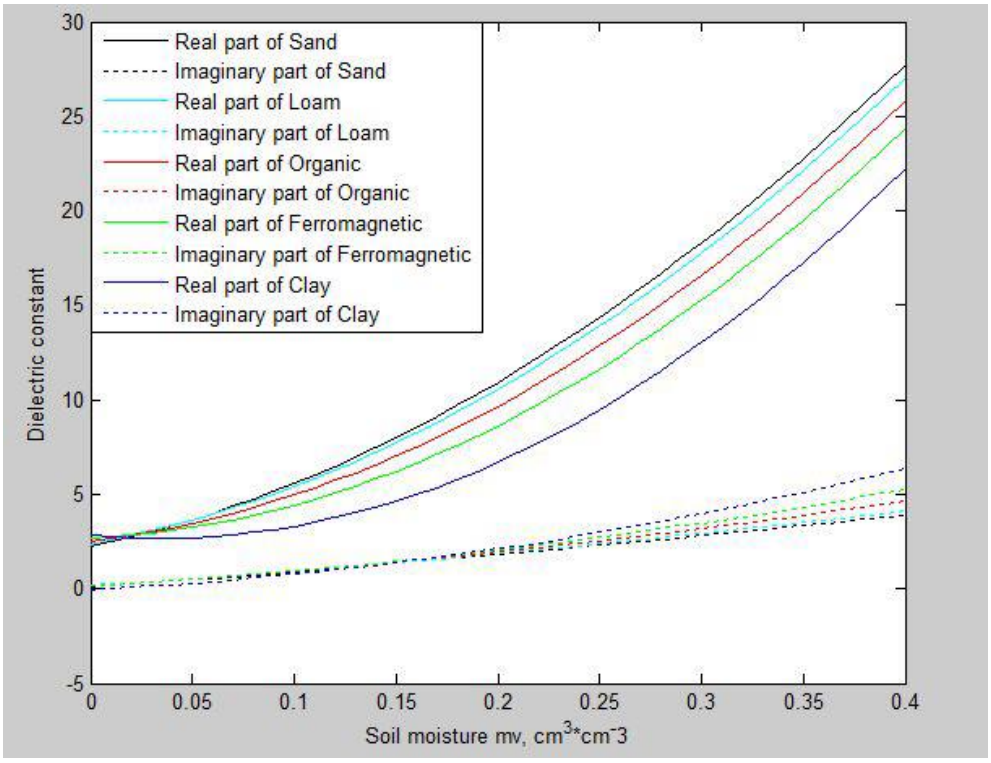

Figure 19: Dielectric constants versus volumetric water content at 1.4GHz (Pei, 2014)

This leads us to ignore the imaginary part of epsilon and consider only the real part, re-writing its equation as:

$$\epsilon_{soil} = \epsilon_r = \frac{\epsilon}{\epsilon_0} \tag{43}$$

6.2. Dielectric Constant determination

Many researches have studied the soil's dielectric constant using GNSS-R systems. In this section some of them are shown, particularly, the most relevant ones conducted by researchers from this university (Politecnico di Torino); together with an analysis about GNSS-R measured data and its interpretation.

i. LHCP measuring Dielectric Constant

The aim of this retrieval process was basically to corroborate the link between received LHCP reflected signals and the soil's dielectric constant, looking forward to retrieving the soil's moisture as well (Pei, 2014).

As seen before, for specular reflection case, the scattering reflected GPS signals are predominately LHCP, so this study focused on this circularly polarized signals' reception.

It has to be noticed that the surface dielectric constant was estimated assuming to neglect soil, what implied precision errors according to the not-perfectly-smoothness of the studied surface.For the realization of these measurements, a GNSS-R setup was used, whose specifications are detailed in chapter 8.1.

Three consecutive 40s data acquisitions were performed, each one corresponding to a different situation of the soil's wetness: dry, moist and soaking wet.

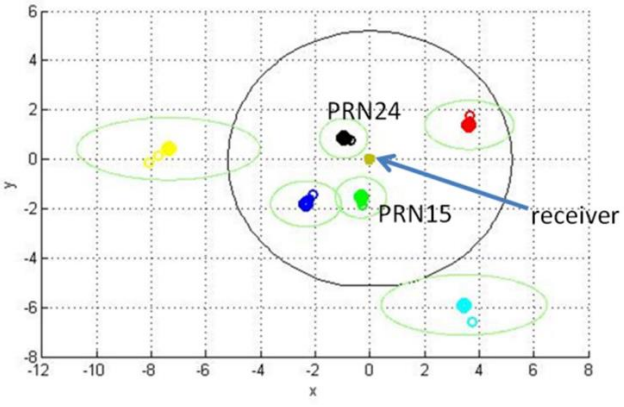

Figure 20: Specular points for dry soil (Pei, 2014)

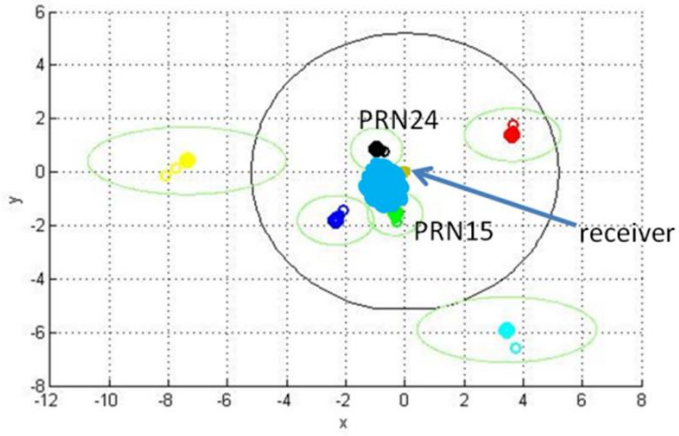

Figure 21: Specular points for wet soil (Pei, 2014)

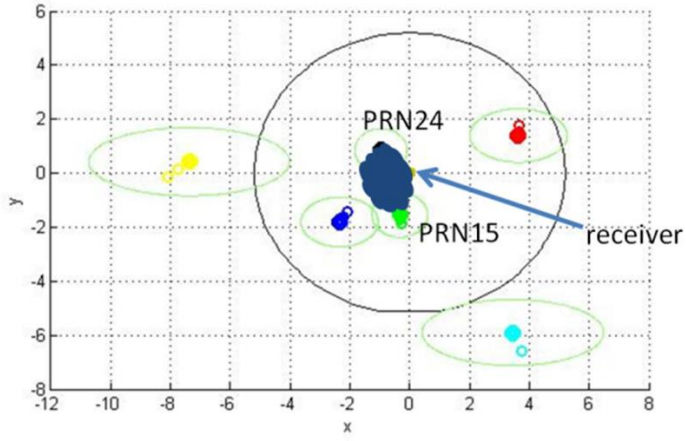

Figure 22: Specular points for soaking wet soil (Pei, 2014)

In Figures 21 and 22 the meaning of the symbols is explained in Table 15.

Brown point	Receiver
Black circumference	LHCP signal ground's footprint
Green circumferences	First Fresnel area for each specular point
Blue mark	Wet areas
Black dots	PRN 24
Green dots	PRN 15
Bold dots	First specular points

Table 15: Moisture measurements (Pei, 2014)

We can notice in Figure 21 and Figure 22 an intrusion of the related to the PRN 24 First Fresnel Zone into the wet area, what could be the reason why the higher SNRs change estimated for the PRN 24, in comparison to the one characterizing the PRN 15 (Figure 23).

From these measurements the following SNR's values were obtained:

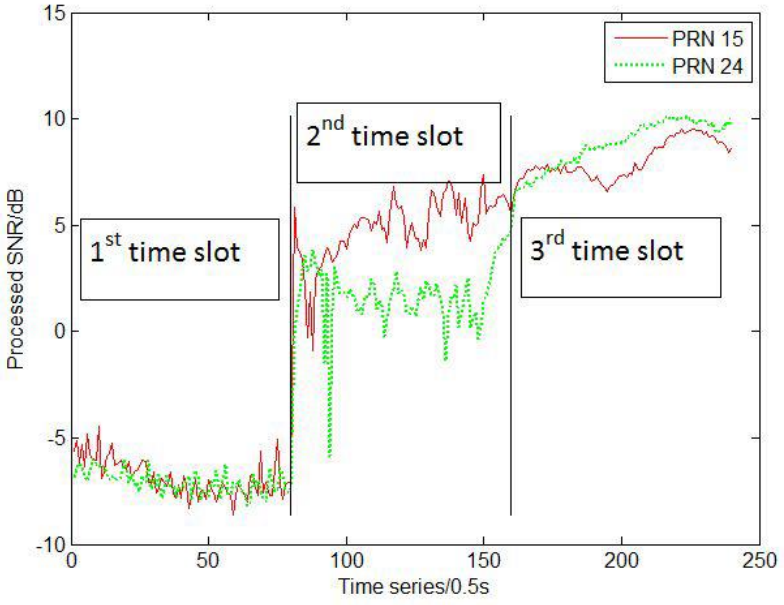

Figure 23:Measured SNR (Pei, 2014)

As expected, SNR increases coherently hand in hand with the terrain moistening.

PRN 15	**Dry**	**Wet**	**Soaking wet**
Median	-7.07	5.10	7.72
Mean	-6.87	4.91	8.05
Standard deviation	0.86	1.48	0.88

Table 16: SNR PRN 15 (Pei, 2014)

PRN 24	Dry	Wet	Soaking wet
Median	-7.05	1.71	8.92
Mean	-7.06	1.72	8.82
Standard deviation	0.53	1.50	1.08

Table 17: SNR PRN 24 (Pei, 2014)

Numerically solving the equations of Hllikainen model (see section 6.1) we can retrieve the dielectric constant (see Figure 24).

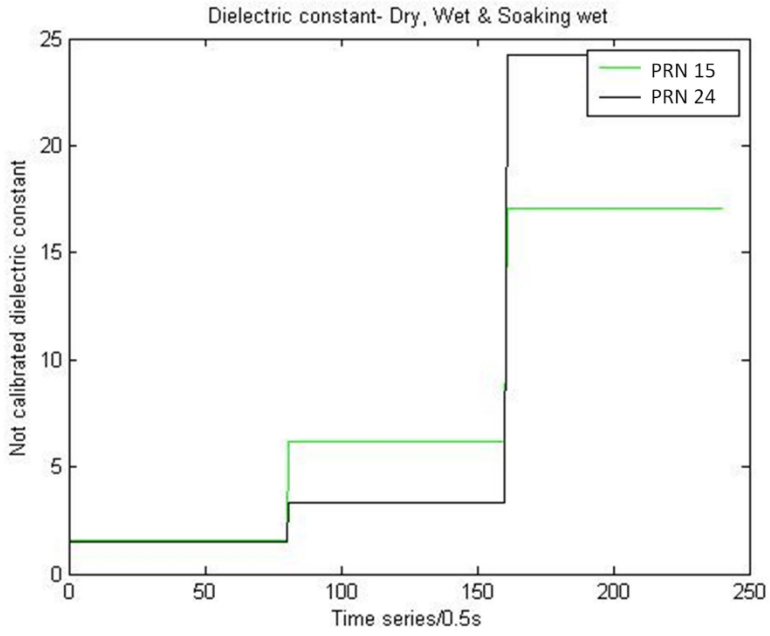

Figure 24: Retrieved dielectric constant

The dielectric constant was meant to follow the SNR's increment trend, what it actually did despite of the third's slot retrieval.

As we can see, during this period the dielectric constant difference between PRN 15 and 24 is much larger that the SNR difference, what was caused by the non-linear relationship between dielectric constant and signal.

It is important to notice that the obtained dielectric constant was retrieved directly from SNR using a calculation without any calibration so, possible wrongly evaluated parameters such as the receiver noise might had influenced the accuracy of the results. Soil moisture was not even precisely controlled so in-situ detailed measurement of it were missing.

However, as the aim of the static measurement was to verify the receiver's SNR sensitivity to soil moisture and the dielectric constant variation, these results are used as a reference to link the LHCP reflected signals and its SNR to the soil's dielectric constant.

ii. Conclusive study 2014

In order to summarize, as further detailed information about measurement campaigns is given in the next section, but with the aim of present a conclusive study of GNSS-R for soil's moisture determination and dielectric constant retrieval, this research will be introduced.

A researching group (Campanella, 2014) carried out GNSS-R measurements in 2014 near to Torino, at Grugliasco exactly, whose particular conditions are detailed in the next Chapter (6.2.iii.Location description).

They conducted several groups of measurements (four groups exactly) in a similar way as (Jia, 2014) did, even using a similar setup, and obtained their corresponding Frist Fresnel Zones maps, SNR measurements and dielectric constant retrievals.

Indeed, they finally obtained relevant results with the satellite 16, providing soil dielectric constant values comparable with those obtained with the probe in particular for measurement 4 and 11. Substituting these values and using the sand and clay percentages given by the USDA, the volumetric water content was computed obtaining the following results:

Measure	Dielectric constant	Volumetric water content
4	13.89	0.21
11	10.87	0.16

Table 18: Results (Campanella, 2014)

iii. Measurement campaign at Grugliasco

The purpose of this study was to determine the dielectric constant and the soil moisture from the generated SNR produced by the scattering of GNSS signals and reflected LHCP.

Four measurements were conducted, all of them using the same setup GNSS-R receiving system, but they were split in two groups of measurements regarding the origin (transmitting satellite) of the most relevant received signals.

An extended description of the used setup is detailed in Chapter 8.1, but it is important to notice that, as the scattered reflecting signal is meant to have a LHCP, the two antennas systems will stand as follows:

- Antenna receiving direct satellite's signal → RHCP
- Antenna receiving scattering reflected signals from the Earth's surface → LHCP

Location description

These measurements were conducted at the Dipartimento Inter-Ateneo di Scienze Progetto e Politiche del Territorio (DIST), which is a controlled environment located in Grugliasco, Torino (45º 03'58.5"N, 7º 35'33.8"E).

What this location had in particular were the well-known soil characteristics, which are the following:

Coarse sand (%)	Fine sand (%)	Very fine sand (%)	Coarse silt (%)	Fine silt (%)	Clay (%)	Organic matter (%)
15.5	50.1	16.1	5.3	8.2	4.8	1.4

Table 19: Grugliasco soil composition

According to the United States Department of Agriculture (USDA) Classification System, the soil of the sites of Grugliasco and Agliano belong to the loamy sand and silty clay loam textural classes, respectively.

Therefore, as far as the soil's composition is well known, conducting dielectric constant measurements in this environment seems to be a good opportunity to check the efficiency of the system.

First and Second measurements

Firstly, the main satellites whose signals were use were plot in order to facilitate its tracking on their way through the sky:

1st Measurement (10:50 hh)							
PRN 1		**PRN 11**		**PRN 28**		**PRN 32**	
Azimuth	Elevation	Azimuth	Elevation	Azimuth	Elevation	Azimuth	Elevation
309.6	64.6	265.8	87.0	287.4	21.7	230.6	86.3

2nd Measurement (10:55 hh)							
PRN 1		**PRN 11**		**PRN 28**		**PRN 32**	
Azimuth	Elevation	Azimuth	Elevation	Azimuth	Elevation	Azimuth	Elevation
312.0	66.6	213.6	87.7	285.1	21.1	250.4	88.6

Table 20: Satellites Grugliasco 1 and 2

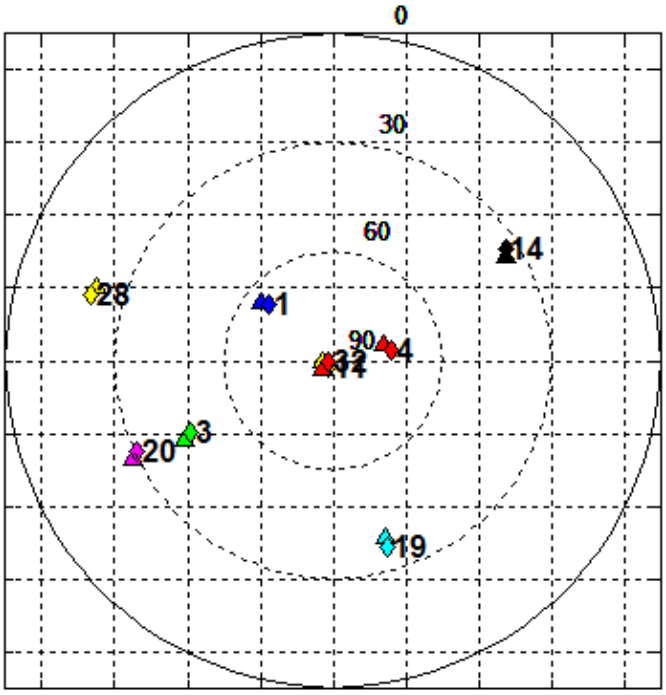

Figure 25: Skyplot Grugliasco 1 and 2

In Figure 25 we can see the position of the satellites relatively to the location of our receiving system, producing the following map of specular points and First Fresnel Zones:

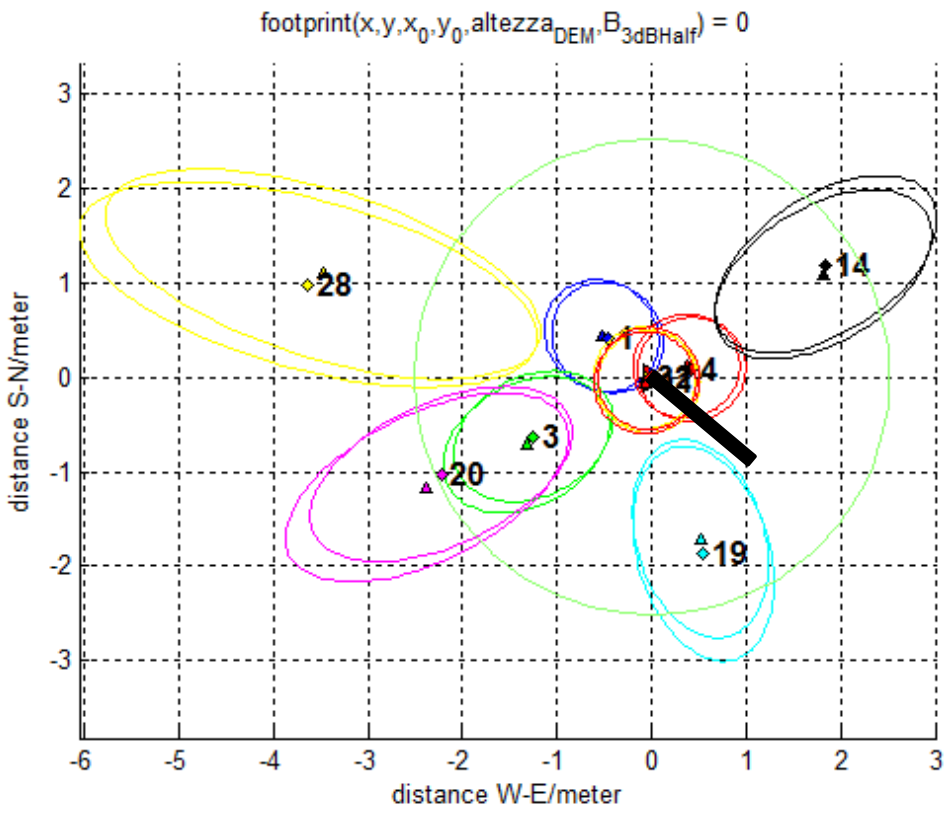

Figure 26: Specular points and First Fresnel Zones Grugliasco 1 and 2

The meaning of the symbol is explained in Table 21 and the SNR is shone in Figures 27 and 28,

Black rectangle	Receiver
Green circumference	LHCP signal ground's footprint
Colourful rhomboids	PRNs
Colourful triangles	Specular points
Colourful circumferences	First Fresnel Zone for each specular point

Table 21: Specular points and First Fresnel Zones Grugliasco 1 and 2

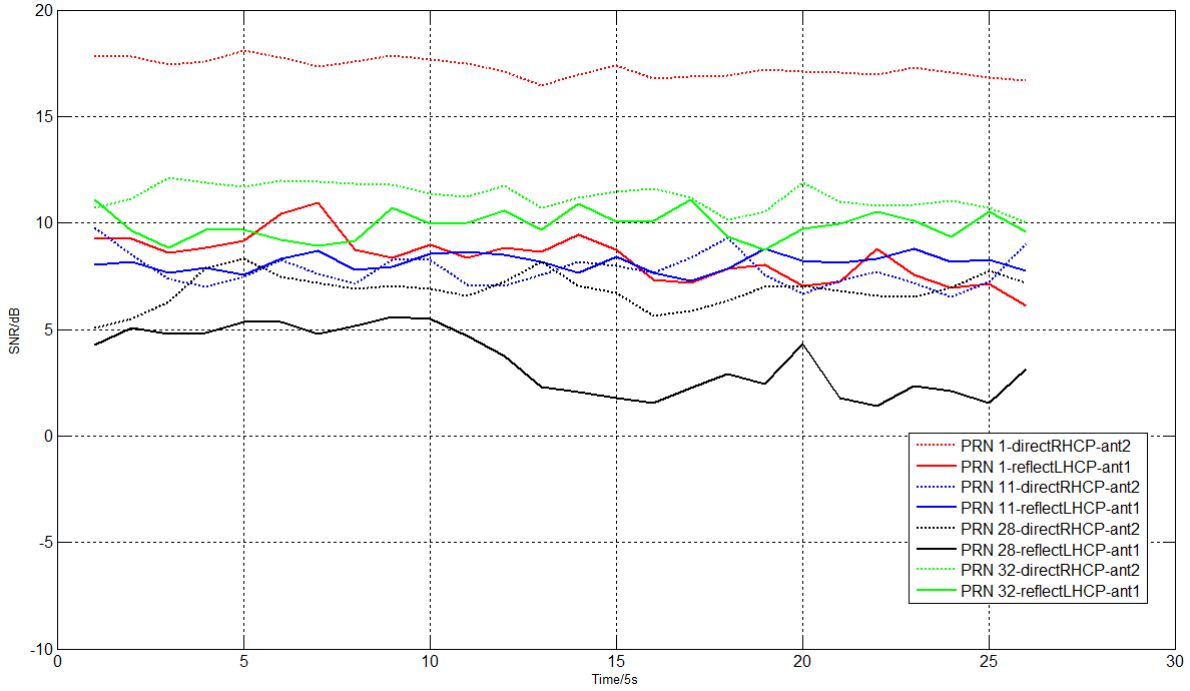

Figure 27: Grugliasco Measured SNR 1

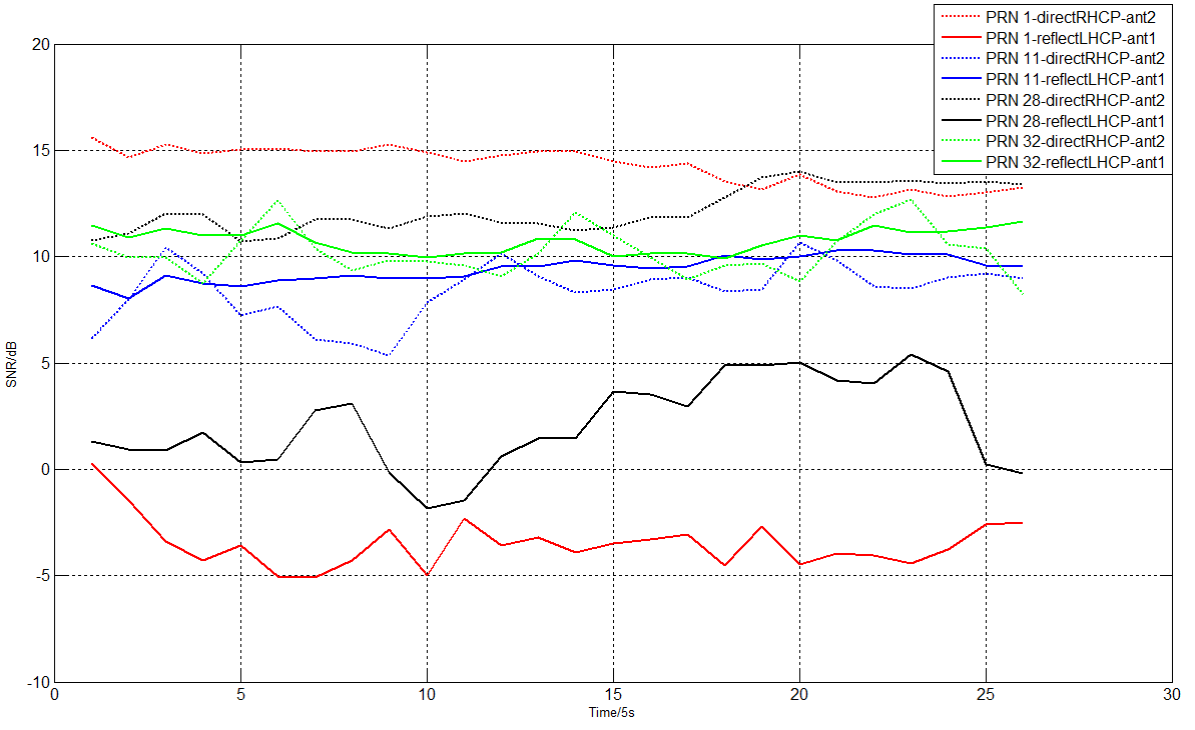

Figure 28: Grugliasco Measured SNR 2

Let's notice that RHCP corresponds to the directly received satellite's signal while LHCP corresponds to the reflected one.

Then, putting all this information together to analyse it we obtain the following table:

Measurement	Polarization	PRN 1	PRN 11	PRN 28	PRN 32
1st	RHCP (direct)	17.27	7.77	6.84	11.25
	LHCP (scattered)	8.38	8.13	3.50	9.89
2nd	RHCP (direct)	14.28	8.40	12.19	10.21
	LHCP (scattered)	-3.48	9.40	2.11	10.75

Table 22: Measured SNR Grugliasco 1 and 2

From where we actually obtain some contradictory values (the ones on red) remarked because of their unexpected nature.

In fact, when measuring these kind of signals, a greater SNR from the RHCP than from the LHCP was supposed to be obtained (mainly because of their signal's power, disregarding the noise contribution) as the first ones are the directly received and the second ones are the scattered ones.

So, logically, the direct ones should loss less signal power, only due to the propagation losses; meanwhile the reflected ones should present lower power due to their additional dispersion losses (scattering on the Earth surface).

Thus, the reason why we are obtaining such controversial value might be caused by some interferences: from a fading in the direct signal (probably caused by any obstacle obscuring the direct transmitter-receiver vision) to an addition of power from other reflected unexpected noisy sources.

Indeed, for this last case, the reason might be a high noisy component of the tripod that is causing signal reactions. These reflections may be creating an additional multipath who decreases the SNR level.

The first supposition make sense regarding the PRN 11 measurements, as far as the direct signal's values seems to be poor compared to the other direct ones while, in the PRN 32 case, the second supposition seems to be the cause.

Apart from those inaccurate values, the other ones lead us to the following dielectric constant's retrievals:

Measurement	PRN 1	PRN 11	PRN 28	PRN 32
1st	~ 4	/	~ 52	/
2nd	/	/	/	/

Table 23: Dielectric Constant Retrieval Grugliasco 1 and 2

Third and Fourth measurements

In the same way as seen before, the satellites' positions and their plotted map are the following:

3rd Measurement (11:00 hh)					
PRN 1		**PRN 3**		**PRN 20**	
Azimuth	Elevation	Azimuth	Elevation	Azimuth	Elevation
314.7	68.7	245.4	48.0	246.7	32.6
3rd Measurement (11:15 hh)					
PRN 1		**PRN 3**		**PRN 20**	
Azimuth	Elevation	Azimuth	Elevation	Azimuth	Elevation
325.2	74.9	251.6	54.2	251.3	38.5

Table 24: Satellites Grugliasco 3 and 4

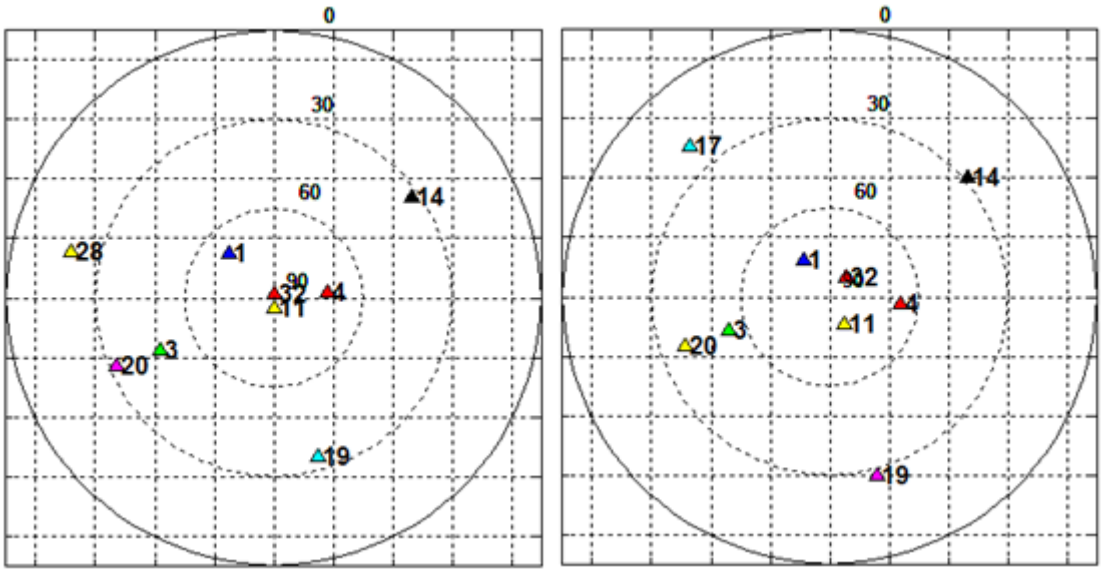

Figure 29: Skyplot Grugliasco 3 and 4

Giving the following First Fresnel Zones map:

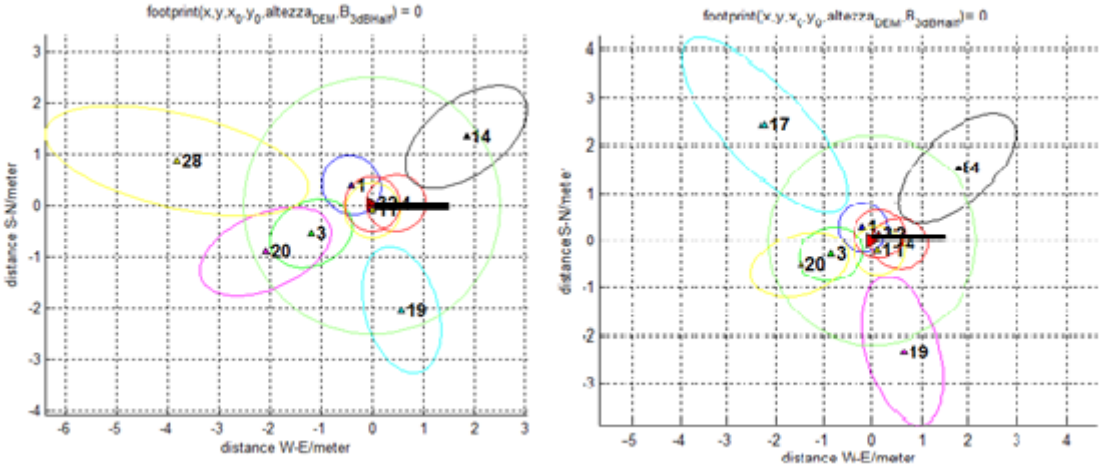

Figure 30: First Fresnel Zone Grugliasco 3 and 4

The meaning of the symbol is explained in Table 25 and the SNR is shone in Figures 31 and 32,

Black rectangle	Receiver
Green circumference	LHCP signal ground's footprint
Colourful rhomboids	PRNs
Colourful triangles	Specular points
Colourful circumferences	First Fresnel Zone for each specular point

Table 25: Specular points and First Fresnel Zones Grugliasco 1 and 2

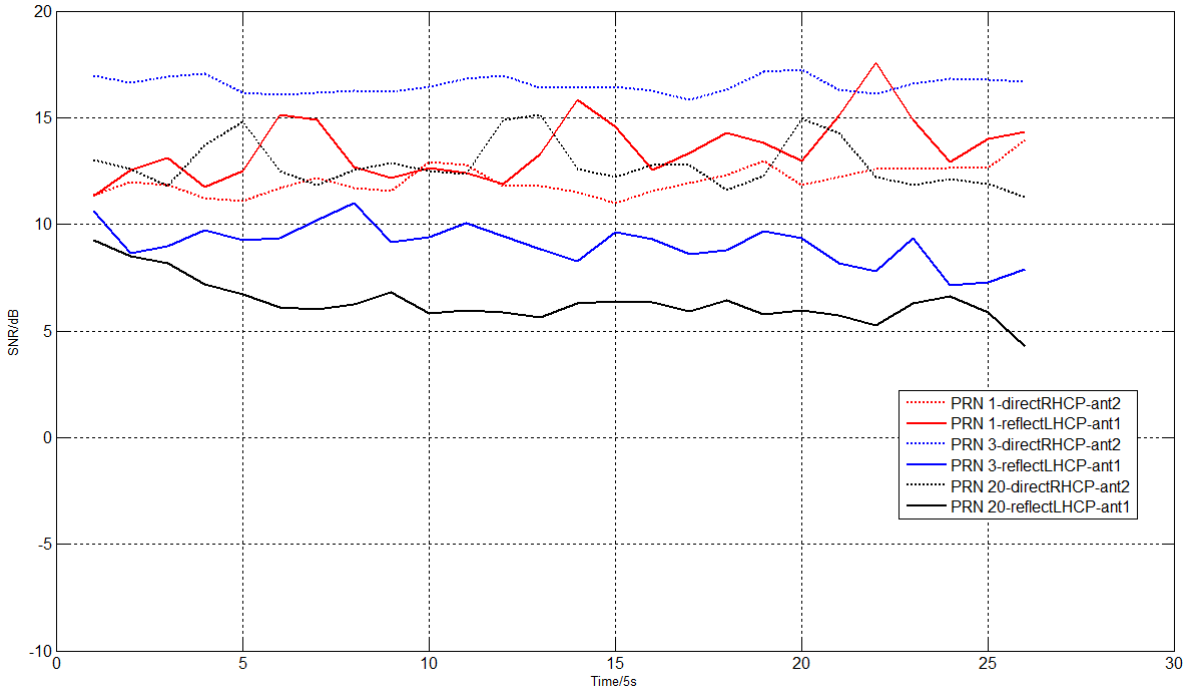

Figure 31: Grugliasco Measured SNR 3

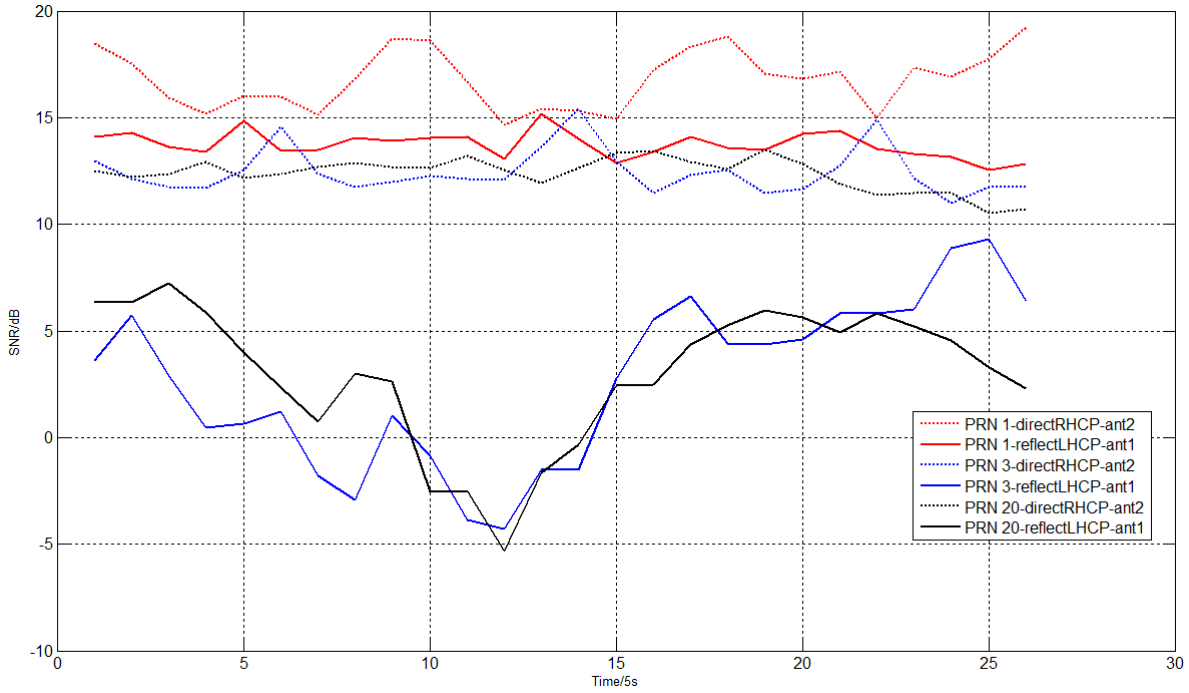

Figure 32: Grugliasco Measured SNR 4

Measurement	Polarization	PRN 1	PRN 3	PRN 20
1st	RHCP (direct)	12.07	16.54	12.82
	LHCP (scattered)	13.56	9.08	6.37
2nd	RHCP (direct)	16.81	12.46	12.38
	LHCP (scattered)	13.73	2.67	3.02

Table 26: Measured SNR Grugliasco 3 and 4

Where we obtain again some contradictory values (the ones on red), which are probably caused by to an addition of power from other reflected unexpected noisy sources as explained before.

And finally obtaining the following Dielectric Constant retrieval:

Measurement	PRN 1	PRN 11	PRN 28	PRN 32
1st	/	~ 6	~ 9	/
2nd	~ 32	~ 4	~ 4	~ 32

Table 27: Dielectric Constant Retrieval Grugliasco 3 and 4

In conclusion, if we disregard the non-coherent SNR measurements, we actually get to determine successfully the dielectric constant of the soil by using the techniques studied on this thesis.

Therefore, it is not difficult to assume that further research has to be done following this path, and even extending its coverage by modifying these GNSS-R circularly polarized systems conducting more measurement campaigns with linearly polarized ones (as theoretically studied in Chapter 5), moving forward to its promising future.

7. Snow Depth Determination

7.1. Snow Depth

Snow is an important component of the climate system and a critical storage component in the hydrologic cycle.

Indeed, measurement of the amount of water stored in the snowpack and forecasting the rate of melt are thus essential for management of water supply and flood control systems (Shi & J.Dozier, 2000).

Unfortunately, due to the complexity of the terrain, many of the snow attributes might present considerable spatial variability even over small distances, making point measurements not enough adequate.

Snow deposition is heterogeneous, with generally greater amounts of snow falling at higher elevations. Even, once on the ground, the snow may be redistributed by wind, avalanching and sloughing.

Furthermore, snowpack ablation is also nonuniform because it is controlled by spatially and temporally varying parameters such as temperature, wind, and radiation (K. M. Larson, 2009).

By analysing the interferometric frequency patterns of multipath reflections (E. D. Gutmann, 2012) (K. M. Larson, 2009) or on both its frequency and amplitude, it is able to infer this depth and equivalent water content with linear polarized antennas.

Using them, it is possible to quantify the number and location of the interference notches and solve for the thickness of the snow layer (Valery U. Zavorotny, December 2014).

7.2. Snow Depth measurements

During the last decade, many researchers' groups have conducted experiments in order to measure the snow depth using GNSS-R systems.

In this chapter two of them will be presented, detailing the measuring setup, the context when they took place (weather, hour, date, etc.), the place where the measurements were done, as well as their results.

i. Politecnico di Torino, Torino 2014

Firstly, it might be useful to look over Yuekun Pei's research (Pei, 2014) mainly because this study is actually one of the most recent ones on this subject, and even because it was carried out at the main Politecnico di Torino.

In Table 29 the detailed information about the weather conditions when the measurements were made is presented, meanwhile Table 28 contains the characteristics of the campaign.

Measurement Campaign	Yuekun Pei - 2014
Location	Politecnico di Torino (roof)
Setup	• Fixed antenna • Elevation of 45° • Compact Hackberry based receiver (Figure 33)

Table 28: Snow Depth Measurements 1 (Pei, 2014)

Figure 33: Snow depth setup (Pei, 2014)

Day	Time	Weather	Snow Level	Humidity
Feb 20th	16:35-17:05	Foggy	null	70%
Feb 21st	13:35-14:15	Snow	1cm	93%
Feb 22nd	09:55-11:05	Snow	2cm	97%
Feb 22nd	11:55-12:35	Snow	3cm	87%
Feb 22nd	16:05-17:05	Snow	0.5cm	78%

Table 29: Yuekun Pei's measurements - Weather

The measurements gave the following outputs:

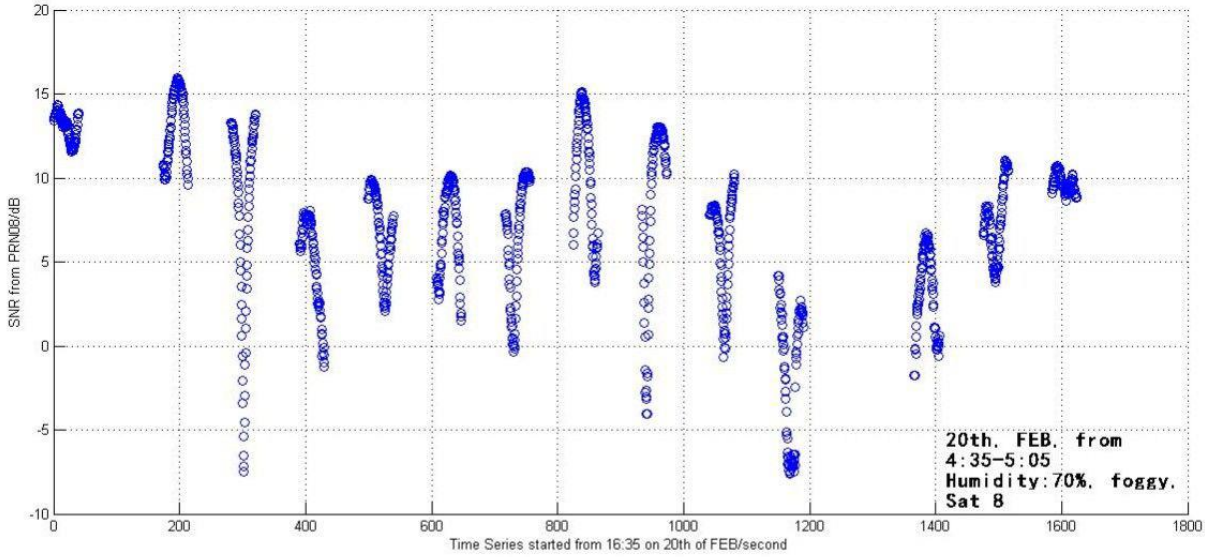

Figure 34: SNR of the measurement on 20th Feb, from 16:35-17:05 (Pei, 2014)

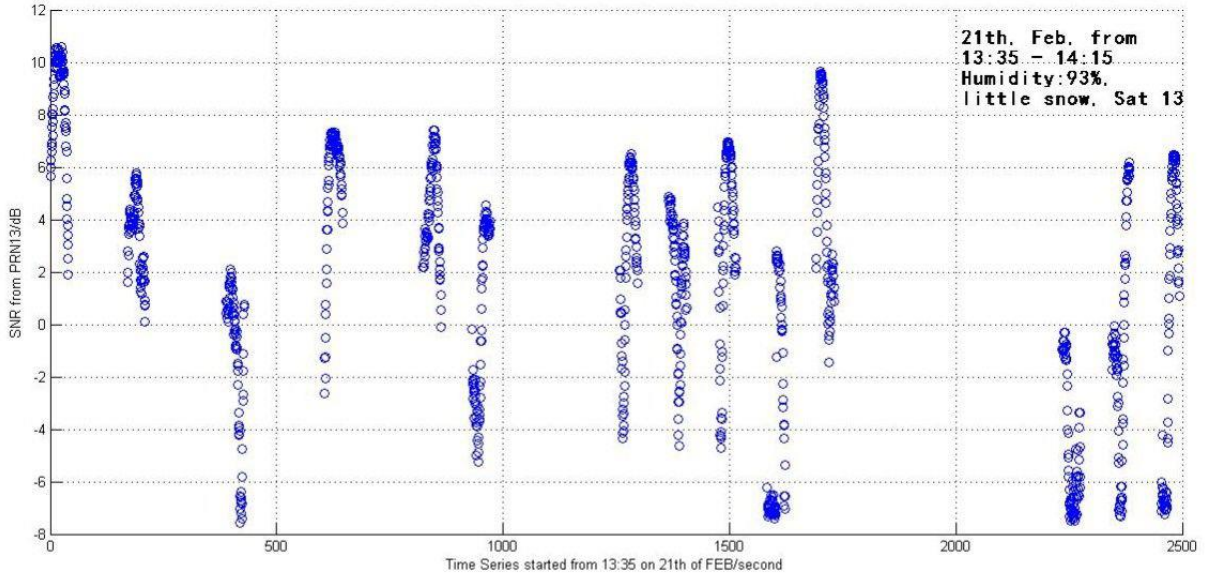

Figure 35: SNR of the measurement on 21st Feb, from 13:35 – 14:15 (Pei, 2014)

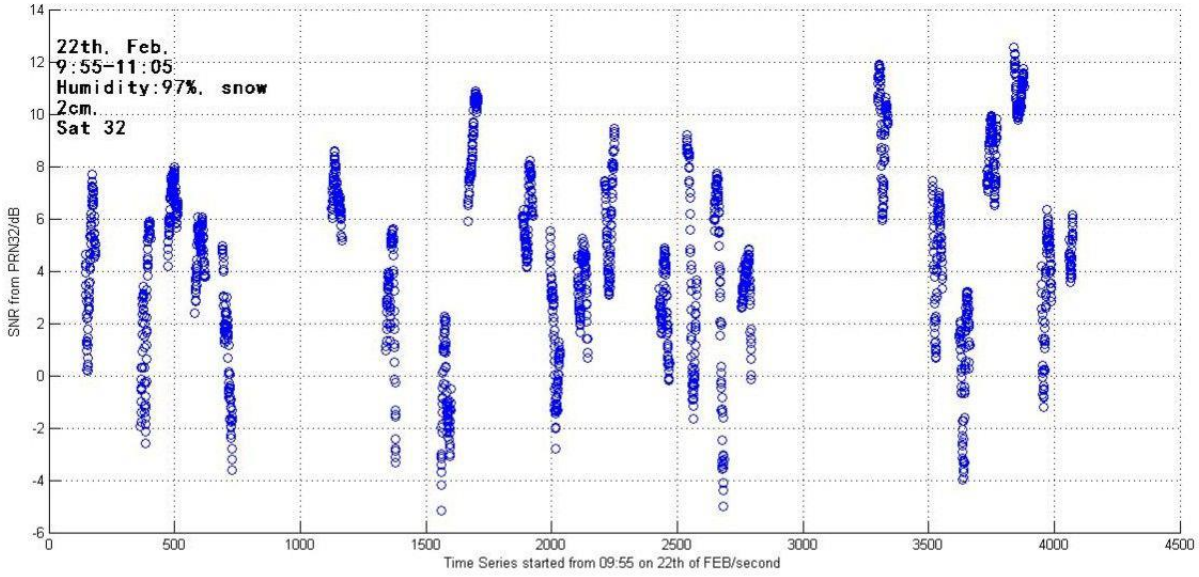

Figure 36: SNR of the measurement on 22nd Feb, from 9:55- 11:05 (Pei, 2014)

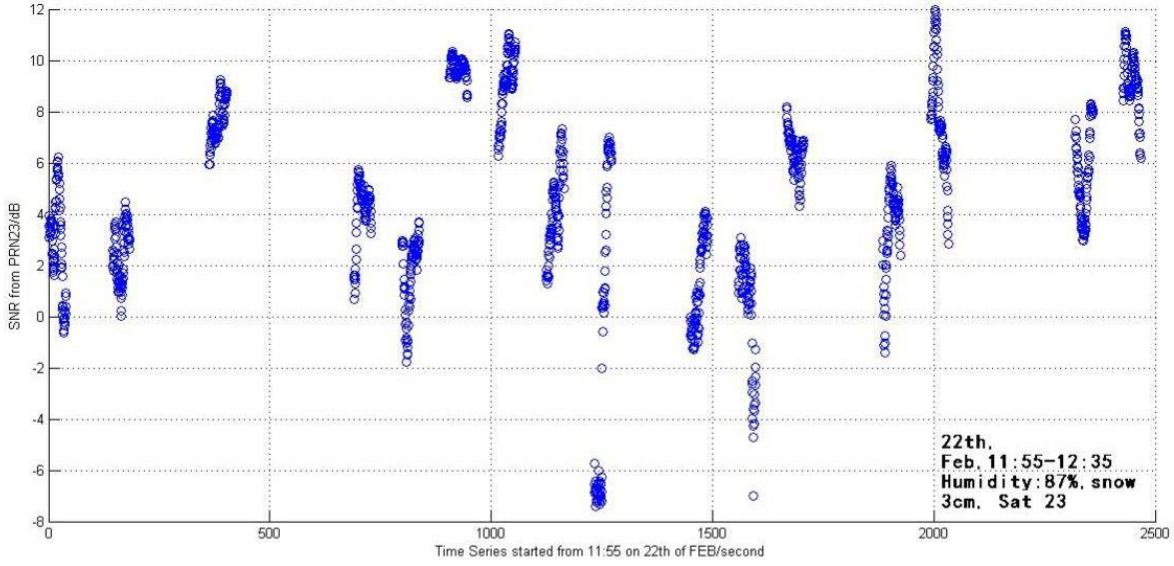

Figure 37:SNR of the measurement on 22nd Feb, from 11:55-12:35 (Pei, 2014)

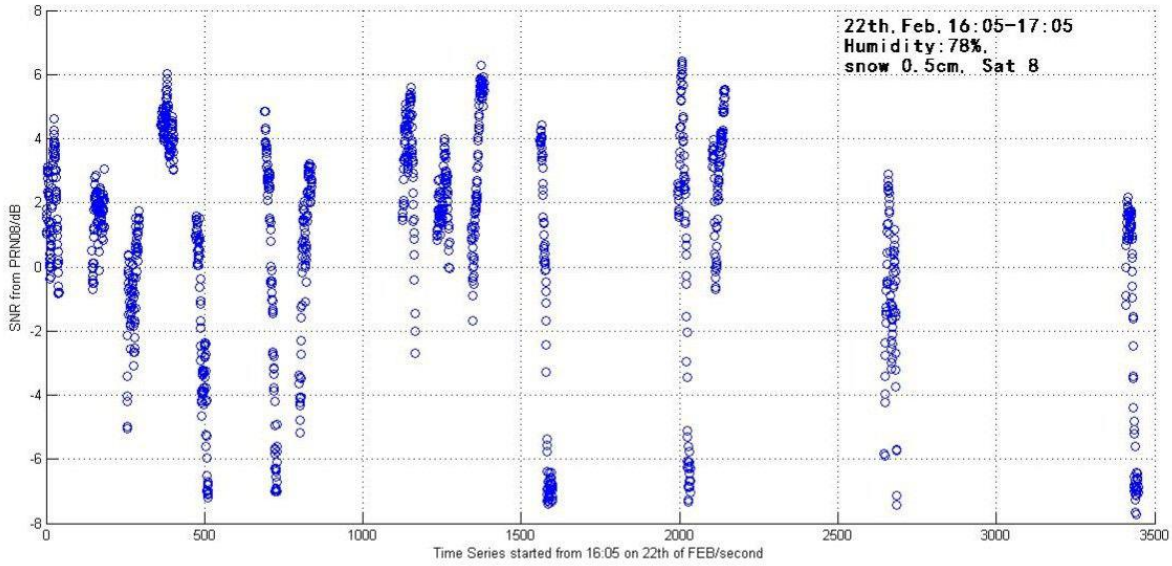

Figure 38: SNR of the measurement on 22nd Feb, from 16:05-17:05 (Pei, 2014)

As we can see, due to the use of the compact receiver, data were not recorded continuously but with a 40 s of recording time for each piece. Around 80 s of time interval between two pieces was expected for the writing of data from ram to SD card, losing some pieces occasionally.

In these figures every dot represents the SNR calculated with 500 ms non-coherent integration time.

Statistics evaluated by grouping each 40 s SNR for all the five measurements, together with information about mean, standard deviation, maximum and minimum value of each time slot are shown the Figure 39.

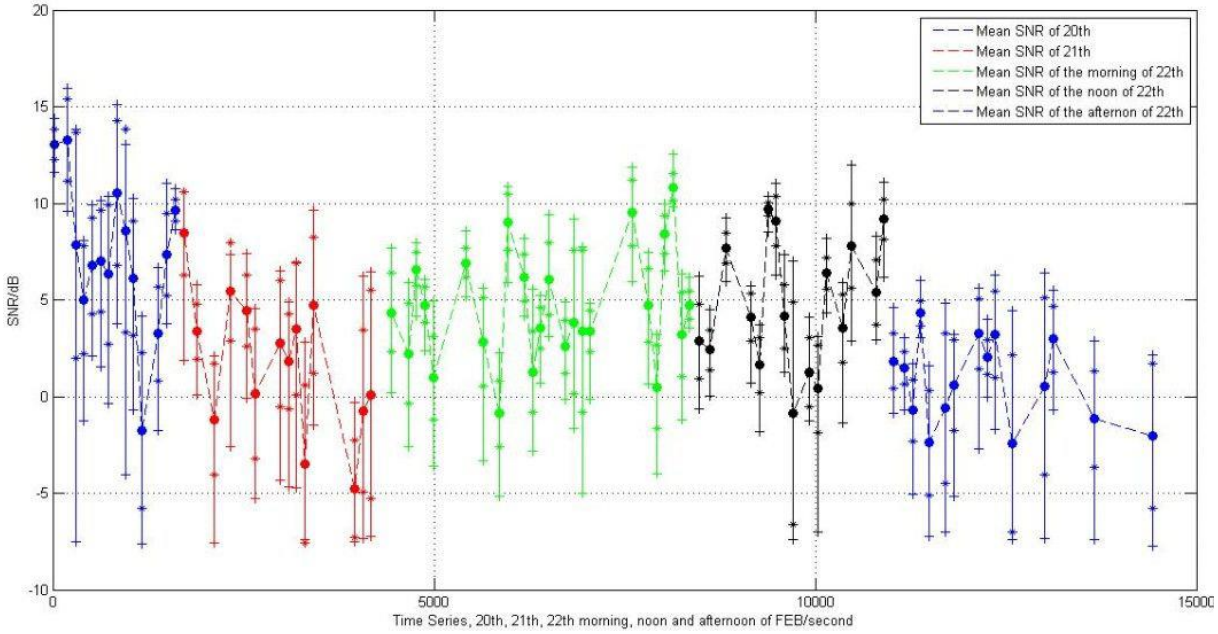

Figure 39: Statistics of measured SNR (Pei, 2014)

As the SNRs have sinusoid-like behaviour, possible interference due to the multipath caused by the buildings was studied, verifying frequency to be close to that revealed by FFT of the SNR series.

Signal amplitude A1 was tried to be extracted from each group of SNR assuming the interference signal had a rotating phase with respect to the specularly-reflected signal which lead to this sinusoid-like SNR performance. Making a second order polynomial fit with the measured snow depth as shown:

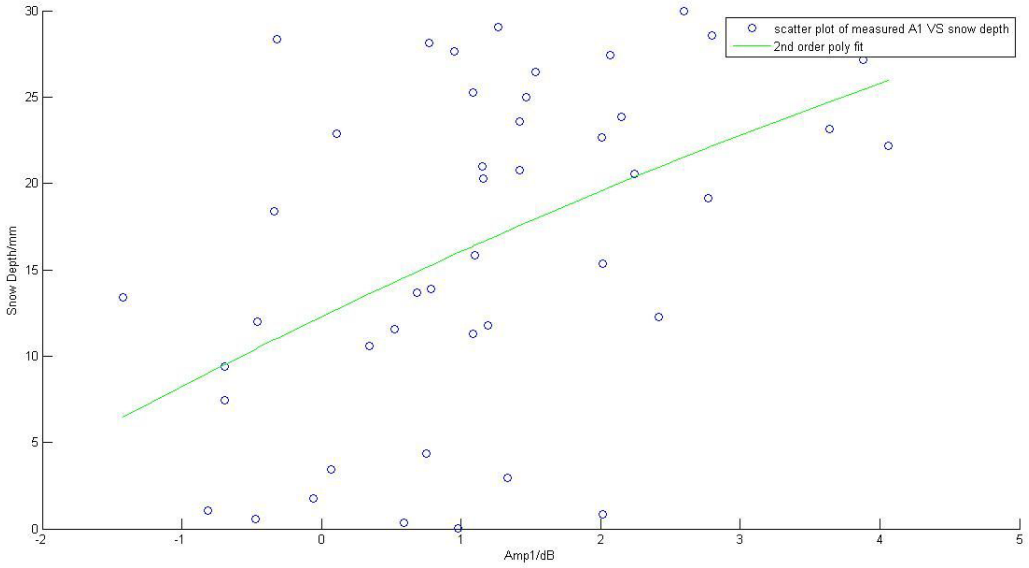

Figure 40: Second order polynomial fit between reflected signal amplitude and snow depth (Pei, 2014)

Unfortunately, the results didn't seem well matched and the research on snow depth was interrupted due to the insufficient theory exploration and limited data. Therefore, it should be notice that the study was not exactly rigorous, but the results shown could be useful as a reference to future studies is expected for the possible future work.

ii. NCAR Marshall Field, Colorado 2009

The second campaign to be mentioned is actually an older one, but which succeeded to produce relevant data and precise measurements about snow depth using GNSS-Reflectivity systems.

Table 30contains the characteristics of the campaign:

Measurement Campaign	**(K. M. Larson, 2009)**
Location	National Center for Atmospheric Research's (NCAR) Marshall Field near Boulder, Colorado (elevation 1728 m)
Setup	• GPS Trimble NetRS receiver with a choke-ring antenna (model TRM29659.00 with SCIT radome), with its phase center ~1.9 m above the ground • Configured to track the L2C signal being transmitted on Block IIR-M GPS satellites: PRN 7, 12, 15, 17, 29, and 31

Table 30: Snow Depth Measurements 2 (K. M. Larson, 2009)

The setup schema could be represented as Figure 41.

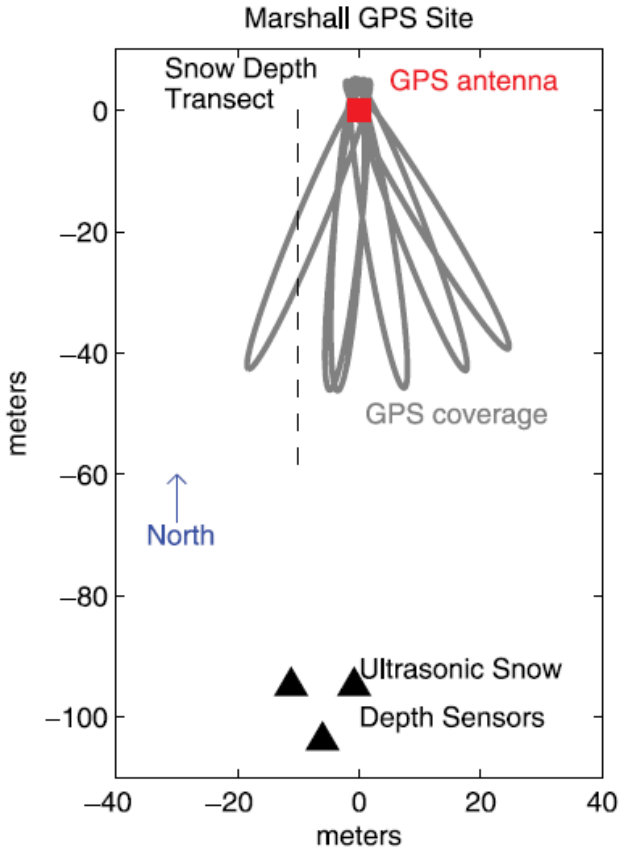

Figure 41: Marshall setup schema (K. M. Larson, 2009)

Which measured two snow falls described in the following table:

Day	Time	Wind	Snow Level	Humidity
March 26th	10:00 UTC (+24hh)	12 m/s	37 mm	70%
April 17th	00:00 UTC (+48hh)	6-10 m/s	105 mm	93%

Table 31: Campaign weather (K. M. Larson, 2009)

Since multipath effects are most pronounced at low elevation angles, only data between 5 and 25 degrees were used in this study.

The resulting measurements were the presented on Figure 42.

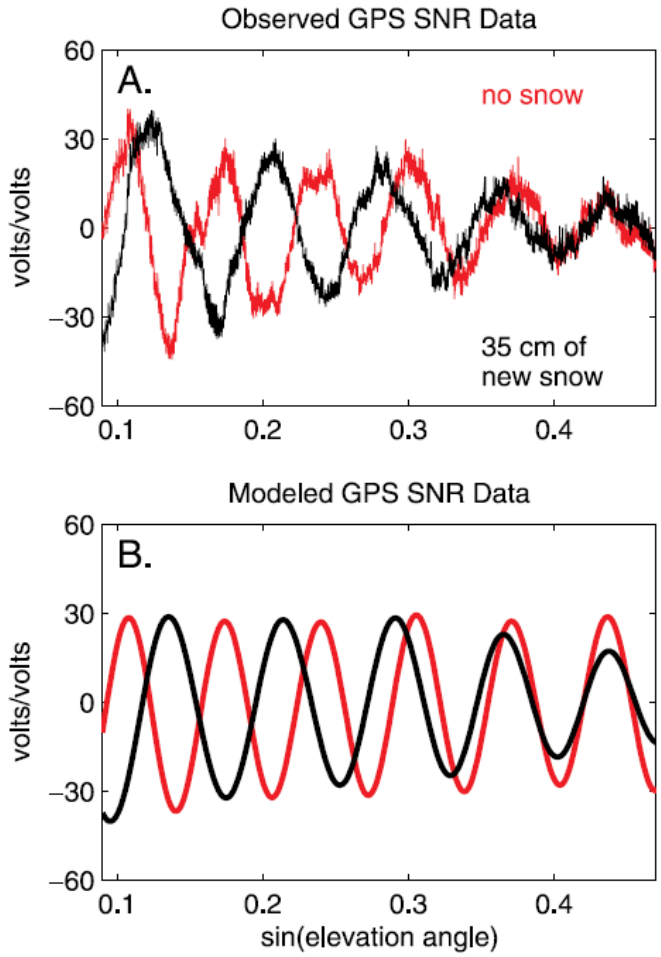

Figure 42: NCAR Marshall measurements (K. M. Larson, 2009)

From these we can observe that GPS SNR measurements for PRN 7 on days 107 (red) and 108 (black), after direct signal component has been removed, approximately 35 cm of snow fell by day 108.

In B there are shown model predictions for GPS multipath from day 107 with no snow on the ground (red), and day 108 after 35 cm of new snow fall had accumulated (black), using an assumed density of 240 kg m^{-3}.

Thus, it can be seen that GPS SNR data is sensitive to but do not directly measure snow depth.

In order to convert changes in GPS multipath data into snow depth Lomb-Scargle periodogram was used to estimate the multipath peak frequency f.

Meanwhile, as seen in Chapter Snow Depth 7.1, other models match the relationship between f and snow depth for various snow densities. But, particularly for the results shown, model calculations for snow density of 240 kg m^{-3} were used.

They tested lower and higher snow densities (150 and 400 kg m^{-3}) based on the measured values and found that this changed GPS snow depth estimates by 10–12%.

It is important to notice that, even when this campaign was meticulous, there were also factors who might produce indeterminateness somehow, as for example the planar snow-layer assumption, the not-optimal elevation angle (for snow depth sensing), or the only transient snowfalls.

But, finally, this study was overall successful because it gave a useful conclusion suggesting that some GPS sites could be used to augment existing snow sensor networks, working with multipath models to estimate snow depth, together with the resolution that GNSS-R linearly polarized systems are a great option for measuring snow depth and equivalent water content.

8. Hardware description

8.1. Dielectric Constant Determination

i. LHCP measuring Dielectric Constant

The GNSS-R system used in this campaign was the same as the one we detail as follows in the section iii about the Grugliasco's campaign, therefore its study will be deeply developed in that section (Pei, 2014).

ii. Conclusive study 2014

In order to have a controlled measurement setup, antennas and front-ends were installed on a metal bar hooked to a tripod (Figure 43) and they were directly powered by the USB port of the PC (Campanella, 2014).

Figure 43: Setup Grugliasco 2014

The antenna was a right handed circular polarized (RHCP) pointing upwards for the measurement of the direct signal, meanwhile a left handed circular polarized antenna (LHCP) was pointing downwards for the measurement of the reflected signal.

ANTCOM Corp. commercial antennas was the selected antenna's brand, providing active devices able to receive a GPS signal in L1 band and L2 band with both LH and RH polarization.

Figure 44: Antenna Grugliasco 2014 (Campanella, 2014)

These antennas are made of aluminium alloy base and they are able to work in a temperature range between -55 and +85 up to an altitude of 70:000 ft. All the electrical specification's taken from the datasheet are listed in the following table:

Frequency	**L1 (1575.42 MHz)**	**L2 (1227.60 MHz)**
Radiation pattern	Hemispherical	Hemispherical
Polarization	RHCP/LHCP	RHCP/LHCP
Impedance	50 ohms	50 ohms
Axial ratio	2 dB	2 dB
LNA gain option	33 dB	35 dB
LNA noise figure	3.0 dB	3.0 dB

Table 32: Antenna Grugliasco 2014 (Campanella, 2014)

The received signal was sent to the front-end by two SMA female connectors: one for the right-hand-circular polarized signal and one for the left-hand-circular polarized signal.

Each front-end was connected to a PC with a software for data acquisition.

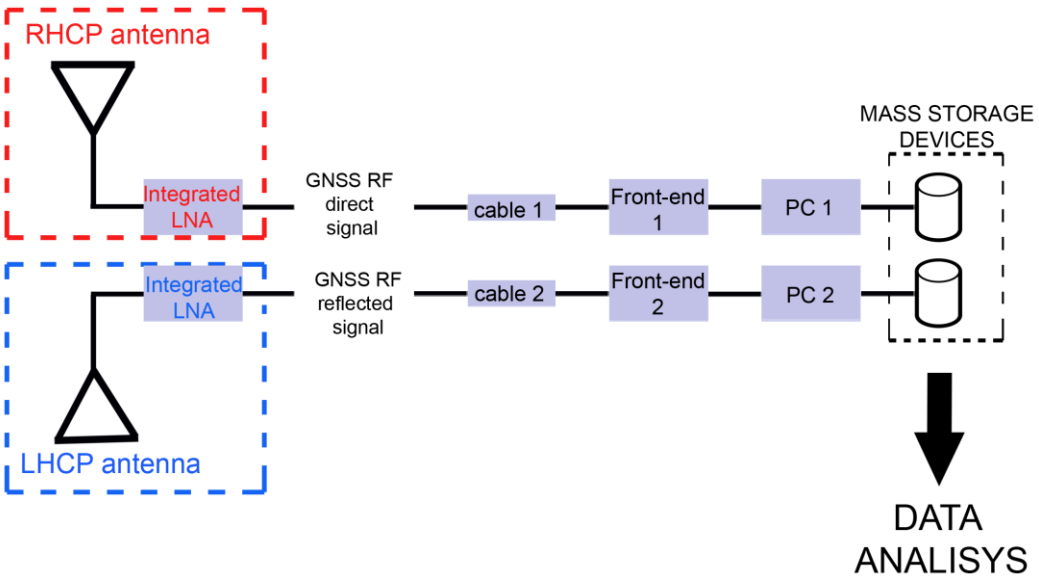

Figure 45: System block diagram (Campanella, 2014)

The receiver used is a SiGe GN3S v2 USB RF front-end, developed By the Colorado Center For Astrodynamics Research, whose information is more deeply explained in section 8.1.iii as the same one is used. Finally, it was connected with the antenna and the pc by a MCX Antenna Connector and mini-USB Connector.

iii. Measurement campaign at Grugliasco

The setup used for the acquisition of the received power can measure both the direct GPS signal and the reflected one by means of two independent acquisition channels: one for the direct signal and one for the reflected signal.

Therefore, two antennas are used for this campaign, a traditional hemispherical GNSS L1 patch antenna JCA001 pointed upwards for the measurement of the direct signal, and a LHCP Antcom antenna pointing downwards for receiving the reflected signal.

The hemispherical RHCP GNSS L1 patch antenna JCA001 has the following profile and the dimensions:

Figure 46: GPS patch Antenna profile

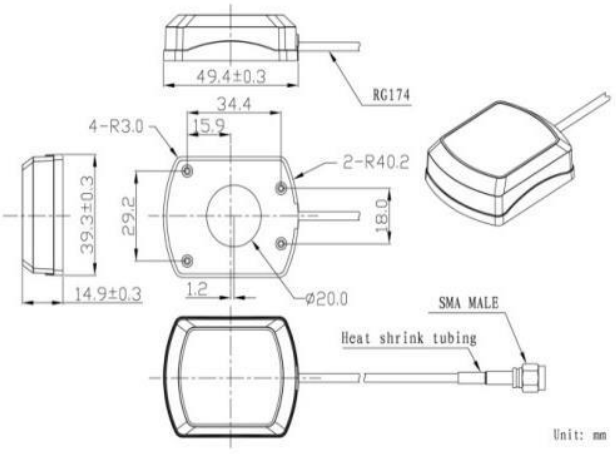

Figure 47: GPS patch Antenna dimensions

The radiation pattern of the antennas is shown in Figure 48 and 49.

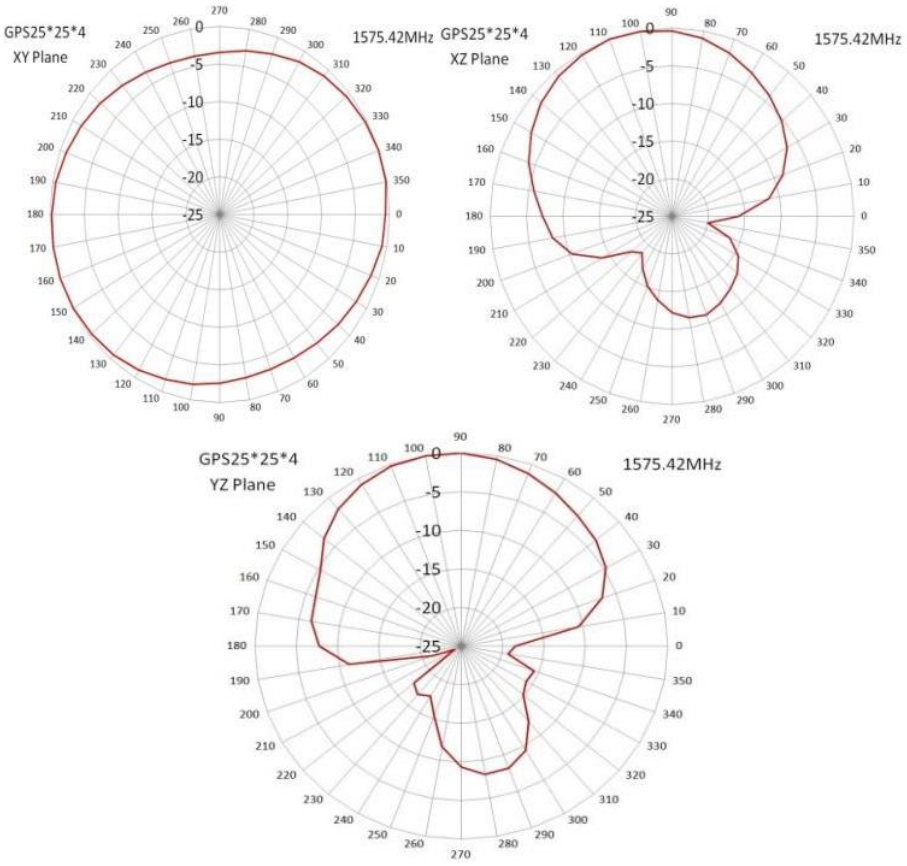

Figure 48: GPS patch antenna Radiation Pattern

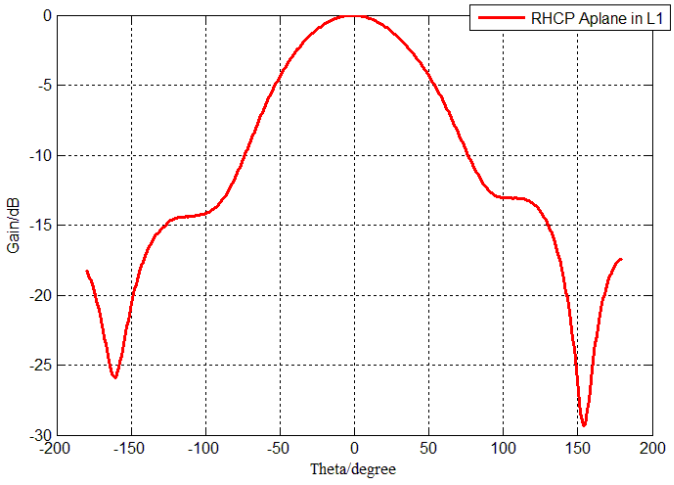

Figure 49: GPS patch antenna measured Radiation Pattern

Meanwhile, the HG-A (High Gain-Antenna) Antcom 1G1215RL-PP-XS-X RevA was used for the reflected link. It is enclosed on a 2 inches square (53 mm x 53 mm) and equipped by an LNA to provide a 33dB gain.

Figure 50: HG-A Antcom antenna

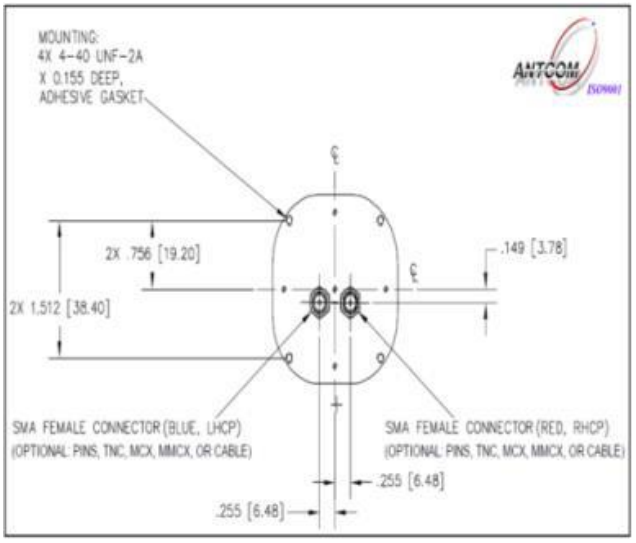

Figure 51: HG-A Antcom antenna dimensions

And whose datasheet is shown on Figure 52.

FREQUENCY:	L1: (1575.42 ±12) MHz			L2: (1227.60 ±12) MHz		
RADIATION PATTERN:	HEMISPHERICAL					
POLARIZATION:	RHCP/LHCP			RHCP/LHCP		
VSWR:	< 1.5:1			< 1.5:1		
IMPEDANCE:	50 ohms			50 ohms		
ANTENNAGAIN (dBic):	Free Space	3 in G.P.	4 ft G.P.	Free Space	3 in G.P.	4 ft G.P.
@ 90 ° (ZENITH):	+ 3.7	+ 4.7	+ 3.1	- 1.7	+ 3.3	+ 4.5
@ 10 ° Elevation	- 2.9	- 1.8	- 1.9	- 7.3	- 3.8	- 3.5
@ 20 ° Elevation	- 1.3	- 0.3	+ 0.6	- 6.2	- 2.0	- 0.8
@ 30 ° Elevation	0.0	+ 1.4	+ 1.7	- 5.2	- 0.5	+ 1.4
@ 60 - 90 ° Elevation:	> 3.0	> 3.9	> 2.4	> - 3.2	> 2.7	> 2.2
BEAM WIDTH(3dB):	108 Deg.	114 Deg.	143 Deg.	100 Deg.	106 Deg.	74 Deg.
AXIAL RATIO:	2 dB			2 dB		
LIGHTNINGPROTECTION:	DC GROUNDING					
LNA GAIN OPTION:	33 dB			35 dB		
LNA NOISE FIGURE:	3.0 dB			3.0 dB		
LNA P1dB Out:	+13 dBm			+13 dBm		
LNA DC POWER:	2.5V/20mA,3V/29mA,3.3V/35mA,(2.5-24)V/<50mA					
REJECTION@ (-50/+50)MHz	-41 dB / -59 dB			-40 dB / -40 dB		
@ (-100/+100)MHz	< -65 dB			< -65 dB		
POWERHANDLING	1 Watt CW, Optional: 10 Watts 1 microsecPulse (-AL-)					

Figure 52: HG-A Antcom antenna datasheet

Indeed, this is a dual polarization antenna, but whose LHCP is the configuration used for the link, as the X-pol level in LH port is better than RH port and satisfies the antenna requirement.

Why we are using this type of antenna is to open the way for further researches on this subject using a more advanced configuration of GNSS-R: adding an RHCP receiving channel (or antenna) to the LHCP antenna in the down-looking direction, in order to overcome possible future problems when separating surface roughness from the geophysical response of the terrain.

The antennas are connected to two commercial front-ends SiGe GN3S v2 USB RF front-ends (Figure 53), developed by the Colorado Center for Astrodynamics Research and licensed as General Public License (GPL) open source.

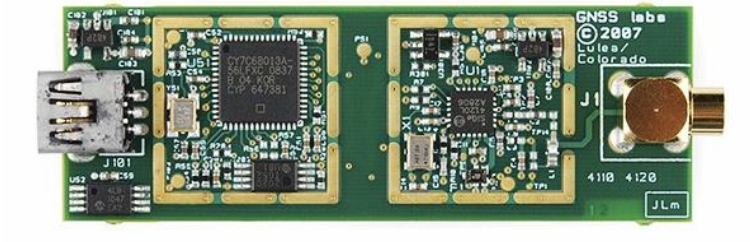

Figure 53: SiGe GN3S Sampler v2 Front-end

These devices are designed to directly capture and sample raw GPS data to a binary file for signal processing, being each of these front-ends composed of two integrated circuits:

- SiGe 4120 GPS Application Specific Integrated Circuit (ASIC) Analog to Digital Converter (ADC).
- Cypress Semiconductors EZ-USB FX2LP USB 2.0 microcontroller.

SiGe 4120 performs RF amplification, filtering, down-conversion, and baseband sampling. They are configured to provide a sample stream with a sampling frequency equal to 16.36 MHz whose samples are sent in In-phase and Quadrature (I/Q) pairs. The specific parameters of the front-ends are the following:

- Sampling frequency: 16.36 MHz;
- Intermediate frequency: 38.400 KHz.

On the other hand, Cypress Semiconductors EZ-USB FX2LP USB 2.0 microcontroller are in charge of reading the digital samples coming from the SiGe 4120 ASIC and sending them in real-time to the PC through the universal serial bus (USB).

SiGe GN3S Sampler v2 is connected with the antenna and the pc by means of a MCX Antenna Connector and mini-USB Connector.

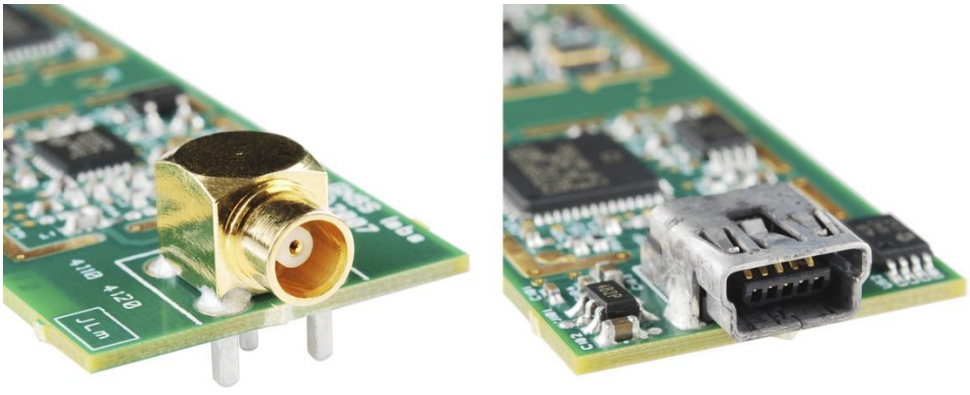

Figure 54: SiGe Front-end antenna's and USB's connectors

The antennas and the front-ends are mounted on a Kevlar bar fixed on a tripod for a more efficient adjustment of the orientation of the antennas which was kept horizontal at a height of 1.45m.

This configuration gives us the possibility of calibrating the system with water identification and extracting the information about terrain characteristics near the reflection points.

However, dielectric constant (relative permittivity) cannot be easily separated with the surface roughness if the soil roughness cannot be negligible or accurately modelled. So, this type of setup might provide inaccurate information in some cases.

Thus, the election of a dual polarized antenna will help the development of further studies which may overcome this issue, using a GNSS-R system composed of one direct receiving antenna and two down-looking ones.

8.2. Snow Depth Determination

i. Politecnico di Torino, Torino 2014

Measurement Campaign	Yuekun Pei - 2014
Location	Politecnico di Torino (roof)
Setup	• Fixed antenna • Elevation of 45° • Compact Hackberry based receiver (Figure 33)

Table 33: Snow Depth POLITO setup

Fixed antenna dual polarization (LHCP/RHCP) antenna working in GPS L1/L2 band produced by Antcom Corporation [Antcom Corperation].

Figure 55: Snow Depth measurement antenna (Pei, 2014)

And whose datasheet is shown on Figure 56.

FREQUENCY:	L1: (1575.42 ±12) MHz		L2: (1227.60 ±12) MHz	
RADIATION PATTERN:	HEMISPHERICAL			
POLARIZATION:	RHCP/LHCP		RHCP/LHCP	
VSWR:	< 1.5:1		< 1.5:1	
IMPEDANCE:	50 ohms		50 ohms	
ANTENNA GAIN (dBic):	Free Space	4 ft G.P.	Free Space	4 ft G.P.
@ 90 ° (ZENITH):	+ 4.7	+ 3.5	+ 3.3	+ 4.9
@ 10 ° Elevation:	- 1.8	- 2.0	- 3.8	- 3.6
@ 20 ° Elevation:	- 0.3	+ 0.8	- 2.0	- 0.1
@ 30 ° Elevation:	+ 1.4	+ 1.8	- 0.5	- 1.8
@ 60 - 90 ° Elevation:	> 3.9	> 2.8	> 2.7	> 3.0
BEAM WIDTH (3dB):	114 Deg.	139 Deg.	106 Deg.	75 Deg.
AXIAL RATIO:	2 dB		2 dB	
LIGHTNING PROTECTION:	DC GROUNDING			
LNA GAIN:	33 dB		35 dB	
LNA NOISE FIGURE:	3.0 dB		3.0 dB	
LNA P1dB Out:	+13 dBm		+13 dBm	
LNA DC POWER:	2.5V/20mA,3V/29mA,3.3V/35mA,(2.5-24)V/<50mA			
POWER HANDLING	1 Watt CW, Optional: 10 Watts 1 Microsec Pulse (-AL-)			

Figure 56: Snow Depth measurement antenna's datasheet (Pei, 2014)

But, as they indicated in their report, the obtained results demonstrated a disagreement with the official data sheet. Thus, they concluded that these antennas are not so ideal for the research, and further verification had to be done.

That is the reason why this researching campaign is presented here barely as a reference point because of its measurements placement, as far as it is a starting point in terms of hardware, software and environment for our study.

ii. NCAR Marshall Field, Colorado 2009

The system used by (K. M. Larson, 2009) was detailed in their research.

Measurement Campaign	**(K. M. Larson, 2009)**
Location	National Center for Atmospheric Research's (NCAR) Marshall Field near Boulder, Colorado (elevation 1728 m)
Setup	• GPS Trimble NetRS receiver with a choke-ring antenna (model TRM29659.00 with SCIT radome), with its phase center ~1.9 m above the ground • Configured to track the L2C signal being transmitted on Block IIR-M GPS satellites: PRN 7, 12, 15, 17, 29, and 31

Table 34: Snow Depth measurements NCAR setup

In short, as far as (K. M. Larson, 2009) measurement campaign got conclusive results about snow depth and equivalent water content, this hardware configuration is to be considered in further studies due to its correctness.

9. Software description

What we manage to do with the software tools is to collect and save on a flash memory all available information on satellites in view and the raw data (direct and reflected signals) and lately be post-process the raw data after the experiment.

9.1. Data acquisition software

i. Skyplot

The prediction of satellite position is a fundamental role for all the measurement campaigns, especially in the GNSS Reflectometry field. Since it exploits the GPS transmitted signal that is reflected off the Earth surface and received by a Low Earth Orbit satellite (LEO) or by a simple GNSS receiver placed at a certain distance from the ground.

For these reasons it is important to know, or better to predict, the satellites position in the sky with respect to a specific space-time coordinates (day, hour, place, etc.) for better signal reception.

Thus, using this web site (https://www.calsky.com/), we are able to locate the satellites' position along their way, obtaining different information.

Particularly, essential information as the satellite identifying number, the azimuth and elevation angle will be reported.

This website also allows you to modify the position of interest where you are around, what makes it possible to calculate the satellite positions from different observation locations.

In order to manage properly the information from the web page, we use a Java program, which generates an output file containing information about the satellites around the observing point (its identification and position), given an input file with specifying the measurement time and date.

Thus, instead of being constantly checking the information from the CalSky web site, we only have to write down an input text file specifying the date and hour when we will be

recollecting data, and then simply running a java program, we are able to obtain an output file with the position of the satellites on the sky relative to our location.

The process should be the following summarized on Figure 57 and Figure 58.

Figure 57: CalSky Software Flow I

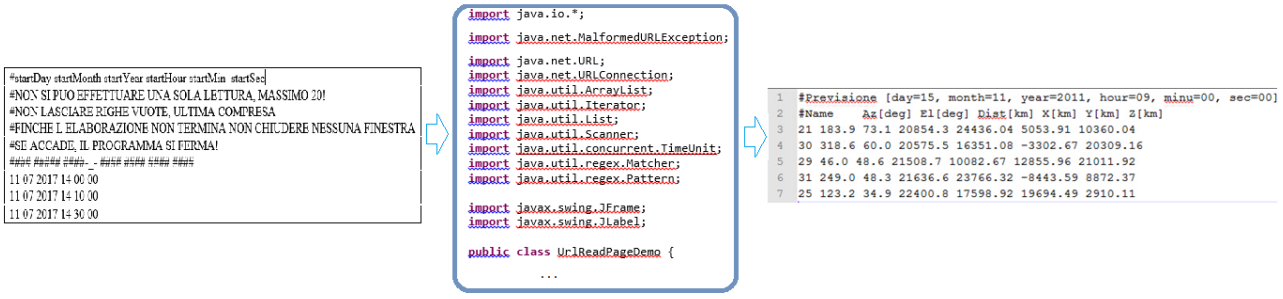

Figure 58: CalSky Software Flow II

Detailed information about the functioning of this software tool can be found in the chapter 1.1. Skyplot from the Appendix.

ii. Matlab scripts for satellite position plots

Helping to complete the prediction of specular point placed on the ground, this software is used to show the sky plot using an input file that will be the output ones from the Java program on step 9.1.i.Skyplot.

Firstly, we have to move these files into a folder, whose oath will be added in the Matlab program in the input file location. Then there are some options providing to modify the height of the antenna, direction of the antenna and the receiver location, which depends on the setup of the measurement:

```
%-----------------------------------------
satelliti=dati_sat('E:\GNSS-Soilmoisure\meas predi_v1\ReflectionMaps\predizioni 20150
%-----------------------------------------
% orientamento antennahelp colormap
%-----------------------------------------
B3dBHalf=120/2; % ang/2 3dB antenna  [gradi]
punt=0;       % antenna elevation. 0 when the boresight is perpendicular to ground
ant_az=0;     % azimuth angle of antenna, clockwise to north
altezza_DEM=1.39;  % receiver height to the ground
zone_limit=[-20 20]; % dimension limit on x-y plane of specular point map
%-----------------------------------------
% Dati di posizione del ricevitore
%-----------------------------------------
centerPoint.lat=45.065278;
centerPoint.long=7.591990;
centerPoint.EGM96_alt=287;        % receiver position ground height wrt mean sea level
```

Figure 59: Matlab parameters

iii. N-Grab

N-Grab has been developed by the NavSAS, which is a joint group from Politecnico di Torino and Istituto Superiore Mario Boella, focused on navigation and localization research topics.

As the NavSAS group specify in the N-Grab User Manual, this is a fully software tool able to record all the samples coming from a GNSS Front End (FE). The key point of N-Grab is that is not locked to a determined FE, so it can record samples from different FEs.

It is able to sample signal from an antenna using 8 bits per sample and pass them to a host PC working with Linux (desirable Linux Kernel posix 2.6 with Debian software packages), to which the FE is connected by a simple USB link.

When the recording is performed, N-Grab creates the output file and automatically chooses the name of the file as for example *usedFE_yyyymmdd_hhmmss_suffix.grab*.

This gives us information about the recording as *usedFE* is a string that represents the FE used for recording, the string *yyyymmdd_hhmmss* represents the date and the time of the start

of the recording (year, month, day, hours, minutes, seconds), and *suffix* gives information about the type of the inner data.

More extended information is given in the chapter 1.3 of the Appendix.

9.2. Data post processing software

This would be the last step we use to measure the soil moisture and dielectric constant of the ground by using this GNSS-R system.

The point of post processing the recollected data is to obtain from the measured values the SNR for both RHCP and LHCP signals (direct and reflected one) in order to extract from there the dielectric constant.

gIndeed, this Matlab software will be in charge of computing the pertinent calculations, as studied in the theoretical explanation of chapters 3 and 6, to retrieve the dielectric constant from the measured data as seen in chapter 6.2.

The main program we are using is the “SNR_computation.mat” file, which should be found in a folder “SNR_computation.mat” (the folder name is not important) together with the following files (schema from the main “SNR_computation.mat”folder):

a) Folder: SNR computation:
    i) Folder: DataTest:
        (1) File: “SIGE_ AAAAMMDD_hhmmss_rawDR.grab” which is the output file ftom the step iii (N-Grab).
    ii) Folder: DDM:
        (1) Floder: risultati

        (The following are Matlab functions used by the main “SNR_computation.mat”)
        (2) File: apribinRangeC2IQ_1bit.mat
        (3) File: codegen.mat
        (4) File: DDM.mat

(5) File: DDMPRCS.mat
(6) File: digitizg.mat
(7) File: longSignalAcquisitionCDC.mat
(8) File: matrice_CDC.mat

iii) File: fc_setting.mat that is a matlab function used by the main "SNR_computation.mat"
iv) File: SNR_computation.mat which is the main function

Once we are sure we have everything correctly, we define the relevant parameters in the "SNR_computation.mat" program as we need and we proceed to run it.

Further information about the functioning of this software tool can be found in the chapter 2. Data post processing software from the Appendix.

10. Conclusions

Global Navigation Satellite System Reflectometry is based on receiving GNSS reflected signals either from the sea or from the Earth, and comparing them in order to obtain information about these surfaces compositions.

In this thesis various applications of GNSS-R systems have been studied both from a theoretical and experimental point of view, together with the inner potential developments for the use of this technology.

Particular attention has been payed on the use of this technique for soil moisture retrieval and for snow depth determination.

First of all, a theoretical approach to the GNSS-R technology is presented in the first chapters. In Chapter 1 an overview of the history and current status of these systems is shown, and in chapters 2 and 3 the functioning principles of GNSS and GNSS-R are conscientiously studied respectively.

Meanwhile, in Chapter 4, we analyse the acquisition method used in the GNSS-R measurements.

Furthermore, deeper study has been conducted about the possible evolution of these GNSS-R schemas, analysing and proposing linearly polarized antennas' setups that could successfully, not only catch up with the functionality of the circularly polarized ones, but also overcome them in many aspects (Chapter 5).

The capability of measuring soil moisture from the signal of Global Navigation Satellite System (GNSS) reflected on the Earth surface has been deeply analysed. Indeed, these studies have given conclusive results that ensure the effectivity of using GNSS-R circularly polarized systems for determining the characteristics of soil and its moisture content (Chapter 6).

When looking up into the recent researches on linearly polarized systems, it comes up the potential of using them for snow depth determination purposes. That is the reason why more investigation about snow depth measurements campaigns has been conducted, leading us to

study the campaign of NCAR Marshall Field (K. M. Larson, Can we measure snow depth with GPS receivers?, 2009).

Taking into account the location where the Politecnico di Torino is and the usual weather conditions in this area, the study of snow depth determination using GNSS-R systems was also possible in previous years.

Giving out relevant and conclusive retrievals from this research, it is easy now to conclude that GNSS-R linearly polarized systems are a great option for measuring snow depth and equivalent water content (Chapter 7).

References

A. Egido, M. C. (2012). Global Navigation Satellite Systems reflectometry as a remote sensing tool for agriculture. In M. C. A. Egido, *Remote Sensing, vol. 4, no. 8* (pp. 2356–2372).

Adnan Kavak, G.-H. X. (1996). GPS Multipath Fade Measurements to Determine L-Band Ground Reflectivity Properties. *20th NASA Propagation Experimenters Meeting.* Texas Univ.; Electrical Engineering Research Lab.; Austin, TX United States.

Agency, E. S. (2016, December 15). *Galileo begins serving the globe*. Retrieved from http://www.esa.int/Our_Activities/Navigation/Galileo_begins_serving_the_globe

BBC. (2012, December 27). *China's Beidou GPS-substitute opens to public in Asia*. Retrieved from BBC: http://www.bbc.com/news/technology-20852150

Beckmann, P., & Spizzichino, A. (1963). *The roughness of the terrain, on which depend the characteristics of the waves from rough surfaces.* Ed. by V. A. Fock and J. R. Wait. Vol. 4. Pergamon Press.

Beckmann, P., & Spizzichino, A. (1963). *The scattering of electromagnetic waves from rough surfaces.* Norwood: Artech House.

Berardelli, P. (2009). GPS: Got plenty of snow? *Science*.

Berginc, G., & Bourrely, C. (2007). Small-slope approximation method: a further study of vector wave scattering from two-dimensional surfaces and comparison with experimental data. *Progress In Electromagnetics Research, Vol. 73*, 251-287.

Block, Y., Wdowinski, S., Fang, P., Zhang, J., Williams, S., Johnson, H., . . . Gurtner, W. (1997, August 10). Southern California Permanent GPS Geodetic Array: Continuous measurements of regional crustal deformation between the 1992 Landers and 1994 Northridge earthquakes. *Journal of Geophysical Research: Solid Earth Volume 102, Issue B8*.

Bock, Y., Wdowinski, S., Fang, P., Zhang, J., Williams, S., Johnson, H., . . . Gurtner, K. S. (n.d.).

Campanella, M. (2014). GNSS-R: Circular Polarization. *GNSS-R: Circular Polarization.* Politecnico di Torino, Torino.

Cardellach, E., Fabra, F., Nogués-Correig, O., Oliveras, S., & Rius, S. R. (2011). GNSS-R ground-based and airborne campaigns for ocean, land, ice, and snow techniques: Application to the GOLD-RTR data sets. *Radio Science, 46(6)*, 1-16.

Carreno-Luengo, H., Amèzaga, A., Vidal, D., Olivé, R., Munoz, J. F., & Camps, A. (2015). First Polarimetric GNSS-R Measurements from a Stratospheric Flight over Boreal Forests. *Remote Sensing 7(10)*, 13120-13138.

Clarizia, M. P. (2009, January 29). *Analysis of GNSS-R delay-Doppler maps from the UK-DMC satellite over the ocean.* Retrieved from Geophysical Research Letters (AGU): https://sites.agu.org/

Commission, E. (2015, December 30). *Galileo's contribution to the MEOSAR system*. Retrieved from http://ec.europa.eu/growth/sectors/space/galileo/sar/meosar-contribution/

Constellation Information | European GNSS Service Centre. (2017, 06 06). Retrieved from https://www.gsc-europa.eu/system-status/Constellation-Information

D. Masters, P. A. (2004). Initial results of landreflected GPS bistatic radar measurements in SMEX02. In P. A. D. Masters, *Remote Sens. Environ., vol. 92, no. 4* (pp. 507–520).

De Roo, R. D., & Ulaby, F. T. (1994). Bistatic Specular Scattering from Rough Dielectric Surfaces. *IEEE transaction on antennas and*, 220-231.

Dobson, M. M., Ulaby, F. T., & Hallikainen, T. (1985). Microwave Dielectric Behavior of Wet Soil-Part II: Dielectric Mixing Models. *IEEE Transaction on Geoscience and remote sensing 23.1*, 35-46.

E. D. Gutmann, K. M. (2012). Snow measurement by GPS interferometric. *Hydrol. Process., vol. 26*, 2951-2961.

Egido, A., Caparrini, M., Ruffini, G., Paloscia, S., Santi, E., Guerriero, L., . . . Floury, N. (2012). Global navigation satellite systems reflectometry as a remote sensing tool for agriculture. *Remote Sens., 4(8)*, 2356–2372.

Egido, A., Paloscia, S., Motte, E., Guerriero, L., Pierdicca, N., Caparrini, M., . . . Floury, N. (2014). Airborne GNSS-R Polarimetric Measurements for Soil Moisture and Above-Ground Biomass Estimation. *IEEE Journal of Selected Topics in Applied Earth Observations and Remote Sensing, 7(5)*, 1532.

Federal Standard 1037C. (n.d.). *Public domain material from the General Services Administration (in support of MIL-STD-188).*

Garrison, J. (2016). Remote Sensing with Signals of Opportunity. *LSGI Distinguished Lecture Series*.

Gleason, S. (2005). Processing of bistatically reflected GPS signals from low Earth orbit for the purpose of ocean remote sensing. *IEEE Transactions on Geoscience and Remote Sensing (Volume: 43, Issue: 6, June 2005)*, 1229 - 1241.

Hegarty, C. G., & Chatre., E. (2008). Evolution of The Global Navigation Satellite System (GNSS). *Proceedings of the IEEE, Vol. 96, Nº 12*, 1902.

Hofmann-Wellenhof, Bernhard, Lichtenegger, Herbert, Wasle, & Elmar. (2008). *GNSS – Global Navigation Satellite Systems.*

http://www.coregalproject.com/pages/technology. (n.d.).

Initial results of landreflected GPS bistatic radar measurements in SMEX02. (2004). In P. A. D. Masters, *Remote Sens. Environ., vol. 92, no. 4* (pp. 507–520).

Jia, Y. (2014). *Global Navigation Satellite System Reflectometry for Land Applications.* Turin: PhD Thesis in Electronics and Telecommunications Eng., Politecnico di Torino.

Jin, S. (2014). Theory of GNSS Reflectometry. In E. C. Shuaggen Jin, *GNSS Remote Sensing: Theory, Methods and Applications* (pp. 175-177). Springer Netherlands.

K. M. Larson, E. D. (2009). Can we measure snow depth with GPS receivers? *Geosci. Res. Lett., vol. 36, p. L17502*.

Kavak, A., Vogel, W. J., & G. Xu. (1998, February 5). Using GPS to measure ground. *Electron. Lett. vol. 34, no. 3*, pp. 254-255.

Kavak, A., Xu, G., & Vogel, W. J. (1996). GPS multipath fade measurements. *Proc. 20th NASA Propagation Experimenters Meeting.*

Kershner, R. B., & McClure, F. T. (1998). *The Legacy of Transit: A Dedication.*

Kristine M. Larson, E. E. (2008, December 24). Use of GPS receivers as a soil moisture network for water cycle studies. *Geophysical Research Letters*.

Larson, K. M., & Small, E. E. (2014). Normalized Microwave Reflection Index: A Vegetation Measurement Derived From GPS Networks. *IEEE Journal of Selected Topics in Applied Earth Observations and Remote Sensing, Volume: 7, Issue: 5*, 1501 - 1511.

Li, W., Rius, A., Fabra, F., Martín-Neira, M., Cardellach, E., Ribó, S., & Yang, D. (2016). The Impact of Inter-Modulation Components on Interferometric GNSS-Reflectometry. *Remote Sensing*.

Li, W., Rius, A., Fabra, F., Martín-Neira, M., Cardellach, E., Ribó, S., & Yang, D. (2016). The Impact of Inter-Modulation Components on Interferometric GNSS-Reflectometry. In W. Li, A. Rius, F. Fabra, M. Martín-Neira, E. Cardellach, S. Ribó, & D. Yang, *Remote Sensing 8 (12)* (p. 1013). Multidisciplinary Digital Publishing Institute.

Martin-Neira, M. (1993, January). A Passive Reflectometry and Interferometry System (PARIS): Application to ocean altimetry. *ESA Journal. 17*, pp. 331-335.

Martin-Neira, M., Kern, M., & D'Addio, S. (2017). Advances in GNSS-R altimetry. *IGARSS (IEEE International Geoscience and Remote Sensing Symposium).*

N. Rodriguez-Alvarez, A. C.-l.-L.-P.-H.-F.-T.-G. (2011). Land Geophysical Parameters Retrieval Using the Interference Pattern GNSS-R Technique. *IEEE Transactions on Geoscience and Remote Sensing, Volume: 49, Issue: 1*, 71 - 84.

National Research Council, D. o. (1995, May 31). The Global Positioning System: A Shared National Asset. *National Academies Press*.

Njoku, E., & O'Neill, P. (1982). Multifrequency microwave radiometer measurements of soil moisture. *IEEE Transactions on Geoscience and Remote Sensing, 4*, 468-475.

Observatory, U. N. (2011, June 7). *USNO NAVSTAR Global Positioning System*. Retrieved from http://tycho.usno.navy.mil/gpsinfo.html

Organization, I. C. (2008). *ICAO Completes Fact-Finding Investigation.*

P. Ferrazzoli, L. G. (1995, 2012 Online). Simulating bistatic scatter from surfaces covered with vegetation. *Journal of Electromagnetic Waves and Applications, vol. 14, no. 2* , pp. 233–248.

Pei, Y. (2014). *GNSS Reflectometry for Land Surface Monitoring and Buried Object Detection.* Turin: PhD Thesis in Electronics and Telecommunications Eng., Politecnico di Torino.

Picardi, G., Seu, R., G. Sorge, S., & Martin Neira, M. (1998, October 10). Vol 46, nº10. *IEEE Transactions On Antennas And Propagation*.

Pinel, N., & Bourlier, C. (2013). *Electromagnetic Wave Scattering from Random Rough Surfaces: Asymptotic Models.* John Wiley & Sons, Inc.

POLARIZATION. (n.d.). Retrieved from RF Cafe: http://www.rfcafe.com/references/electrical/ew-radar-handbook/polarization.htm

Radio spectrum. (2018, April 7). Retrieved from Wikipedia: https://en.wikipedia.org/wiki/Radio_spectrum

Rocken, C. (1997, December 1). Analysis and validation of GPS/MET data in the neutral atmosphere. *Journal of Geophysical Research: Atmospheres Volume 102, Issue D25*, pp. 29849–29866.

Rodriguez-Alvarez, N., Bosch-Lluis, X., Camps, A., Aguasca, A., Vall-llossera, M., Valencia, E., . . . Park, H. (2011). Review of crop growth and soil moisture monitoring from a ground-based instrument implementing the Interference Pattern GNSS-R Technique. *Radio Science, 46(6).*

Shi, J., & J.Dozier. (2000). Estimation of snow water equivalence using SIR-C/X-SAR, Part I: Inferring snow density and subsurface properties. *IEEE Transactions on Geoscience and Remote Sensing, 38*, 2465 – 2474.

Shuanggen Jin, G. F. (2011). Remote sensing using GNSS signals: Current status and future directions. *Advances in Space Research, Volume 47, Issue 10*, 1645-1653.

Stillman, D. (2009). *Plotting surveying data in Google Earth.* Retrieved from http://code.google.com/p/google-earth-plotter

Tao, Z. (2018, 03 02). *BeiDou global expansion*. Retrieved from BeiDou satellite system takes next step in global expansion drive: http://eng.chinamil.com.cn/view/2018-03/02/content_7956923.htm

Ticconi, F., Pulvirenti, L., & Pierdicca, N. (2011). Models for scattering from rough surfaces. In F. Ticconi, L. Pulvirenti, & N. Pierdicca, *Electromagnetic Waves, vol. 10* (pp. 203-226).

Tsang, L., & Kong, J. A. (2002). *Scattering of Electromagnetic Waves: Advanced Topics*. John Wiley & Sons, Inc.

Tsang, L., Kong, J. A., & Ding, K.-H. (2000). *Scattering of Electromagnetic Waves: Theories and Applications.* John Wiley & Sons, Inc.

Ulaby, F. T., Hallikainen, M. T., & Dobson, M. C. (1985). Microwave Dielectric Behavior of Wet Soil-Part I: Empirical Models and Experimental Observations. *IEEE Transaction on Geoscience and remote sensing GE-23.1*, 25-34.

Ulaby, F. T., Moore, R. K., & Fung, A. K. (1982). *Microwave remote sensing: Active and passive, vol. 2.*

Valery U. Zavorotny, S. G. (December 2014). Tutorial on Remote Sensing Using GNSS Bistatic Radar of Opportunity. *IEEE Geoscience and Remote Sensing Magazine, Volume: 2 Issue: 4*, 8-45.

Voronovich, V. U. (2000, March). Scattering of GPS signals from the ocean with wind remote sensing application. *IEEE Trans.Geosci. Remote Sens. Vol 38, nº2*, pp. 951-964.

Wang, J., & Schmugge, T. (1980). An empirical model for the complex dielectric permittivity of soils as a function of water content. *IEEE Transactions on Geoscience and Remote Sensing, 4*, 288-295.

Wang, L. (2016, December 6). *Directions 2017: BeiDou's road to global service*. Retrieved from GPS World: http://gpsworld.com/directions-2017-beidous-road-to-global-service/

Worth, H. E., & Warren, M. (2009). *Transit to Tomorrow. Fifty Years of Space Research at The Johns Hopkins University Applied Physics Laboratory.*

Worth, H. E., & Warren, M. (n.d.). *Transit to Tomorrow. Fifty Years of Space Research at The Johns Hopkins University Applied Physics Laboratory.*

Zavorotny, V., & Voronovich, A. (2000). Scattering of GPS signals from the ocean with wind remote sensing application. *IEEE Transactions on Geoscience and Remote Sensing, 38(2)*, 951-964.

Abbreviations

ADC	Analog to Digital Converter
AFSPC	Air Force Space Command
ASIC	Application Specific Integrated Circuit
BeiDou-1	BeiDou Navigation Satellite System
BeiDou-2	COMPASS
BOC	Binary offset carrier modulation
BPSK	Binary phase-shift keying
CBOC	Cosine BOC
CDMA	Code Division Multiple Access
CDMA	Code Division Multiple Access
DARPA	Defense Advanced Research Projects Agency
DDM	Delay-Doppler Map
DW	Delay Waveform
ECEF	The Earth-centered Earth-fixed
EOC	Early Operational Capability
ESA	European Space Agency
FDMA	Frequency division multiple access
FE	Front End
FFT	Fast Fourier Transformate
FOC	Full Operational Capability
FOC	Full Operational Capability

GDOP	Geometric Dilution of Precision
GLONASS	Global'naya Navigatsionnaya Sputnikovaya Sistema
GNSS	Global Navigation Satellite System
GNSS-R	GNSS reflectometry
GPS	Global Positioning System
HG-A	High Gain-Antenna
IEEE	Institute of Electrical and Electronics Engineers
IEM	The Integral Equation Method
IOC	Initial Operational Capability
IPT	Multipath and Interference Pattern Technique
ITU	International Telecommunication Union
KA	Kirchhoff Approximation
KGO	KA in Stationary-Phase Approximation (Geometric Optics, KGO)
KPO	KA in Physical Optics Approximation
LEO	Low Earth Orbit satellite
LHCP	Left-Handed Circular Polarization
LNA	Low Noise Amplifiers
MBOC	Multiplexed binary offset carrier
MEO	Medium Earth Orbit 20000km and above
NATO	North Atlantic Treaty Organization
NAVSTAR-GPS	NAVigation System and Ranging - Global Position System
NCAR	National Center for Atmospheric Research’s
PGGA	Southern California Permanent GPS Geodetic Array
PRN	Pseudo-Random Noise

PVT	Position, Velocity and Time
QPSK	Quadrature phase-shift keying
RF	Radio Frequecy
RHCP	Right-Handed Circular Polarization
SD	Secure Digital (SD card)
SMP	The small perturbation method
SNR	Signal to Noise Ratio
SSA	The Small Slope Approximation
TDR	Time Domain Reflectometry
UHF	Ultra High Frequencies
USB	universal serial bus.
VSWR	voltage standing wave ratio
WGS84	World Geodetic System
X-pol level	Cross-polarization level

APPENDIX

1. Data acquisition software

1.1. Skyplot

The prediction of satellite position is a fundamental role for all the measurement campaigns, especially in the GNSS Reflectometry field. Since it exploits the GPS transmitted signal that is reflected off the Earth surface and received by a Low Earth Orbit satellite (LEO) or by a simple GNSS receiver placed at a certain distance from the ground.

For these reasons it is important to know, or better to predict, the satellites position in the sky with respect to a specific space-time coordinates (day, hour, place, etc.) for better signal reception.

In order to manage properly the information from the web page, we use a Java program, which generates an output file containing information about the satellites around the observing point (its identification and position), given an input file with specifying the measurement time and date.

The process should be the following:

Figure 60:Process Skypot

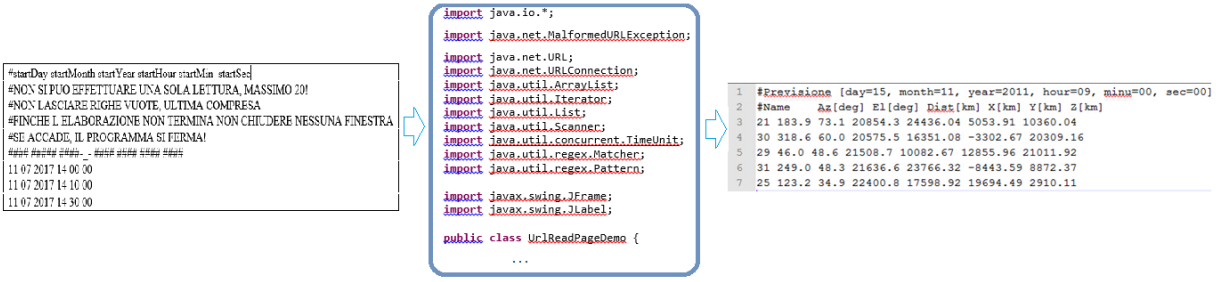

Figure 61: Process Skypot (2)

The first required operation mentioned is implemented through a Java script that analyzes the time information given by user on a simple txt. file, respecting a specific format, specifying the time elapsing between each sampled point and ensuring the black space presence at the end of each written text line as in the following.

The following steps describes how to use the acquisition software, but first of all the equipment needed in order to do so is specified:

- PC with Java, preferably a Developer Kit.
- Optional: an integrated development environment (IDE) as Eclipse (https://www.eclipse.org/downloads), for example. I recommend to use the latest version for developers.
- Internet connection.
- Folder "site_reader" corresponding to the Java Project with the same name. If already downloaded the full project, it should contain the following folders:
    - .metadata
    - .settings
    - src
        - UrlReadPageDemo.class
        - UrlReadPageDemo.java

      As well as it should contain the following files:
    - Text file "file_input.txt"
    - .classpath
    - .project

If not, you should create a Java Project as "site_reader" was supposed to be, containing in its package "src"(default) at least the Main Class "UrlReadPageDemo", which should contain the code explained later on this chapter.

Apart from it, inside the Project folder must be the "file_input.txt" file.

The rest of the folders inside "site_reader" should be automatically generated when compiling and executing the main java class from its "src" package.

Example of "file_input.txt":

```
#startDay startMonth startYear startHour startMin  startSec
#NON SI PUO EFFETTUARE UNA SOLA LETTURA, MASSIMO 20!
#NON LASCIARE RIGHE VUOTE, ULTIMA COMPRESA
#FINCHE L ELABORAZIONE NON TERMINA NON CHIUDERE NESSUNA FINESTRA
#SE ACCADE, IL PROGRAMMA SI FERMA!
#### ##### ####-_- #### #### #### ####
11 07 2017 14 00 00
11 07 2017 14 10 00
11 07 2017 14 30 00
```

Once we created the input file, it is required to calculate the real-time satellite movements in the space on website www.calky.com.

Please note that the Calsky website goes back of two years, thus you should define a valid date for the measurements in the "file_input.txt".

This website allows also to modify the position of interest where we are around which is possible to calculate the satellite positions, thus you should specify your position. In the main page of the website, we choose "astronomer" from the pop menu.

The program flow should be the following:

1. Edit/Create "file_input.txt".
2. Run UrLReadPageDemo.java
    a. Option 1 - Using an IDE as Eclipse: Run directly the java class.
    b. Option 2 - Without an IDE:
        i. Open CMD (Windows → Search "CMD")
        ii. Open the "site_reader" directory using *dir* to see the files names along the folders; *cd \myFolder* to go inside a directory; *javac UrLReadPageDemo.java* to compile the JDK program ("UrLReadPageDemo.java"); and finally *java UrLReadPageDemo* to run the program.
3. A file called "output_DDMMYYYY_HHMM.txt" should appear as a result of this process inside the "site_reader" folder.

The Java program “UrLReadPageDemo” should be as follows:

```
import java.io.*;
import java.net.MalformedURLException;
import java.net.URL;
import java.net.URLConnection;
import java.util.ArrayList;
import java.util.Iterator;
import java.util.List;
import java.util.Scanner;
import java.util.concurrent.TimeUnit;
import java.util.regex.Matcher;
import java.util.regex.Pattern;

import javax.swing.JFrame;
import javax.swing.JLabel;

public class UrlReadPageDemo {

	static Satellite[] sat_array = new Satellite[20]; // NUMERO MASSIMO DI
PREVISIONI
	static Previsione[] Prev_curr = new Previsione[20]; //NUMERO MASSIMO DI
PREVISIONI
	static int num_previsioni = 1;
	static int j = 1;

	public static void main(String[] args) {

		//ATTENZIONE!!
		//SE PER CASO I FILE DI USCITA CHE DOVREBBERO CONTENERE XYZ SONO
VUOTI
		// E' PERCHE NON SEI AUTENTICATO SULLA PAGINA, QUINDI ENTRA ED
IMPOSTA LE TUE COORDINATE

	//http://www.calsky.com/?GPS=obs=86401006796313&cha=12&sec=12&sub=0&startDa
y=28&startMonth=8&startYear=2011&startHour=16&startMin=2&startSec=51&startHSec=0&t
imebuild=&interval=1&step=1&Go.x=19&Go.y=21
		//QUESTA è UNA RICERCA D'ESEMPIO DELL URL-ENCODED

		//FILE DI NOME "data[0-n]" CONTENGONO LA PAGINA HTML FINO ALLE RIGHE
DI XYZ[INCLUSE!] E'UTILE
		//PER VEDERE SE C'E QUALCOSA CHE NON VA', E NEL CASO CHE XYZ NON
VENGANO RESTITUITI, SI PUO VERIFICARE COSA
		//QUAL' E' STATA L
		int num_letture = 1;

		try {
			List<String> ls = URL_maker_from_file();
	///QUESTA è LA PARTE DOVE ITERO SUGLI
			Iterator<String> it=ls.iterator();                    ///
			ELEMENTI PRESENTI SUL FILE IN INGRESSO
			createAndShowGUI(new JFrame() ,"Loading...");
```

```
                    while(it.hasNext()) {
                          URL url = new URL(it.next().toString());
                          //////Output.println(line);
                          set_satellite(url);
                          createAndShowGUI(new JFrame(), "stampato file " +
num_letture);
                          print_file_and_clean_all(num_letture++);
                    }
                    createAndShowGUI(new JFrame() ,"PROGRAM FINISHED! CLOSE ALL
THE WINDOWS");
                    // writer.close();                    ///PRINT DATA.HTML
              } catch (MalformedURLException e) {
                    e.printStackTrace();
              }  catch (IOException e) {
                    e.printStackTrace();
              }
              return;
        }

        public static void set_satellite(URL url) throws IOException {
              URL satellite_url;

              BufferedReader reader = new BufferedReader(new
InputStreamReader(openUrlStream(url)));

              ////FileOutputStream printer = new FileOutputStream("full_page.htm");
              ////PrintStream html_printer = new PrintStream(printer);

              //////FileOutputStream file = new
FileOutputStream("tabella_satelliti.htm");
              //////PrintStream Output = new PrintStream(file);

              ///FileOutputStream file_out = new FileOutputStream("file_link.htm");
              ///PrintStream Output_link = new PrintStream(file_out);

              Matcher m;

              String line;
              String new_L;
              int line_skipped = 450;
              int line_curr = 1;

              while ((line = reader.readLine()) != null) {
                    /*
                    if (line_curr <= line_skipped)
                    {
                     line_skipped++;
                     continue;
                    }
                     */

                    //html_printer.println(line);
```

```
                    if(line.contains("csrender"))//csrender
                    {

                          int start=line.indexOf("csrender");
                          int end=line.indexOf("\"><IMG");
                          new_L=(String) line.subSequence(start,end) ;
                          ////
                          line=line.substring(end).replace(" ", " ");
                          ////

      //////Output_link.println("http://www.calsky.com/"+new_L);      ///PRINT
FILE_LINK.TXT
                          satellite_url=new URL("http://www.calsky.com/"+new_L);
                          ///ADESSO MI PROCURO IL NOME J-ESIMO
                          //reader.readLine();

                          m = Pattern.compile("PRN (\\d+)/GPS").matcher(line);
                          m.find();
                          sat_array[j]=new Satellite(m.group(1));


                          get_coordinate(satellite_url,j);

                          // {
                          m =
Pattern.compile("az:.*?(\\d+\\.?\\d*)&deg;.*?h:.*?(\\d+\\.?\\d*)&deg;.*?dist:.*?(\
\d+\\.?\\d*)km").matcher(line);
                          m.find();
                          sat_array[j].setAz(Double.parseDouble(m.group(1)));
                          sat_array[j].setEl(Double.parseDouble(m.group(2)));
                          sat_array[j].setDist(Double.parseDouble(m.group(3)));
                          ////////////////////////////////////////////////
                          j++; //incremento dovuto all allocazione di un nuovo
satellite.
                    }
                    // }
                    if(line.contains("smallprint"))
                          break;
      ///salto tutto l'html intuile
            }
      }


      public static void get_coordinate(URL url, int n) {
            try {

                    BufferedReader reader = new BufferedReader(new
InputStreamReader(openUrlStream(url)));
                    // BufferedWriter writer = new BufferedWriter(new
                    // FileWriter("data_"+n+".html"));
```

```
                    // FileOutputStream file = new
                    //
FileOutputStream("file_coordinate"+n+"_"+getDateTime()+".txt");
                    // PrintStream Output = new PrintStream(file);

                    String line;
                    while ((line = reader.readLine()) != null) {
                          if (line.contains("Rotating Coordinates"))// è la prima
riga
                                // utile dell html
                          {
                                reader.readLine();

                                while ((line = reader.readLine()) != null) {

                                      // Output.println(line);
///FILE_COORDINATE%D.....TXT
                                      // writer.write(line); ///FILE DATA_%D.HTML
                                      // writer.newLine(); ///FILE DATA_%D.HTML

                                      int start = line.indexOf("X     =")
                                      + ("X     =".length());
                                      int end = line.indexOf("km    Y     =");
                                      String num_str = line.substring(start,
end);
                                      double X = new Double(num_str);
                                      sat_array[n].setX(X);

                                      start = end + ("km    Y     =".length());
                                      end = line.indexOf("km    Z     =");
                                      num_str = line.substring(start, end);
                                      double Y = new Double(num_str);
                                      sat_array[n].setY(Y);

                                      start = end + ("km    Z     =".length());
                                      end = (line.length() - 5);
                                      num_str = line.substring(start, end);
                                      double Z = new Double(num_str);
                                      sat_array[n].setZ(Z);

                                      return;
                                }

                                reader.close();
                                // writer.close(); ///FILE DATA_%D.HTML
                                return;
                          }

                          else {
                                // writer.write(line); ///FILE DATA_%D.HTML,
parte prima di
                                // quella che cerco
```

```
                                    // writer.newLine(); ///FILE DATA_%D.HTML
                              }
                        }

                        reader.close();
                        // writer.close();; ///FILE DATA_%D.HTML

                  } catch (MalformedURLException e) {
                        e.printStackTrace();
                  } catch (IOException e) {
                        e.printStackTrace();
                  }
                  return;
            }

            public static InputStream openUrlStream(URL url) throws IOException {
                  URLConnection hc = url.openConnection();
                hc.setRequestProperty("User-Agent", "Mozilla/5.0 (Macintosh; U; Intel
Mac OS X 10.4; en-US; rv:1.9.2.2) Gecko/20100316 Firefox/3.6.2");
                  return hc.getInputStream();
            }

            public static List<String> URL_maker_from_file() throws
MalformedURLException, FileNotFoundException {

                  // BufferedWriter writer = new BufferedWriter(new
                  // FileWriter("data.html"));
                  List<String> list = new ArrayList<String>();

                  // String NL = System.getProperty("line.separator");
                  Scanner scanner = new Scanner(new FileInputStream("file_input.txt"));
                  scanner.useDelimiter(" ");

                  try {
                        while(scanner.hasNextLine()) {
                              String first_word=new String(scanner.next());
                              if(first_word.contains("#")) {
                                    //scanner.
                                    scanner.nextLine();
                                    continue;
                              }

                              String day = new String(first_word);
                              String month = new String(scanner.next());
                              String year = new String(scanner.next());
                              String hour = new String(scanner.next());
                              String minu = new String(scanner.next());
                              String sec = new String(scanner.next());

                              Prev_curr[num_previsioni++] = new Previsione(day, month,
year, hour, minu, sec);
```

```
      list.add("http://www.calsky.com/?GPS=obs=86401006796313&cha=12&sec=12&sub=0
&startDay="
                                          + day
                                          + "&startMonth="
                                          + month
                                          + "&startYear="
                                          + year
                                          + "&startHour="
                                          + hour
                                          + "&startMin="
                                          + minu
                                          + "&startSec="
                                          + sec
                                          +
"&startHSec=0&timebuild=&interval=1&step=1&Go.x=19&Go.y=21");
                              scanner.nextLine();
                        }
                } finally {
                        //scanner.close();
                }
                return list;
        }

        public static void print_file_and_clean_all(int number) throws
FileNotFoundException {

                FileOutputStream file_out = new FileOutputStream("output_" +
                              Prev_curr[number].getDay() + Prev_curr[number].month +
Prev_curr[number].getYear() +
                              "_" + Prev_curr[number].getHour() +
Prev_curr[number].getMinu() + ".txt");
                PrintStream Output = new PrintStream(file_out);

                Output.println("#" + Prev_curr[number].toString());
                Output.println("#Name    Az[deg] El[deg] Dist[km] X[km] Y[km]
Z[km]");

                for(int i = 1; i < j; i++) {
                        Output.println(sat_array[i].getName() + " " +
sat_array[i].getAz()
                                        + " " + sat_array[i].getEl() + " " +
sat_array[i].getDist()
                                        + " " + sat_array[i].getX() + " " +
sat_array[i].getY()
                                        + " " + sat_array[i].getZ());
                }
                sat_array = new Satellite[15];
                j=1;
                return;

        }
```

```
	public static int first_number_index(String str, int start) {
		int i = start;
		Character c;
		while(i < str.length()) {
			c=str.charAt(i);
			if(Character.isDigit(c)) {
				return i;
			} else
				i++;
		}
		return -1;
	}

	public static int last_double_number_index(String str, int start) {
		int i = start;
		Character c;
		while(i<str.length()) {
			c=str.charAt(i);
			if(Character.isDigit(c) || c.compareTo('.') == 0) {
				i++;
			} else
				return i-1;
		}
		return -1;
	}

	public static void print_txt_from_html(URL url) throws IOException {
		BufferedReader reader;
		FileOutputStream printer;
		try {
			printer = new FileOutputStream("main_page.html");
			reader = new BufferedReader(new
InputStreamReader(openUrlStream(url)));
			PrintStream html_printer = new PrintStream(printer);
			String line;
			while((line = reader.readLine()) != null)
			{
				html_printer.println(line);
			}
			printer.close();
			reader.close();
			html_printer.close();
		} catch (FileNotFoundException e) {
			e.printStackTrace();
		}
	}

	private static JFrame createAndShowGUI(JFrame frame,String str) {
		//Create and set up the window.
		frame = new JFrame("Site_reader ----> RUNNING");
		frame.setDefaultCloseOperation(JFrame.EXIT_ON_CLOSE);
```

```
            //Add a label.
            JLabel label = new JLabel(str);
            frame.getContentPane().add(label);
            //Display the window.
            frame.setSize(200, 100);
            //frame.pack();
            frame.setVisible(true);
            return frame;
    }

}
```

The Java program creates one output text file for each point that previously set in the input file. In this file, different information will be reported, especially the satellite identifying number, the azimuth and elevation angle, the most useful data in the experimental applications. An example of output text file is shown in Figure 62: Output.

It is important to notice that the Java program has been redefined to read the web site autonomously and modifying the url's user agent when doing so in order to not be identified as a bot by the web's security.

Thus, it is recommendable not to be constantly running this code, what could appear to be a bot's action.

```
1  #Previsione [day=15, month=11, year=2011, hour=09, minu=00, sec=00]
2  #Name    Az[deg] El[deg] Dist[km] X[km] Y[km] Z[km]
3  21 183.9 73.1 20854.3 24436.04 5053.91 10360.04
4  30 318.6 60.0 20575.5 16351.08 -3302.67 20309.16
5  29 46.0 48.6 21508.7 10082.67 12855.96 21011.92
6  31 249.0 48.3 21636.6 23766.32 -8443.59 8872.37
7  25 123.2 34.9 22400.8 17598.92 19694.49 2910.11
```

Figure 62: Output

1.2. Matlab scripts for satellite position plots

Helping to complete the prediction of specular point placed on the ground, this software is used to show the sky plot using an input file that will be the output ones from the Java program on step 1.1 (Figure 62: Output).

Firstly, we have to move these files into a folder, whose path will be added in the Matlab program in the input file location. The main. m file contains all the function that will be used.

Then there are some options providing to modify the height of the antenna, direction of the antenna and the receiver location, which depends on the setup of the measurement:

```
%-------------------------------------------
satelliti=dati_sat('E:\GNSS-Soilmoisure\meas predi_v1\ReflectionMaps\predizioni 20150
%-------------------------------------------
% orientamento antennahelp colormap
%-------------------------------------------
B3dBHalf=120/2; % ang/2 3dB antenna  [gradi]
punt=0;       % antenna elevation. 0 when the boresight is perpendicular to ground
ant_az=0;     % azimuth angle of antenna, clockwise to north
altezza_DEM=1.39;  % receiver height to the ground
zone_limit=[-20 20]; % dimension limit on x-y plane of specular point map
%-------------------------------------------
% Dati di posizione del ricevitore
%-------------------------------------------
centerPoint.lat=45.065278;
centerPoint.long=7.591990;
centerPoint.EGM96_alt=287;        % receiver position ground height wrt mean sea level
```

Figure 63: Matlab parameters

The MATLAB® prediction script is used for showing the sky plot. So, we created a table that contains the detailed description of the files and functions.

A list of files and functions that can help us to get a brief view of the structure of the software is presented as follows:

name	type	description
Magazzino	folder	Folder stores output file
Predizioni3	folder	Folder stores output file
EGM96.DAC	.DAC	Data file used in EGM96_undulation.m and EGM96_undulation_reverse.m
EGM96_undulation.m	.m	Sub-function of main.m;
EGM96_undulation_reverse.m	.m	Sub-function of main.m;
IsoRange.m	.m	Compute the isotropic range
Lampedusa.kml	.kml	
dati_sat.m	.m	Sub-function of main.m; Used to retrieve output files
deg2utm.m	.m	Convert lat/lon vectors into UTM coordinates (WGS84)
ecef2lla.m	.m	Sub-function of main.m; Convert earth-centered earth-fixed (ECEF) Cartesian coordinates to latitude, longitude, and altitude
footprint.m	.m	Sub-function of main.m; Obtain the footprint of specific coordinates and antenna parameters
getLatLong.m	.m	Get the latitude and longitude from a specific file
get_google_map.m	.m	Sub-function of main.m; Gets a Google Maps™ using the Google Static Maps API
lla2ecef.m	.m	convert latitude, longitude, and altitude to earth-centered, earth-fixed (ECEF) Cartesian

main.m	.m	Main function
main_Fresnel.m	.m	Main function of Fresnel field graph
main_skyplot.m	.m	Main function of sky plot graph
main_spec_google.m	.m	Main function of Google Maps™ projection graph
mappa_riflessioni.m	.m	One specific function to resolve satellite position
mappa_riflessioni_new.m	.m	One specific function to resolve satellite position
plottaTracciaSatelliti.m	.m	Plot the trace of satellites on Google Maps™
polar_plot.m	.m	Sub-function of main.m; invoke polar plot
polargrid.m	.m	adds grid lines to axes
resolveF.m	.m	Resolve the first input argument which satisfy the specific conditions
rotazione.m	.m	Sub-function of main.m;
trovaRaggio.m	.m	Resolve the radius given latitude in degree

1.3. N-Grab

N-Grab has been developed by the NavSAS, which is a joint group from Politecnico di Torino and Istituto Superiore Mario Boella, focused on navigation and localization research topics.

As the NavSAS group specify in the N-Grab User Manual, this is a fully software tool able to record all the samples coming from a GNSS Front End (FE). The key point of N-Grab is that is not locked to a determined FE, so it can record samples from different FEs.

All the descriptions and procedures explained in this chapter are extracted from the N-Grab User Manual (N-Grab GNSS data grabber User Manual SW Version 1.5.3, NavSAS Group, 19/04/2010).

It is able to sample signal from an antenna using 8 bits per sample and pass them to a host PC working with Linux (desirable Linux Kernel posix 2.6 with Debian software packages), to which the FE is connected by a simple USB link.

1.3.1. Minimum Requirements to Install N-Grab

N-Gene can be installed in any modern personal computer PC (desktop or laptop) having the following minimum requirements:

- Operating System: Linux Kernel posix 2.6 with Debian software packages (*.deb*)
- RAM: 512 MB;
- Free HD space: 20 GB suggested for data recording; in order to be able to record samples, used hard disk should be at least 7200 rpm.;
- Hardware: GPS antenna, a compatible USB front-end, and relative cables are needed to elaborate in real-time samples from an antenna; USB 2.0 port is needed to meet required throughput.

It is possible to verify the presence of the chosen FE executing the command *lsusb* in a terminal window, it will show any of these outputs:

FE	VID	PID
Fraunhofer	0x04b4	0x0085
SIGE	0x16c0	0x072f
NavSAS prototype	0x04b4	0x0085

Figure 64: FEs

1.3.2. Installation

For initiating the installation, you should ensure that you are logged in an user account with administrative privileges, as well as ensure a good internet connection.

N-Gene installation process will detect automatically the presence of all required packages in the system and will connect to the standard Linux repository in order to download and install the missing ones.

Then follow the next steps:

I. Put the N-Grab DVD in the driver (Ubuntu should mount automatically the DVD and open a File Manager window showing the content of the DVD)

I. Double click on the icon *gnss-frontend-fw-0.1.deb*: this opens the installation packet (Figure 65). Now user can launch the installation procedure by clicking the button labeled *Install Package*: after this, the packet manager asks the user for the password to administrate the system. After this password has been entered correctly, the packet manager installs all the required files and, finally, shows the message of *Installation Finished* (Figure 66). Now user can close the installation windows.

II. Double click on the icon *ngrab-1.5.2-i386.deb*. Requested operations are the same as in the installation of *gnss-frontend-fw-0.1.deb.*

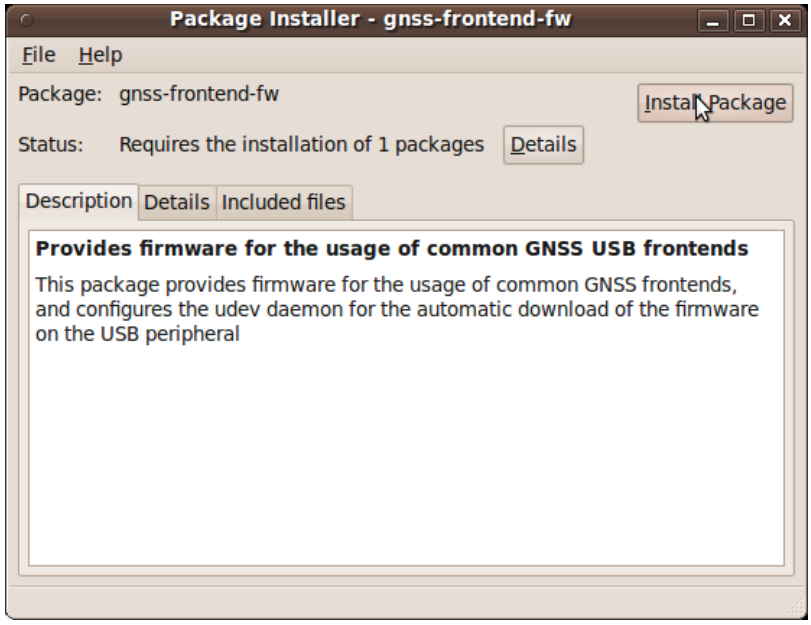

Figure 65: Opening and installing the package

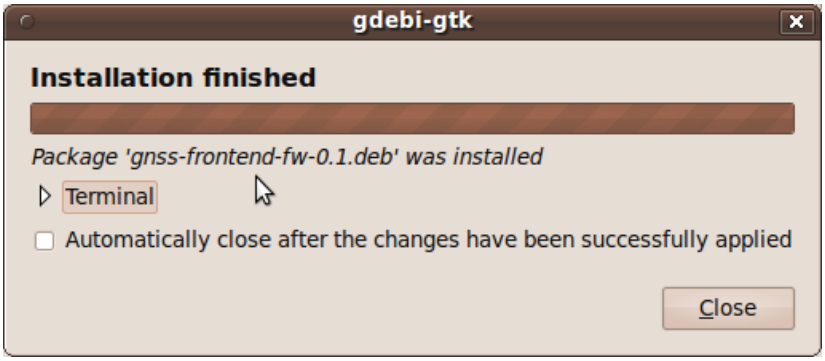

Figure 66: The conclusion of installation procedure

1.3.3. Launching and Recording

- From the terminal: command *ngrab &*.
- Directly executing the program from the directory *Applications/Accessories/NGrab.*

When before start collecting data, you should fix the available parameters in the *Options* menu.

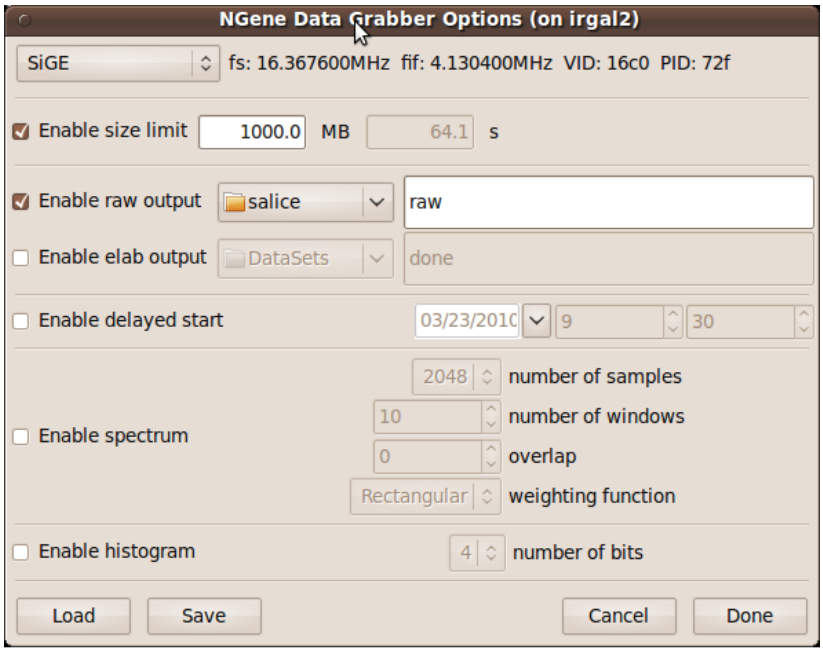

Figure 67: N-Grab options window

The selectable options are the following, corresponding to each section in the Figure 68:

(1) FE choice: choose the used FE, then the Vendor ID (VID), Product ID (PID), the sampling frequency (fs) and the intermediate frequency (fif) will appear on the right.

(2) *Enable size limit:* N-Grab automatically stops the recording when the file reaches the size limit chosen. The size limit is indicated in megabytes that are automatically converted into seconds.

(3) Type of output data: FE native format (raw), 8 bit signed integer format (elaborated) or even both of them. The raw format is compatible with N-Gene software receiver, whereas the elaborated format is useful for all the receivers that are not specifically suited for the used FE.

It is possible to choose the folder where data will be saved as well as the file's suffix.

(4) Delayed start: then, after pressing the *Start Grabber* N-Grab until the clock of the PC reaches the time chosen by the user to start writing samples on the disk. It will stop only when pressing the *Stop Grabber* button.

(5) Signal analysis options: real time spectrum analysis of the samples:

- *number of samples* per FFT
- *number of windows* (FFTs) per results
- o*verlap:* adjacent windows can be overlapped to reduce the number of samples
- *weighting function* for input, as *Rectangular*, *Triangular*, *Hanning*, and *Hamming* functions

(6) Histogram of the Analog to Digital Converter (ADC) outputs.

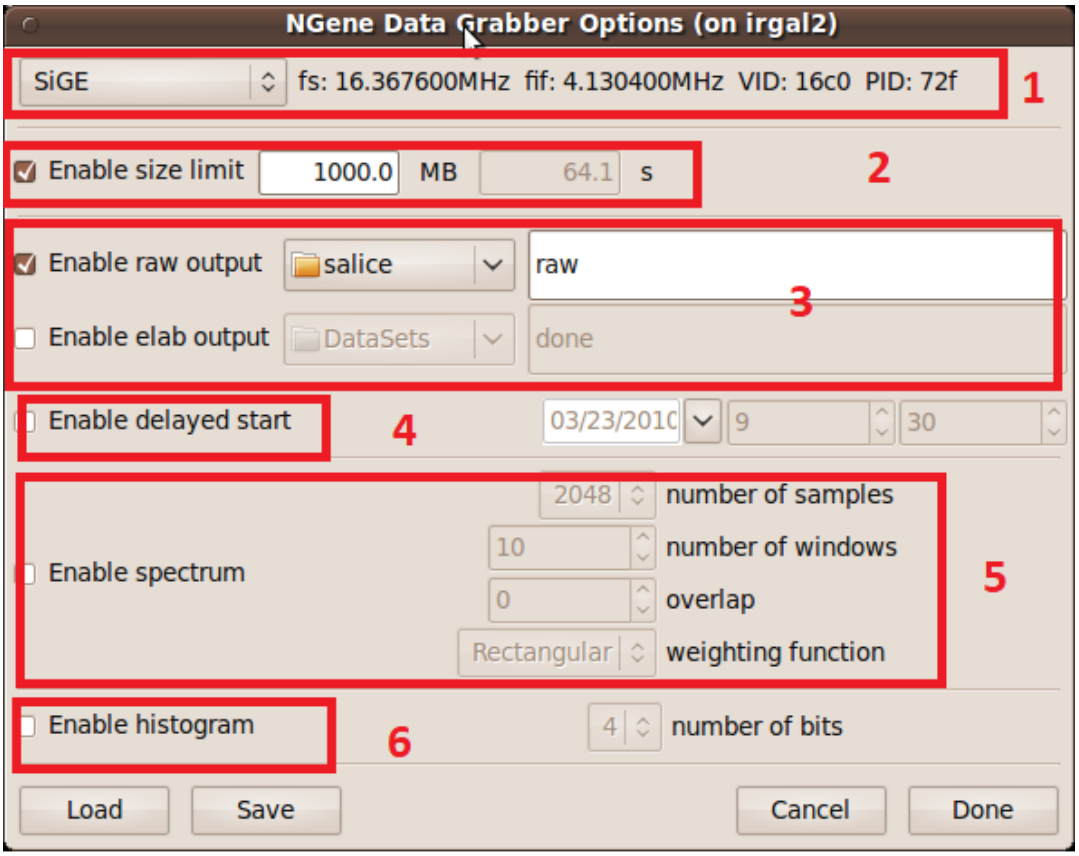

Figure 68: N-Grab options window (Detail)

When the recording is performed, N-Grab creates the output file and automatically chooses the name of the file as for example *usedFE_yyyymmdd_hhmmss_suffix.grab*.

It must be noticed that every data recording performed with N-Grab creates new files, old files aren't overwritten or deleted.

2. Data post processing software

This would be the last step we use to measure the soil moisture and dielectric constant of the ground by using this GNSS-R system.

The point of post processing the recollected data is to obtain from the measured values the SNR for both RHCP and LHCP signals (direct and reflected one) in order to extract from there the dielectric constant.

The main program we are using is the “SNR_computation.mat” file, which should be found in a folder “SNR_computation.mat” (the folder name is not important) together with the following files (schema from the main “SNR_computation.mat”folder):

b) Folder: SNR computation:
   i) Folder: DataTest:
      (1) File: “SIGE_ AAAAMMDD_hhmmss_rawDR.grab” which is the output file ftom the step iii (N-Grab).
   ii) Folder: DDM:
      (1) Floder: risultati
      (The following are Matlab functions used by the main “SNR_computation.mat”)
      (2) File: apribinRangeC2IQ_1bit.mat
      (3) File: codegen.mat
      (4) File: DDM.mat
      (5) File: DDMPRCS.mat
      (6) File: digitizg.mat
      (7) File: longSignalAcquisitionCDC.mat
      (8) File: matrice_CDC.mat
   iii) File: fc_setting.mat that is a matlab function used by the main “SNR_computation.mat”
   iv) File: SNR_computation.mat which is the main function

Once we are sure we have everything correctly, we define the following parameters in the "SNR_computation.mat" program:

1. *addpath('.\DDM\')*
2. *addpath('C:\Data\')*
3. *list=dir('C:\ Data\')*

Using these we have access to the folders and have a variable to work with its inner data.

4. *Nsat:* is the tracked satellite's number, depending on the data we need to compute, if defined in vector, the only procedure changed is the number of loops.
5. *fc:* carrier frequency.
6. *flprt:* controls the plot function inside DDM(), 1 to print and 0 otherwise.

All the operations can be done in the Main script (SNR_computation.m), some main parameters including: Nsat: input one of the satellites you want to observe. coh_int_time and ncoh_int_time : the two paramters can be adjusted to see the performance of the DDM. The vector x including all the satellites you want to observe as shown in the following figure:

```
ls_freq=range_freq(1):deltaf:range_freq(2);
coh_int_time=1
ncoh_int_time=100;
N=5;
coh_int_time_samples=ceil(coh_int_time*fs*1e-3);
% start_series=1;                                  %%%%%%%%%%%%%%% start from 1, inte
%total_samples=4883790000;% total length of data in number of byte

loop=floor(total_samples/(2*N*ncoh_int_time*coh_int_time_samples));
loop
SNR=zeros(1,10);
Nsat=13;
fc=38400;
% fc=fc_setting( fs,range_freq,Nsample_freq,deltaf,deltaf_prcs,ls_freq,coh_int_time,
i=7;
tic
 for x=[13,28,15,30]      %line 145 end

    Nsat=x;
```

Figure 69: Important parameters in post processing

List of files and functions can help us get a brief view of the structure of the software. Here is the file and function list (Table):

Table 1.3 List of Files and Functions

name	type	description
DDM	folder	Folder stores sub-routing files
SNR_computation.m	.m	Main script
DDM.m	.m	Sub-function of main script
DDMPRCS.m	.m	Sub-function of main script
longSignalAcquisitionCDC.m	.m	Sub-function of DDM.m and DDMPRCS.m